ADVANCED FUNCTIONAL MATERIALS
www.afm-journal.de

3D Printing of Functional Magnetic Materials: From Design to Applications

Chengqian Zhang, Xiangjia Li, Laiming Jiang, Daofan Tang, Han Xu, Peng Zhao, Jianzhong Fu, Qifa Zhou, and Yong Chen**

The research of functional magnetic materials has become a hot topic in the past few years due to their fast, long-range, and precise response in diverse environments. Functional magnetic devices using different magnetic materials and structure designs have been developed and demonstrated good advantages to enable various applications. However, the required magnetic materials and structure designs for diverse functions also increase the fabrication difficulties while developing such devices. 3D printing technology presents a powerful and promising manufacturing approach to rapidly fabricate functional magnetic devices of complex geometries in multiple materials and scales. Here, various 3D printing strategies and the underlying mechanisms of functional magnetic materials for several primary applications are systematically reviewed, including, magnetic anisotropy for property enhancement, magnetic robots, magnetic components in electronics, and magneto-thermal devices. Finally, the current challenges and future perspectives in engineering 3D printed functional magnetic devices are discussed.

1. Introduction

Recent progress in embedding magnetic materials to impart objects with various functions, such as, mechanical reinforcement,[1] controlled motion,[2] efficiency improvement,[3] deformation sensing,[4] and thermogenesis,[5] enables a wide and rising interest in functional magnetic material and its applications. For instance, a magnetic field can be utilized as a non-contacting operation source to orientate magnetic fillers inside composites, which exhibits anisotropic performances in mechanical,[1a] electrical,[6] thermal,[7] and optical properties[8] after alignment. The objects with embedded magnetic domains also show excellent characteristics of controlled motion under an external magnetic field. Magnetically actuated microrobots are widely recognized as a promising engineering solution to mimic the motions of plants and animals.[9] In electronics, the employment of soft magnetic components significantly increases the performance of radio-frequency devices and transformers due to the capability of concentrating magnetic flux using such components.[10] Besides, when exposed to an alternated magnetic field (AMF), magnetic particles can generate stable heat due to energy dissipation,[11] which makes magnetic materials important in the field of thermogenesis. In these fields, magnetic materials that serve as functional fillers exhibit various properties. Therefore, the manufacturing methods that can precisely construct such magnetic materials with well-designed structures are critical to fabricate functional parts with better performance. Unlike conventional subtractive and forming manufacturing processes that have limited ability to create products with intricate internal structure, additive manufacturing (AM, a.k.a, 3D printing) is able to build complex functional 3D structures directly from computer-aided design models using various materials.[12] With the ability of rapid fabrication and multi-material printing, 3D printing shows great potentials in manufacturing parts with novel designs that are previously unachievable.

Currently, over 50 types of 3D printing methods have been developed based on different principles. According to the American Society for Testing and Materials (ISO/ASTM 52 900:2015), these diverse 3D printing/additive manufacturing technologies can be classified into seven different processes: Material jetting, material extrusion, vat photopolymerization,

C. Zhang, D. Tang, Prof. P. Zhao, Prof. J. Fu
State Key Laboratory of Fluid Power and Mechatronic Systems
Zhejiang University
Hangzhou 310027, China
E-mail: pengzhao@zju.edu.cn
C. Zhang, D. Tang, Prof. P. Zhao, Prof. J. Fu
Key Laboratory of 3D Printing Process and Equipment of Zhejiang Province
Zhejiang University
Hangzhou 310027, China
C. Zhang, Dr. L. Jiang, H. Xu, Prof. Y. Chen
Epstein Department of Industrial and Systems Engineering
Viterbi School of Engineering
University of Southern California
Los Angeles, CA 90089, USA
E-mail: yongchen@usc.edu
Prof. X. Li
Department of Aerospace and Mechanical Engineering
School for Engineering of Matter
Transport and Energy
Arizona State University
Tempe, AZ 85287, USA
Dr. L. Jiang, Prof. Q. Zhou
Department of Biomedical Engineering
Viterbi School of Engineering
University of Southern California
Los Angeles, CA 90089, USA
The ORCID identification number(s) for the author(s) of this article can be found under https://doi.org/10.1002/adfm.202102777.

DOI: 10.1002/adfm.202102777

binder jetting, powder bed fusion (PBF), energy deposition, and sheet lamination.[13] Several well-known 3D printing technologies were derived from these methods, such as, direct ink writing (DIW), fused deposition modeling (FDM), stereolithography apparatus (SLA), two-photon polymerization (TPP), inkjet printing (IJP), and selective laser sintering/melting (SLS/SLM). These manufacturing methods are broadly applicable to metals, polymers, ceramics, and composites, and each technique has its advantages and limitations in constructing objects with some structures and functions. For instance, IJP is usually employed to print parts of small size due to its characteristics of high-resolution printing ability. FDM is one of the most commonly used 3D printing techniques to print thermoplastic polymers. DIW has excellent tolerability of polymer selections and multi-material printability due to its mechanical extrusion method and simple equipment. Particularly, a multi-material multi-nozzle 3D printing system was recently developed based on DIW, which allows the high-speed building rate with complex materials designed at the voxel level.[14] Based on SLA, TPP is a relatively new 3D printing process that provides a means of activating chemical or physical processes with a high spatial resolution (≈100 nm) in three dimensions, capable of micro and nanofabrication.[15] Moreover, a developed dynamic mask projection-based method, continuous liquid interface production, was invented to cure the photopolymer without the time-consuming intermediate recoating step at each layer, reducing the building time from hours to minutes.[16] Metal materials can be printed with high quality and fine resolution by SLS/SLM and binder jetting methods, where the printed part is supported by uncured powders.[17] Purposely, this review will not focus on the detailed development of various 3D printing technologies, which were covered in several recent reviews.[13,18] However, recent developments in 3D printing technologies further result in better performance and finer structures. Hence, understanding the characteristics of these printing techniques such as printing resolution, multi-material printability, and printing material requirements can be a good guideline for choosing the appropriate method to print magnetic materials and improve specific functions.

Well-designed 3D structures based on a deep understanding of the mechanism in magnetically functional applications were reported to have a potential for increasing the performance of structural parts, magnetic robots, transformers, and heat generators.[19] For example, inspired by the orientation of reinforcing elements in natural composites, the active magnetic materials are assembled to microarchitectures with special reinforcement and unique orientation by incorporating magnetic fields during printing.[1,19a] Fabricated objects can be magnetically manipulated by mixing magnetic fillers into a polymer base. However, this driving method is inefficient, and the transformation is simple.[20] To achieve the design and fabrication of magnetic robots with high-ratio deformation and fast responding, novel 3D printing methods were developed to embed programmed magnetic moments into planar structures at the micrometer scale and millimeter scale.[19b,21] To reduce the energy loss in high-frequency transformer, SLM of multi-alloys were proposed to replicate the layered structure of laminated stacks,[3] which was tedious in the conventional manufacturing process. The energy loss by combining the layered structure and the slits was reduced to 7% of the sample. Additionally, magnetic fillers were also employed in hyperthermia materials and shape memory polymers (SMPs) to take advantage of its uniform and noninvasive heating under a high-frequency magnetic field.[19d,22] Thus, by combining the benefits of 3D printing and the understanding of critical mechanisms in magnetic functions, engineers can achieve high-performance functional magnetic structures/systems with an emphasis on optimizing structural design and the choice of materials.

This review is intended to discuss the mechanism of functional magnetic material in different applications and the involved 3D printing techniques and to provide insight into the construction of high-performance magnetic parts through an optimized combination of design and fabrication methods based on such mechanism (**Figure 1**). In this review, we first introduce the mainstream magnetic materials and 3D printing technologies (Section 2), then focus on the recent advancements in 3D printing of magnetic anisotropic materials with property enhancement (Section 3), magnetic robots (Section 4), magnetic electronics (Section 5), and magnetic thermology (Section 6). Discussions of the key mechanisms, design requirements of magnetic materials and functional structures, and the fabrication using the developed 3D printing technology are presented in each section. Finally, we conclude the review with our outlook offering current benefits, challenges, and future perspectives on 3D printing technologies of functional magnetic materials.

2. Overview of Magnetic Material and 3D Printing Methods

2.1. Magnetic Functional Fillers

The functional fillers under the magnetic field can be aligned into polymer network matrixes with highly ordered structures.[1b] After removing the external magnetic field, most magnetic fillers will return to a non-magnetized state due to the low remanence magnetization, except for the permanently magnetized materials.[26] So far, either ferromagnetic materials or superparamagnetic particles have been used as magnetic active fillers in most researches to fabricate structures for specific properties.[13,27]

According to the intrinsic magnetic response, the functional fillers can be categorized into ferromagnetic materials and weakly magnetic materials. The ferromagnetic materials, like iron (Fe) and iron (III) oxide (Fe_2O_3) can be magnetized quickly in the magnetic field due to their unpaired electrons.[1a] Conversely, the weakly magnetic materials cannot be significantly magnetized in the external magnetic field until the ferromagnetic materials are added on the surface by multiple different processes, such as, chemical synthesis,[28] surface modification,[29] coating,[30] etc.

Currently, ferromagnetic materials are widely used to fabricate functional composites and structures through 3D printing methods. According to the coercivity (Hc), ferromagnetic materials can be divided into hard magnetic materials (Hc > 1000 A m^{-1}) and soft magnetic materials (Hc ≤ 1000 A m^{-1}).[31] Generally, once magnetized (exposed to a strong external

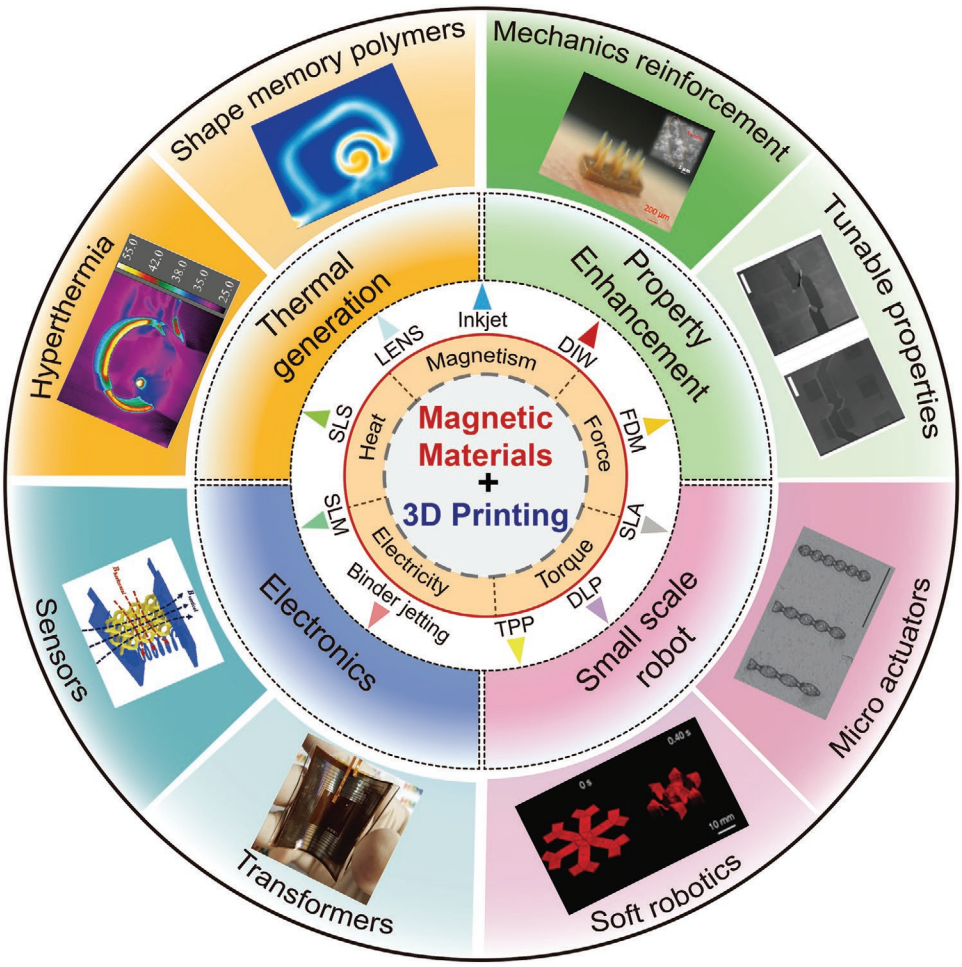

Figure 1. The functions and applications of 3D printed magnetic materials. The reviewed functions of magnetic materials include magnetism, force, torque, electricity, and heat. Primary applications include property enhancement, small-scale robots, electronics, and thermal generation. Representative functionality and applications (by clockwise) are mechanics reinforcement (Reproduced with permission.[1a] Copyright 2020, Wiley VCH.), anisotropic structure (Reproduced with permission.[1b] Copyright 2015, Springer Nature.), microactuators (Reproduced with permission.[23] Copyright 2014, Wiley VCH.), soft robotics (Reproduced with permission.[21a] Copyright 2018, Springer Nature.), transformers (Reproduced with permission.[24] Copyright 2017, Wiley VCH.), sensors (Reproduced with permission.[4] Copyright 2020, Wiley VCH.), hyperthermia (Reproduced with permission.[5b] Copyright 2019, Wiley VCH.), and shape memory polymers (Reproduced with permission.[25] Copyright 2019, Elsevier.).

magnetic field, and then removed), the high remnant characteristics (i.e., high B_r) allow hard magnetic materials, such as, Alnico, SmCo alloys, and NdFeB alloys, to retain strong magnetism. The high coercivity (i.e., high H_c) helps them to sustain the high residual magnetic flux density over the applied magnetic fields below the coercive field strength. In contrast, soft magnetic materials retain weak magnetism and are easy to be demagnetized. Therefore, hard magnetic materials are usually employed as functional fillers to fabricate customized-structure magnets and programmable shape-morphing robots due to their outstanding remnant magnetism after magnetization. Currently, four mostly utilized families of hard magnetic materials include Alnico, hard ferrite, SmCo alloys, and NdFeB. Research efforts on 3D printing have been mainly concentrated on NdFeB due to its highest magnetic strength at room temperature. Soft magnetic materials like Fe,[32] Fe_2O_3,[1a] and iron (II, III) oxide (Fe_3O_4),[33] ferrite, and Fe-Si alloys have high relative permeability and fast response to the applied field. They are widely used to fabricate magnetic-aligned composites with anisotropic property enhancement, novel magnetic components in electronics, and guiding part of microrobots. Due to low coercivity and hysteresis loss, soft magnetic microparticles are also employed to build devices that can generate heat under AMF, which can be applied in shape memory composites.

Another commonly used ferromagnetic functional material is superparamagnetic nanoparticles (NPs). Due to nanoscale size (usually < 3–50 nm), the magnetization of NPs can randomly flip direction under the influence of temperature. Therefore, when no magnetic field is applied, their average magnetization is zero.[34] In this state, an external field can magnetize the NPs, like paramagnetic materials, while they have much larger susceptibility. The conventional superparamagnetic materials contain Fe_3O_4, Fe_2O_3, $MnFe_2O_4$, FePt, and FeCo.[35] Among all these materials, Fe_3O_4 NPs are widely used for various applications, such as micro-robot, hyperthermia therapy, supporting, and shape-changing due to their good

biocompatibility, relatively high magnetic susceptibility, and low cost. For example, Fe_3O_4-based magnetic heating devices are commonly used in trachea and occlusion surgery, as well as, vessel stents.[5b] The magnetic nanomaterials can be synthesized into different structures using numerous approaches, such as, template-assisted process, electrodeposition, laser ablation, hydrothermal chemical reaction, etc.[36] The synthesized nanomaterials, including nanoparticles, nanorods, nanowires, nanotubes, nanobelts, nanosprings, nanoribbons, nanorings, nanofiber, and nanoclusters, have been attracting attention for the fabrication of magnetic-aligned composite due to their unique functional properties.[36,37] For example, nickel (Ni) nanowires were assembled and printed under the magnetic field to form aligned Ni rod arrays for semiconductive applications.[38]

Weakly magnetic fillers, which are difficult to be magnetized, can also be aligned in the external magnetic field to form composites with tunable properties when coated with ferromagnetic materials.[36] With the decoration of ferromagnetic materials, weakly magnetic materials, such as, carbon nanotube,[39] graphene,[40] carbon fibers (CNFs),[41] alumina platelets,[42] boron nitride,[43] silica,[1b] glass fiber,[44] calcium phosphate,[45] silicon carbide,[46] liquid crystals,[47] etc., can self-assemble in the magnetic field. The related magnetic-aligned composites exhibiting exceptional mechanical, electrical, thermal, and optical properties play a crucial role in various application fields.[48]

2.2. 3D Printing Methods

Most of the magnetic field-based self-assembly is limited to construct 1D and 2D structures for microelectronics and microrobotics.[36,38] During the past thirty years, numerous 3D printing processes have been developed, and the revolution of 3D printing has enabled advances in producing products with complex shapes that are novel and sustainable.[13,49] Besides the mainstream 3D printing techniques, different magnetic field-assisted 3D printing processes were investigated by integrating a designed magnetic field in the current 3D printing processes to fabricate anisotropic composites.[1a,19a,21a,32,33,45] The innovations of magnetic field-assisted 3D printing technologies open intriguing perspectives for designing functional materials and structures based on the magnetic field-enabled self-assembly.[13] The following sections give a general introduction to the commonly used 3D printing technologies and some related magnetic field-assisted 3D printing methods.

2.2.1. Commonly Used 3D Printing Technologies

The categories of 3D printing technologies were briefly introduced in Section 1, with each technology having its advantages and limitations in constructing objects with designed structures and functions. These manufacturing methods are broadly applicable to metals, polymers, ceramics, and composites. The selection of fabrication processes depends on the starting materials, requirements of processing speed and resolution, and performance requirements of final products. Here, we will review these commonly used 3D printing technologies as a guideline for choosing appropriate magnetic material printing methods to improve specific functions of 3D-printed parts.

Material IJP, also widely known as IJP, is a commonly used 3D printing technique for selectively depositing materials on a substrate to form the object.[50] With high-resolution and multi-materials abilities, the IJP process is widely used to fabricate magnetic substrates with small thicknesses,[51] which can impart flexibility to 3D-printed parts.[19c,24] However, when employing this method, it is essential to choose an adequate low-viscosity liquid polymer and nanoscale magnetic particles as functional fillers to avoid clogging of the printhead. Due to the use of a large amount of solvents evaporated during printing, using IJP to build complex 3D structures is difficult.[52]

Materials extrusion, in which the print materials are extruded through a movable print head to form a continuous filament and then selectively deposited into 2D layers, is one of the most widely used 3D printing processes, particularly when working with polymers and thermoplastic composites.[53] According to the differences in extruding materials, there are two main methods—FDM and DIW. When printing magnetic materials, FDM is mainly used to print permanent magnets with near-net-shape and 3D structures.[54] Compared to traditional manufacturing processes, FDM is becoming an alternative method that can rapidly fabricate magnets with general performance and complex geometry. However, the existence of nonmagnetic thermoplastic polymers reduces the magnetic performance of the 3D-printed magnets. In contrast, DIW is a widely used fabrication method to print magnetic materials due to its good tolerability of polymers selections. The great multi-material printing ability makes DIW the leading method to apply magnetic materials into various applications, such as magnetic robot[21a] and bone regeneration.[22]

Vat photo-polymerization (VPP) is a 3D printing process that selectively solidify light-sensitive liquid polymers using a specific light source to form solid objects layer-by-layer. Various VPP processes, including SLA, TPP, and mask image projection-based stereolithography (MIP-SL), were developed based on this principle. The main advantage of VPP is the ability to print parts with high resolution, high-quality surface finish, and wide material selection. However, when the printing materials are confined to magnetic materials, the magnetic particle content is limited to a low level due to poor curing performance related to particle-induced absorption.[23] Magnetic microrobots with complicated structures and good biocompatibility were fabricated using TPP for biomedical applications. Compared with SLA, the TPP process provides flexibility in fabricating 3D structures at a micrometer scale. Two strategies are applied to couple the 3D structures with magnetic materials. The first one is to deposit magnetic coating like Ni/Ti bilayers on the surface of the helical swimmer by electron beam evaporation,[55] which can not only be actuated by the magnetic field but also improve microrobots' surface biocompatibility. The second method is to embed superparamagnetic NPs in the printed structures.[23,56] During the printing process, a magnetic field was built to trap and align magnetic microparticles to control their magnetization directions.[23] In general, the TPP method makes it possible to fabricate in vivo microrobots for therapeutic operations by magnetic propulsion.

Binder jetting is a 3D printing method in which powders are fused and selectively bonded with binders, a liquid bonding agent, in each layer.[57] It is mainly used for metal or ceramic powders, and there are no thermal gradient-induced stresses inside the printed part. Until now, only a few attempts have been made to print magnets and shape memory alloys using this method.[58] However, due to its capacity of printing complex 3D structures by using powders as supporting structures, this method will show more applications in fabricating novel soft magnetic components with the diversification of soft magnetic devices.

PBF is a 3D printing process that uses a focused laser or an electron beam as the power source to fuse powdered materials on a bed layer-by-layer.[59] According to the differences in the powders' phase state during printing, it is also known as SLS or SLM. Compared with binder jetting, PBF has the potential of combining geometrical freedom with an improved magnetic performance by increasing the volume content of magnetic materials since a polymer binder is not needed.[60] Moreover, the multi-material printing ability of PBF opens up new possibilities, such as using different materials within a single transformer to create areas of changing magnetism and conductivity, which will reduce eddy current losses significantly.[3]

Directed energy deposition (DED) utilizes thermal energy to fuse materials by melting while being deposited rather than after deposition of a new layer. Like other powder-based 3D printing methods, DED is mainly focused on the fabrication of soft and hard magnetic parts with near-net-shape and superior magnetic performance.[61]

2.2.2. Magnetic Field Assisted 3D Printing

Magnetic fillers are usually suspended in liquid solution for 3D printing magnetic-aligned composites. The magnetic fillers are randomly distributed in the liquid polymer matrix without applying the magnetic field. Magnetic fillers can be assembled and manipulated into 1D, 2D, and 3D structures using external and locally applied magnetic fields.[21b] For example, magnetic fillers can be assembled into micro chains in 3D printing of magnetic-aligned composites. The magnetic fillers interact with each other through dipolar-dipolar forces and tend to aggregate to form chains in the orientation controlled by the magnetic field direction. The morphology of the aligned magnetic filler chains can be modulated by changing the fillers' concentration, the fillers' size, and the strength of the magnetic field.[62] Due to the magnetic dipole-dipole and electrostatic repulsive forces, the assembled magnetic particle chains are separated with uniform interchain spacing at the final equilibrium state.[19a,21a] The interchain spacing can be adjusted by changing the particle concentration and the strength of the magnetic field.[1a]

Based on the magnetic field-assisted self-assembly, several new 3D printing processes have been developed. For example, MIP-SL is a 3D printing method in which layers of liquid photocurable polymer are selectively solidified when the liquid resin is exposed to the irradiation of UV light beam.[63] By incorporating the magnetic field generated by either permanent magnet or computer-controlled solenoids (**Figure 2**a), the active magnetic materials are assembled into special microarchitectures with unique orientations in the photocurable polymer matrix.[1,32,33,41] Compared with MIP-SL, the DIW-based 3D printing process enables the fabrication of non-photocurable polymer-based composite. It is more convenient for DIW to deposit multiple types of materials at the same layer.[64] A magnetic field was applied to DIW as well as the tape casting-based printing processes to overcome the fibers' shear alignment during the extrusion process. For example, calcium phosphate microrod coated with superparamagnetic iron oxide nanoparticles (SPIONs) were successfully aligned during extrusion by using the magnetic-assisted DIW process.[45] In the magnetic-assisted DIW and tape casting approaches, the magnetic active fibers were aligned when a localized magnetic field was applied at the printing location (refer to Figure 2b).[19a,21b,45,62] Also, a new 3D printing process was developed to fabricate magnetic aligned composite by combining a well-established slip-casting process with an external magnetic field (Figure 2c).[65] With the deposition of active magnetic suspension in the added magnetic field, heterogeneous composites with controllable orientations and particle distributions were fabricated.[65]

When printing functional materials with embedded magnetization, DIW[21a,69] and the SLA-based methods[21b] can program the internal magnetization of printed structures by orientating the magnetized NdFeB particles during the printing process. For example, the electromagnetic coil or ring magnet was set around the writing nozzle of a DIW system to generate a uniform magnetic field along the flow direction of the ink (refer to Figure 2d).[21a] The magnetized NdFeB microparticles that are initially non-oriented will reorient along the magnetic field, remaining a durable magnetic moment within the magnetized filament. By switching the magnetic field direction, the magnetic domains of the printed filaments can be programmed, enabling the transformation of printed structures controlled by the added magnetic field. Like the DIW method, the SLA-based methods also apply magnetic fields to encode the magnetization of the magnetic particles in the resin vat. With an applied magnetic field, the dispersion and distribution of the magnetic microparticles in the resin can be controlled by reorienting them (refer to Figure 2e). Diller et al.[21b] illustrated the feasibility of printing a dual-layer structure with different magnetization components. Compared with DIW, the SLA-based methods can fabricate soft robots with more complex magnetizations and morphologies, since the resolution of the used digital light allows for higher accuracy in patterning 3D magnetization.

The self-assembly of magnetic fillers in the polymer-based composite can be instant. The fast response is one of the main benefits of magnetic field-assisted self-assembly compared with the field-assisted 3D printing approaches based on electrical and acoustic fields. For example, IJP is widely used in electronics manufacturing due to its high resolution, simultaneous multi-material fabrication, and large-scale printing abilities.[70] As shown in Figure 2f, a magnetic field was applied below the inkjet nozzle by an electromagnet, so the magnetic particles in the jetted droplets were aligned during the printing process.[66] Furthermore, electrospinning exhibits strengths in the fabrication of thin films with composite nanofibers over a large area.[71] In the magnetic field-assisted electrospinning, the external magnetic field enables the alignment of electrospun

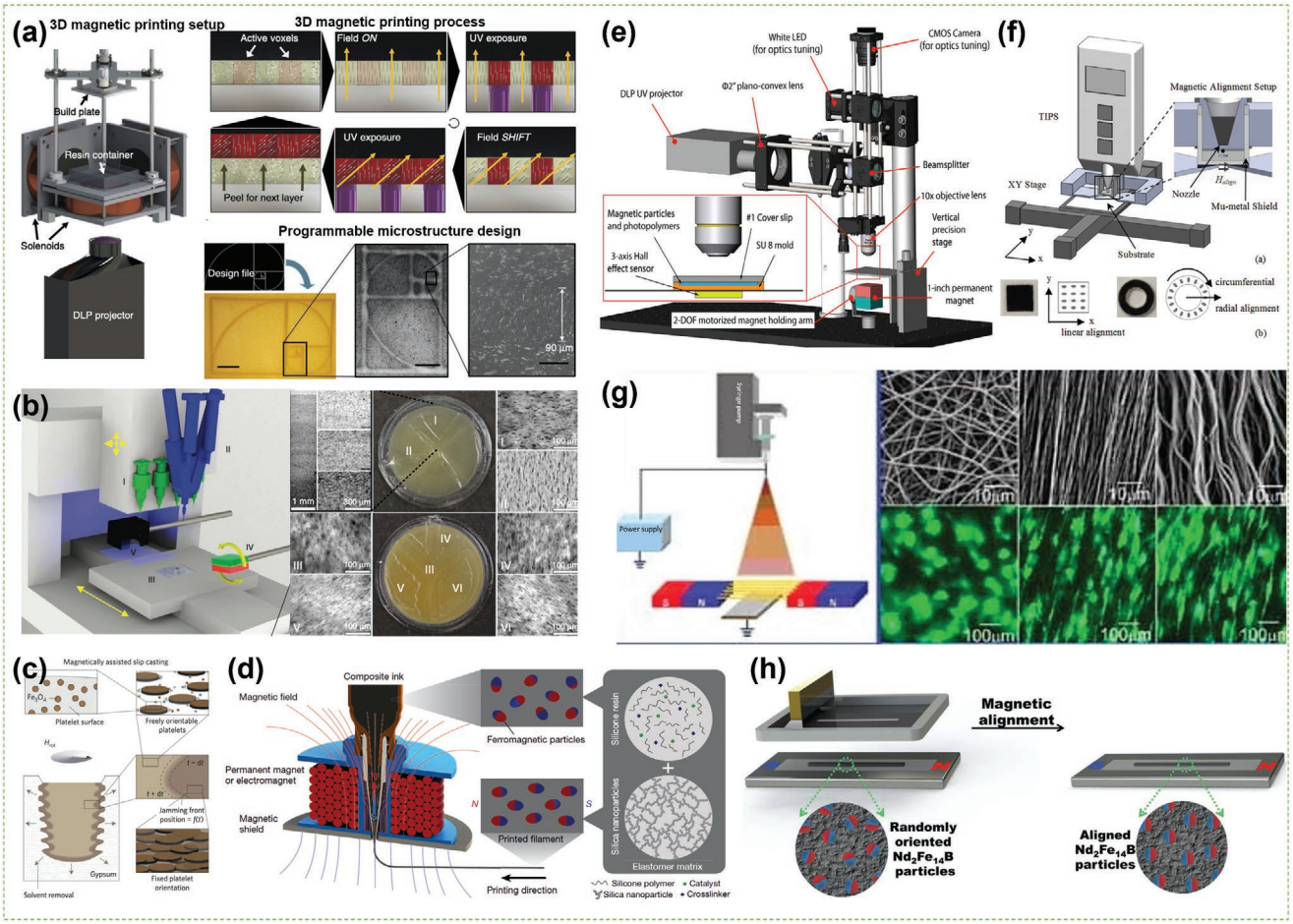

Figure 2. Magnetic-field-assisted 3D-printing technology: a) Magnetic field-assisted SLA technology. Reproduced with permission.[1b] Copyright 2015, Springer Nature. b) DIW-based multi-material magnetic 3D printing. Reproduced with permission.[19a] Copyright 2015, Springer Nature. c) Magnetically assisted slip casting. Reproduced with permission.[65] Copyright 2015, Springer Nature. d) DIW-based 3D printing for orientating magnetization. Reproduced with permission.[21a] Copyright 2018, Springer Nature. e) Permanent magnet assisted SLA technology. Reproduced with permission.[21b] Copyright 2019, American Association for the Advancement of Science. f) Magnetic field-assisted inkjet printing. Reproduced with permission.[66] Copyright 2014, AIP Publishing. g) Magnetic field-assisted electrospinning. Reproduced with permission.[67] Copyright 2010, Wiley-VCH. h) Magnetic field-assisted screen printing. Reproduced with permission.[68] Copyright 2016, American Association for the Advancement of Science.

polymer nanofibers. Furthermore, it brings a new opportunity to assemble and align ultralong nanowires on a large scale (refer to Figure 2g).[67] Magnetic field-assisted screen printing was also developed by placing the magnet under the fabrication substrate in the screen printing, a long-established technology for fabricating organic electronics.[72] Hence, the magnetically self-healing ink was aligned along the magnetic field direction in the screen printing process (refer to Figure 2h).[68]

To summarize, the newly developed magnetic field-assisted 3D printing processes can realize the functional fillers' alignment in spatial directions by applying a designed magnetic field.[27] Compared to other field-assisted 3D printing approaches, the magnetic field-assisted 3D printing process is fast, taking no more than a few seconds for the magnetic fillers to assemble in the polymer matrix.[1a] Besides, the magnetic field-assisted alignment has good robustness, high dynamic, and excellent static performance. The magnetic field enables one to control the orientation and spatial arrangement of fillers remotely since the permanent magnet or computer-controlled solenoids can generate the magnetic field without contact with the composites. The magnetic field-assisted 3D printing processes have provided a powerful fabrication tool to produce complex composites with tailored structures and functionalities due to the advantages mentioned above.[13]

3. 3D Printing of Magnetic Anisotropy for Property Enhancement

The magnetic field-assisted assembly has been widely used in the manufacturing of functional magnetic material for various applications, owing to their unique capability in controlling the orientation and spatial arrangement of fillers, including 1D, 2D, and 3D aggregates.[73] For example, the high-rate performance of lithium-ion batteries can be improved dramatically because of aligned graphite particles in the fabricated electrode by applying

magnetic alignment technology.[74] However, due to the limited fabrication capability, traditional manufacturing technologies can only construct the magnetic-aligned composite into simple geometric shapes, which restricts the applications of magnetic-aligned composite in acoustic, optical, electronic, mechanical, and thermal fields.[75] Recently, 3D printing provides a potential solution to fabricate the magnetic-aligned composite with complex structures and precise arrangement of functional fillers.[13] This section will discuss the recent advances in 3D printing of magnetic anisotropy for property enhancement, including the principle and mechanism, material selection, innovative magnetic field-assisted 3D printing processes, and 3D printing of magnetic aligned composite with various tunable properties.

3.1. Property Enhancement Principle and Mechanism

Over the millions of years of evolution, natural material with optimized architectures exhibits specific functions that even sophisticated human-made materials cannot match.[26] Natural material with anisotropic properties, attributed to unique hierarchical architectures, has attracted significant attention for various applications because of better economic benefits and broader applied perspectives.[76] Such natural hierarchical architectures are regularly arranged and composed in a variety of alignments and make up whole biological materials with optimized constituent and aspect ratio.[28] For example, the delicate arrangement of micro and nanostructures can manipulate light to create fantastical structure color in nature.[29] The feathers of hummingbirds show iridescent blues and greens generated by aligning keratin, air hole, and melanin into nanoarrays (**Figure 3**a).[30] Similarly, the spines of polychaete worms exhibit iridescent color due to hexagonally packed cylindrical hollow channels, which selectively reflect long-wavelength light (Figure 3b).[29] Besides, the ring teeth of squid sucker, composed of oriented tubular structures with graded pore size, reveal anisotropic physicochemical and thermomechanical properties (Figure 3c).[77]

In addition, there are some examples of biological materials with unique microarchitectures that demonstrate brilliant mechanical enhancement.[78] For example, the cross lamellar structures of seashell (Figure 3d) enable the absorption of more energy during the deformation without fracturing. The seashell's underlying toughness enhancement mechanisms, such as channel cracking, interlocking, and crack deflection of lamellar structures, contribute to the fracture resistance of seashells.[79] The brick-mortar architectures learned from bone and nacre also reveal significant enhancement of the fracture resistance (Figure 3e).[80] For example, the underlying mechanism of anisotropic mechanical behavior of nacre results from the specific topological arrangement of a soft and ductile mortar layer and stiff and hard bricks.[80] Moreover, biological materials across different species, such as, fish scales, beetles, crabs, lobsters, mantis shrimps, demonstrate outstanding toughness and

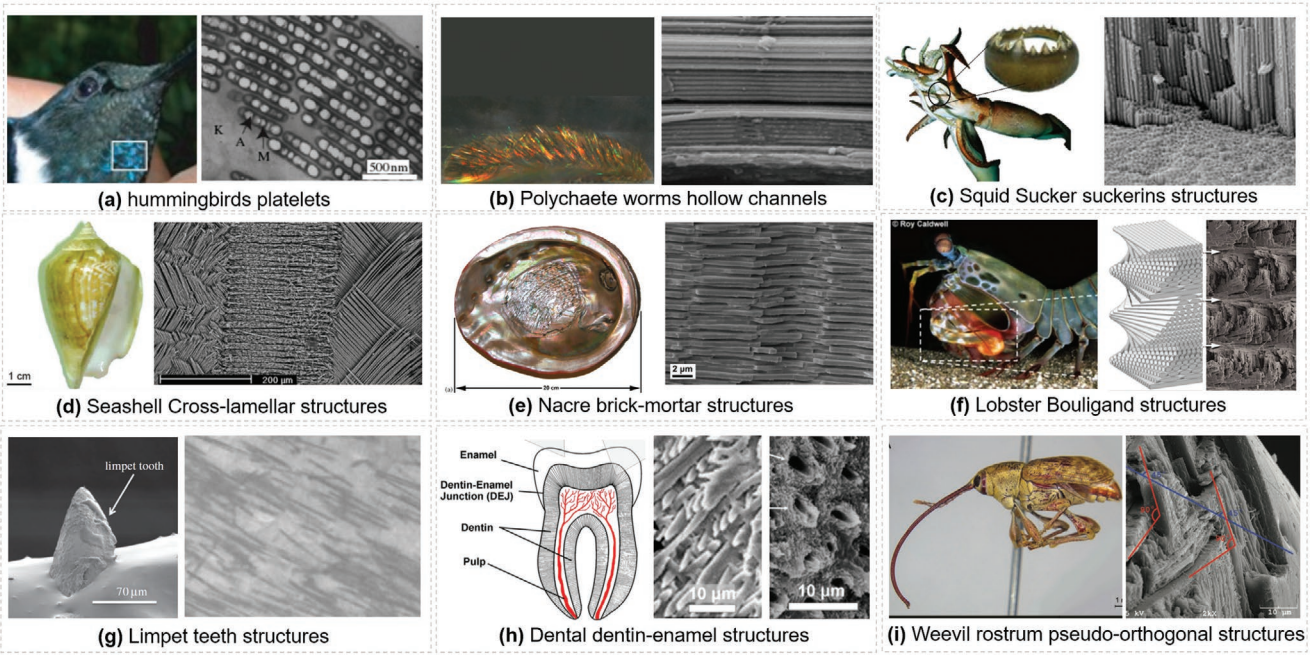

Figure 3. Examples of natural functional composite with hierarchical architectures. a) Aligned platelets of a hummingbird for structural color. Reproduced with permission.[30] Copyright 2009, Royal Society. b) Hollow channels array of polychaete worms for structural color. Reproduced with permission.[29] Copyright 2012, American Society for Photobiology. c) Suckerins structures of squid sucker. Reproduced with permission.[77a] Copyright 2017, American Chemical Society. d) Cross-lamellar structures of a seashell. Reproduced with permission.[79] Copyright 2003, Royal Society of Chemistry. e) Brick-mortar structures of nacre. Reproduced with permission.[80] Copyright 2007, Elsevier. f) Bouligand structure of lobster. Reproduced with permission.[48] Copyright 2017, Elsevier. g) Aligned goethite nanofiber inside limpet teeth. Reproduced with permission.[81] Copyright 2015, Royal Society. h) Dentin-enamel structures of mouse teeth. Reproduced with permission.[82] Copyright 2010, Elsevier. i) Pseudo-orthogonal structures of weevil rostrum. Reproduced with permission.[83] Copyright 2019, Wiley-VCH.

stiffness owing to Bouligand structures (Figure 3f).[48,84] Such Bouligand structures play a significant role in the remarkable damage tolerance with the mechanism that energy dissipates and stress mitigates along the twisting microcracks without leading to catastrophic failure.[84] Recently, limpet teeth were identified as the strongest natural material, whose tensile strength is even higher than that of spider silk.[81] This distinctive mechanical reinforcement results from aligned goethite nanofiber in the goethite/protein composite (Figure 3g). Unlike the hierarchical microarchitectures of limpet teeth, natural mammal teeth offer excellent mechanical strength with architectures of specific arrangements of rigid enamel layer and flexible dentin.[85] As shown in Figure 3h, reinforcing blocks are aligned parallel and perpendicular to the loading force's direction in the enamel layer and the dentin layer of mouse teeth.[82,86] The endocuticle of the weevil rostrum consists of macro fiber laminae piled in a pseudo-orthogonal manner (Figure 3i) so that the crack formation and propagation can be effectively prevented. Although the pseudo-orthogonal structures are less rigid, they exhibit better toughness compared to the Bouligand structures.[83]

Biological materials with hierarchical architectures in nature provide design inspiration of functional structures with property enhancement.[82] The enhanced functionalities can be accurately modulated by controlling the spatial distribution and orientation of functional fillers in the hierarchical architectures.[82] However, due to the fabrication capability limitation, there are several challenges in reproducing hierarchical biological architectures with special spatial orientations of functional fillers by using traditional manufacturing technologies. Utilizing advanced 3D printing with the assistance of physical fields opens the way toward the fabrication of bioinspired structures for performance enhancement.[82] Different strategies, such as magnetic field,[1b] electric field,[87] mechanical shear force,[88] freeze-casting,[89] self-assembly,[90] have been developed to achieve the fabrication of highly ordered structures.[27] Compared with other strategies, the magnetic field exhibits advantages in remote control and no restriction on the orientation direction. Specifically, the magnetic dipole moment m of a magnetic particle under the external magnetic field is determined by the volume susceptibility of the particle, the magnetic field strength, and the particle size. The magnetic moment m of the magnetic particle will increase with the magnetic field until it reaches a saturated value.[21b] The magnetized particle generates the local magnetic field, and the adjacent magnetic particles will be attracted by its local magnetic field. The interparticle magnetic dipole-dipole force will drive the alignment of particles into micro chains along the external magnetic field direction.[21b] To align the magnetic fillers in the external magnetic field, the attractive forces, including the magnetic force, electrostatic force, and van der Waals' force, should be big enough to overcome the repulsive force and fluid drag force.[45] The assemble force drives the magnetic particles to move to regions with the maximum magnetic field strength.[45] The formation and the length of magnetic particle chains will be diminished by decreasing the magnetic field strength.[21b] The use of magnetic field-assisted 3D printing to fabricate anisotropic structure for mechanics reinforcement is the focus of this section.

3.2. 3D Printing of Magnetic Aligned Composite for Mechanical Reinforcement

Biological material exhibits anisotropic mechanical properties because of different reinforcing structural features (refer to Figure 3d-i).[41] Bio-mimicking such hierarchically organized reinforcing features are challenging for traditional composite fabrication methods.[41] Physical field-assisted 3D printing opens a new way to replicate reinforcing structural architectures inspired by biological material, such as, bone, seashells, limpet teeth, shrimp, lobsters, etc.[13] The integration of 3D printing and dynamic control of the magnetic field enables the fabrication of composite with specific alignments of functional fillers, enhancing the strength, stiffness, and toughness of the 3D printed materials.[42a]

The mechanical property of the structures fabricated by the magnetic field-assisted 3D printing process improves dramatically by spatially controlling the alignment of functional fillers during the printing process.[1a] For example, alumina Al_2O_3 microparticles decorated with iron oxide nanoparticles (IOPs) were aligned under the magnetic field to form the reinforcement architectures.[1b] As shown in **Figure 4**a, the particle orientation was adjusted by controlling the magnetic field. The assemble orientation played a significant role in either strengthen or weaken the mechanical properties of the 3D-printed composite. When the alignment of the alumina microparticles was parallel to the loading direction, the printed composite was reinforced and revealed high compression strength. The alignments of magnetic fillers induced by the magnetic field provide a new way to create programmable composites with anisotropic mechanical properties. To achieve mechanical enhancement, natural herringbone and Bouligand structures were replicated with aligned micrometer-sized nickel-coated carbon fibers (NiCFs) in the photocurable polymer matrix by using magnetic field-assisted slurry-based SL (refer to Figure 4b).[41] The toughness and compression strength of the printed composite were determined by the mass fraction of NiCFs and the morphology of microarchitectures formed under the magnetic field.[41] The young's modulus of 3D-printed parts with alignments of NiCFs is more than ten times of the one of pure polymer. The magnetic field is not only able to modulate the static mechanical properties of the 3D-printed composite but also can change the mechanical index of the 3D-printed structures dynamically.[91] For example, magnetoactive lattice structures were printed by MIP-SL using elastomers and ferromagnetic nanoparticles. The modulus of printed lattice structures can be adjusted from positive to negative with the increase of magnetic field (refer to Figure 4c).[91a] The dynamic regulation of the mechanical performance of 3D-printed composite has an extensive prospect in diverse applications. Additionally, the magnetic-aligned composite showed advantages in the mechanical reinforcement for biomedical application. For instance, bioinspired painless microneedles (MNs) were fabricated using the magnetic field-assisted MIP-SL with biocompatible polymer and IOPs (refer to Figure 4d).[1a] The magnetic iron oxide particles (IOPs) were assembled in the magnetic field to generate the limpet teeth-inspired reinforcement architecture during printing. It opens intriguing perspectives for designing MNs with high mechanical strength based on the limpet teeth-inspired hierarchical structures.

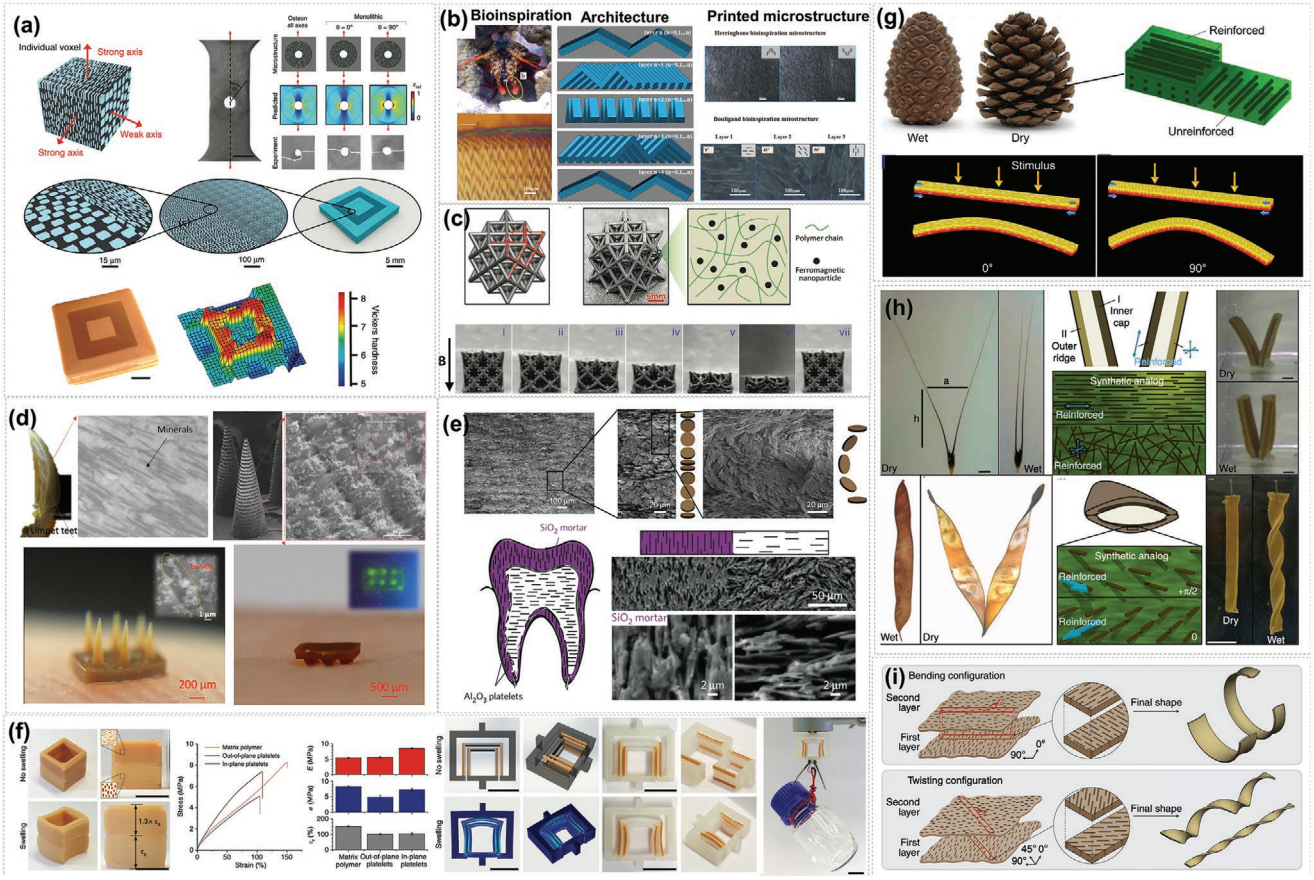

Figure 4. Magnetic-field-assisted 3D printing of the mechanically reinforced composite. a) Mechanical properties of composite with programmable reinforcement architectures printed by magnetic field-assisted SLA. Reproduced with permission.[1b] Copyright 2015, Springer Nature. b) Bioinspired composites with tunable mechanical properties created by 3D magnetic printing. Reproduced with permission.[41] Copyright 2018, Springer Nature. c) Magnetic actuation of elastomer lattices printed with ferromagnetic nanoparticle-based composite. Reproduced with permission.[91a] Copyright 2018, Wiley VCH. d) Limpet teeth-inspired microneedles printed by magnetic field-assisted SLA for drug delivery. Reproduced with permission.[1a] Copyright 2020, Wiley VCH. e) Scanning electron images of 3D printed composite with tuning the local orientation of fillers to reproduce the heterogeneous architecture of natural teeth. Reproduced with permission.[65] Copyright 2015, Springer Nature. f) Multi-material magnetic 3D printing of heterogeneous composites with programmable mechanical performance. Reproduced with permission.[19a] Copyright 2015, Springer Nature. g) Schematics of shapeshifting of pinecone-inspired composite with different microfibril arrangement. Reproduced with permission.[92] Copyright 2019, Elsevier. h) Wheat awn and orchid tree seedpod inspired reinforced composites with aligned cellulose microfibrils. Reproduced with permission.[42b] Copyright 2013, Springer Nature. i) Schematics of bending and twisting of self-shaping ceramic bilayer result from the different alignment of platelets magnetic field-assisted screen printing. Reproduced with permission.[93] Copyright 2016, Springer Nature.

High volume fraction particulate composite with tunable stiffness and toughness can be designed and fabricated using magnetically assisted slip casting, which addresses the current challenges on the specific functional demands in the biomedical field.[65] For example, the dentin-enamel layers of the natural tooth were reproduced by assembling 20 vol% of alumina platelets and 13 vol% of alumina nanoparticles for dentin-like layer, and 20 vol% of alumina platelets, 4% isotropic silica, and 9 vol% of alumina nanoparticles for enamel-like layer in a 5wt% poly(vinyl pyrrolidone) aqueous solution (Figure 4e).[65] The hardness of the 3D-printed composite can be adjusted by changing the particulate content and particle orientations.[65] Besides, anisotropic stiff platelets were assembled in a ceramic, metal, or polymer functional matrix to create programmed microstructural designs using magnetically assisted slip casting.[65] For instance, the alumina composite with reinforcement alignment exhibits a threefold increase in fracture toughness than the one without alignment.[65] As shown in Figure 4f, heterogeneous material with anisotropic mechanical properties was fabricated by the magnetic field-assisted DIW, by which multiple materials can be deposited using separate syringes.[19a] The used composite ink consisted of polyurethane acrylate, polyhydroxy ethyl methacrylate, photo-initiator, magnetically modified alumina platelets, and fumed silica. When the ink was extruded, the alumina platelets were aligned by a permanent magnet during the printing process. The strength and elastic modulus of the aligned 15 wt% alumina platelets composite in the tensile loading direction increased by 49% and 52%, respectively, than those of the samples whose alignment is perpendicular to the loading direction. Moreover, the alignment of the alumina platelets influences the local swelling response of the 3D-printed parts. The *Z* directional swelling ratio of 3D-printed parts with the perpendicular alignment of 15 wt% alumina platelets was 30% higher than the one with the alignment parallel to the *Z*-axis.[19a]

The reinforcing fillers improve the mechanical properties and endow the printed composite with anisotropic shape deformation capabilities.[42b,92,94] For example, pinecone-inspired stripes were fabricated using 40 wt% short steel fiber-based composite by the slurry-based SLA. The shape-changing ratio of the 3D-printed strip with aligned fibers parallel to the force loading direction was much larger than the one with the alignment direction orthogonal to the force loading direction (refer to Figure 4g).[92] Besides, the reinforced composite demonstrated anisotropic swelling/ shrinkage due to the aligned fillers. The shape-changing performance of bioinspired composite cellulose microfibrils can be modulated by changing the reinforcement orientation.[42b] For instance, the swelling and shrinkage of 7.5 vol% alumina platelets aligned perpendicular to the reinforcement direction is 250% and 200% higher than the one with alignment parallel to the reinforcement direction, respectively (Figure 4h).[42b] The bending and twisting of the fabricated layers can be programmed by controlling the orientation of the magnetic fillers in the 3D-printed composite. Moreover, the printed composite can be converted into a fully ceramic part after removing the inside polymer matrix.[94] For example, magnetic alumina platelets were aligned inside the alumina nanopowders-based slurry. Then the self-shaping ceramics were obtained after the sintering, owing to the orthogonal anisotropic shrinkage in the reinforced microstructures.[93] The ceramic's final shape after sintering can be regulated by the geometry and the particles' reinforced microstructures (Figure 4i).

Owing to the reinforcement microstructures, the shape-changing of 3D printed objects provides a programmable method to fabricate parts with complex geometries in a simple manner. It also paves the way for 4D printing of the magnetic-aligned composite with anisotropic swelling/shrinkage for various applications in the future.[13,49] The bioinspired structural material with aligned fillers can be successfully fabricated using magnetic field-assisted 3D printing.[1,41,65] Magnetically aligned fillers not only enhance the anisotropic mechanical properties of the 3D-printed composite but also trigger the anisotropic shape-changing under the external stimulus.[42b,92,94,95] The discussed achievements would be helpful to understand the effect of aligned architectures on mechanical reinforcement, shape-changing, and the dynamic control of the magnetic field for anisotropy mechanical performance with programmable alignments.

3.3. Magnetic Aligned Composites for Other Tunable Properties

Magnetic fillers are aligned in the polymer matrix in the magnetic field, and the magnetic aligned composite is further built by different types of 3D printing processes.[1a,19a,21a,32,33,45] Because the functional fillers are oriented in a particular direction, the mechanical, electrical, thermal, and optical properties of the magnetic-aligned composite exhibit anisotropic performances compared with the composite where the fillers are randomly distributed.[27] The anisotropic performance of functional composite can be modulated by controlling the aligned microarchitectures and adjusting the material composition.[40,41] The magnetic field-assisted 3D printing also promotes possibilities in manipulating and mimicking natural heterogeneous microstructures with tunable electric, thermal, and optical characteristics.[13]

3.3.1. Electrical Conductivity

Magnetic nanoparticles, nanotubes, nanowires, and nanoplates have become popular active fillers in inducing remarkable electrical performance.[96] The alignment of functional fillers can induce anisotropic electrical conductivity and enhance electronic performance.[97] Current magnetic-aligned composites have potential applications in electronic coatings, electronic devices, energy storage and supply, etc.[98] For example, Kimura et al. were the first to align multiwalled carbon nanotubes in a polyester matrix by applying the external magnetic field for the anisotropic electrically conductivity.[99] Later, single-walled carbon nanotubes (SWCNTs)/epoxy resin composite were fabricated with the uniform alignment of SWCNTs. The electronic conductivity of 3% SWCNT/ epoxy composite perpendicular to the alignment direction is 1.4 times of the one along the alignment direction.[100] Additionally, graphene is another form of carbon material discovered with outstanding electrical properties.[87,101] To align the graphene inside the polyimide composite using the magnetic field, the Ni nanoparticles were tethered to the graphene. The electrical conductivity of aligned 1.3v% Ni-graphene composite was 2.5 times higher than the randomized 1.3v% Ni-graphene composite.[102]

The electrical conductivity enhancement of magnetite CNFs/ epoxy nanocomposite was also studied.[103] For instance, the electrical conductivity of the composite measured parallel to the alignment is consistently over one order of magnitude higher than that of the randomly-oriented nanocomposites, of which the concentration of CNFs ranges from 0.2 to 0.6 wt% (refer to **Figure 5**a).[103] Moreover, the alignment of metallic fillers (nanoparticles and nanowires) in the composite can also enhance the composite's electrical conductivity. For example, the electrical conductivity of silicon/Ni composite with the alignment of Ni is more than sevenfold compared with the composite with randomly distributed Ni fillers (refer to Figure 5b).[6,104] In summary, the bioinspired arrangement of functional fillers can dramatically increase the electrical conductivity of the composite, and magnetic field-assisted 3D printing of aligned composite with anisotropic electrical properties can further facilitate promising applications such as flexible sensor, supercapacitor, battery, and solar cell in the future.[105]

3.3.2. Thermal Conductivity

Thermally conductive fillers, including ceramic, metal oxides, metals, and carbon material, exhibit excellent thermal performance, and composites with magnetically aligned thermally conductive fillers offer great efficiency in heat conduction and heat transfer.[106] Thermal ceramic fillers, such as hexagonal boron nitride (hBN) microplates,[43,107] boron nitride nanoplatelets (BNNP),[108] and aluminum nitride[7] platelets were coated with IOPs to enhance the magnetic responsibility in the magnetic field. For example, the aligned hBN microplates/epoxy

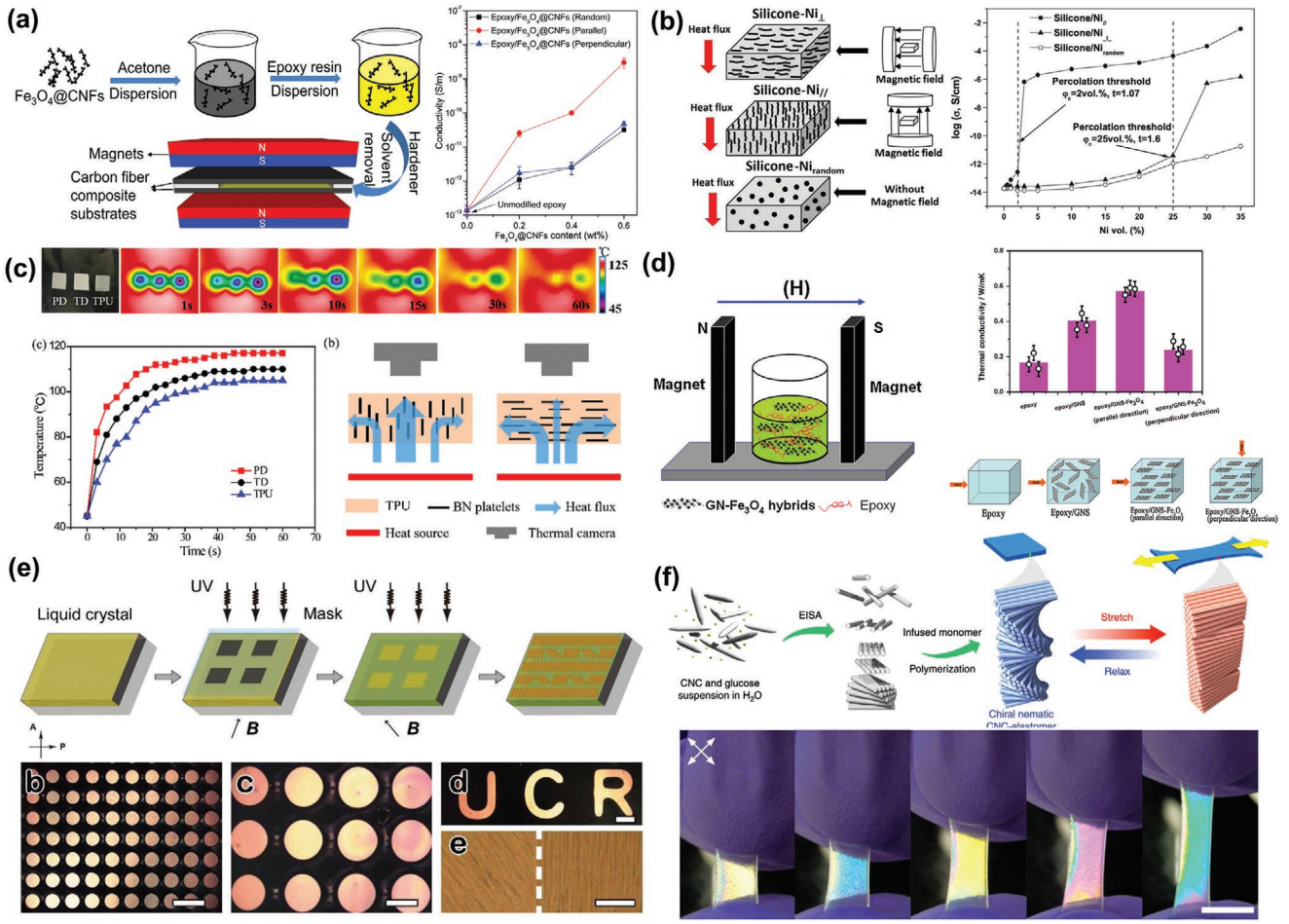

Figure 5. Magnetic aligned composite with tunable electrical, thermal, and optical properties. a) The electrical conductivity of Fe_3O_4 CNFs/epoxy composite with different volume fractions of Fe_3O_4-CNFs. Reproduced with permission.[103] Copyright 2015, Elsevier. b) Electrical conductivity of Ni/Silicone composite with different volume fractions of Ni. Reproduced with permission.[6] Copyright 2014, Elsevier. c) Thermal conductivity of aligned boron nitride/polyurethane composite. Reproduced with permission.[109b] Copyright 2019, Elsevier. d) Thermal conductivity of polyvinylidenefluoride composites with magnetic oriented carbon nanotube. Reproduced with permission.[110] Copyright 2014, Springer Nature. e) Fabrication of different polarization structures with aligned liquid crystal via lithography. Reproduced with permission.[8] Copyright 2014, American Chemical Society. f) Spiral aligned cellulose nanocrystals for stretchable optics. Reproduced with permission.[111] Copyright 2019, Springer Nature.

composite induces a significant reduction of thermal expansion and improves thermal conductivity along the alignment direction.[43,107] The measured thermal conductivity of the 9.14 vol% hBN microplates/silicone composites in the parallel and perpendicular directions to the alignment are 44.5% higher and 37.9% lower than that of unaligned composites, respectively.[107] The thermal conductivity and the thermal conductivity enhancement factor of aligned 20 wt% BNNP/epoxy composite can reach 1.07 W mK^{-1} and 463.2%, respectively.[108a] When the BN filler loading ratio was increased to 30 vol%, the thermal conductivity of aligned BN/epoxy composite measured parallel to the alignment increased to 3.445 W mK^{-1}, which is 1.96 times that of the BN/epoxy composite with randomly oriented BN fillers.[108b] Currently, both hBN/thermoplastic polyurethane (TPU) composites and BN/alumina (Al_2O_3)/polydimethylsiloxane (PDMS) composites were fabricated using advanced 3D printing technologies.[109] The thermal conductivity of aligned 35 wt% BN/ 30 wt% Al_2O_3 /PDMS composite reached 3.64 W mK^{-1}.[109a] The thermal conductivity of the 40 wt% hBN microplates/TPU composites measured parallel to the alignment is 2.8 times higher than that of samples measured perpendicular to the alignment (Figure 5c).[109b] Besides, the alignment of hBN platelets significantly affects thermal expansion (TE) of the 3D printed hBN microplates/TPU composite.[109b]

Due to low conductivity, a thermally insulating polymer matrix was formed with the random dispersion of the spherical Al_2O_3 particles. With the decoration of Fe_3O_4, Al_2O_3 particles can be aligned inside the epoxy resin under the external magnetic field. The assembled Al_2O_3 particles form direct contact with each other, enhancing the thermal conductivity of Al_2O_3/epoxy composite.[112] The Ni/silicone composite with the alignment of Ni particles displayed anisotropic thermal conductivity and diffusivity.[6] For instance, the thermal conductivity of aligned 15 vol% Ni/silicone composite was 1.8 and 2.0 times of that of the composites filled with random and perpendicular distribution of Ni particles.[6] Besides, the carbon material is one type of attractive thermal material due to its exceptional

thermal properties. For example, the thermal conductivities of graphene and carbon nanotubes are in the range of 2000–6000 and 2000–5000 W mK^{-1}, respectively.[6] The magnetic carbon nanotube (mCNT) can be prepared by coating the iron oxide or Ni particles. The thermal conductivity of the aligned mCNT/polyvinylidene fluoride composite was 1.62-fold that of the unaligned composite.[39] Graphene nanosheets (GNSs) coated with Fe_3O_4 particles were aligned in the magnetic field. The thermal conductivity of aligned GNSs/epoxy composite measured in the parallel direction was more than two times the one measured in the perpendicular direction (refer to Figure 5d).[110] The outstanding thermal properties can be achieved by controlling the alignment of thermally conductive fillers in the magnetic field. The heat transfer of the magnetically aligned composite can be further programmable for applications in numerous fields, such as fuel cells, thermoelectricity, and thermal barrier coating.[106,113]

3.3.3. Optical Properties

The magnetic-aligned photonic material displays anisotropic light propagation, scatting, and emission owing to the unique photonic architectures, such as, multi-layer structures, Bouligand structure, photonic crystals, ordered networks, etc.[114] For example, aligned photonic crystals showed splendid structural colors by modulating the refractive index for controllable light propagation.[114] The visible light can be selectively diffracted by helical structures, of which the distance of one rotation approximates the wavelength of light.[115] Besides, the jewel beetle has iridescent elytra due to the Bouligand structures made by chitin nanocrystals.[115a] The attractive color of Pollia condensata is also attributed to the Bouligand-type structure of cellulose.[115b] To mimic such intense color, cellulose nanocrystals (CNCs) were self-assembled into a chiral nematic liquid crystal with Bouligand structure-shaped arraignments that demonstrated attractive optical properties and enabled the development of mirrorless lasing and security film.[116] CNCs can be aligned vertically to generate crossed polarizer images of the fingerprint texture in the magnetic field with a strength of 10 T.[117] Furthermore, the flexible iridescent film was fabricated by assembling the CNCs in the polymer matrix, which generated a wide spectrum range of structural color from blue to red.[118] The high concentration of polymer in the composite enables multi-color domains visible at the microscopic level due to the increase of photonic bandgap.[118] Aligned CNCs with Bouligand structures in the iridescent films produced photonic structures that reflected both right and left circularly polarized light.[119]

The transmittance intensity of polarized light of the 3D-printed film can be modulated by changing the orientation of magnetic liquid crystal (LC) nanorods.[8] As shown in Figure 5e, the area with the arrangement of the LC nanorods parallel to the transmission axis of the polarizer appeared dark under the polarizing optical microscope, and the one with the arrangement of the LC nanorods oriented 45° to the transmission axis of the polarizer appeared bright.[8] Besides, with the help of a magnetic field, ellipsoidal photonic crystals were assembled into superlattices that showed striking structural color, and the displayed structural color can be changed by adjusting the sizes of the photonic crystals.[120] Also, CNCs were assembled into a helical arrangement in an elastomer matrix to mimic natural Bouligand structures, enabling stimuli-responsive stretchable optics (refer to Figure 5f).[111] The arrangement of the CNCs changed from a chiral nematic to pseudo-nematic upon stretching, inducing the color changing of the composite from white to green. This bioinspired photonic sensory mechanism facilitates flexible optics and sensors to visualize mechanical stresses and detect critical failures. Due to their tunable optical performance, the magnetically aligned photonic composites will reveal attractive prospects in numerous fields, such as light guiding, chemical sensing, responsive display, and energy harvest.[47,111,114]

3.4. Discussion

The bioinspired architectures, made with aligned magnetic fillers, show remarkable anisotropic properties and excellent property enhancement.[13] Many magnetic field-assisted 3D printing processes were developed, and functional ferromagnetic and paramagnetic fillers were aligned to reproduce bioinspired architectures (**Figure 6**a). Compared with the shear force-assisted alignment in which the alignment is only limited to the printing direction, the magnetic field-assisted 3D printing approach offers a much flexible approach to dynamic control of the alignment orientation in the 3D space.[1a] Besides, magnetic field-assisted 3D printing enables composite fabrication with complex geometric shapes and 3D filler alignment for anisotropic properties. It provides more potential opportunities to reproduce the smart materials in nature for mechanical, electrical, thermal, and optical applications.[19a,41,45] Magnetic field-assisted 3D printing process has successfully produced several natural materials with excellent mechanical properties, which are not accessible for the homogeneous composite fabricated by conventional manufacturing processes (Figure 6b).[19a,41] Furthermore, the development of magnetic field-assisted 3D printing technology provides more potential opportunities to investigate the aligned composite with tunable electrical, thermal, and optical properties.[19a,41,47,73,75,101] For example, electrically conductive fillers were assembled in the polyimide-based resin, and the electrical conductivity of the 3D-printed composite showed enhancement in the direction that are parallel to the alignment orientation (refer to Figure 6c).[102] Similarly, the thermal conductivity of polymer matrix with magnetic fillers assembled under the magnetic field showed dramatic improvement (Figure 6c).[39] Also, photonic nanocrystals assembled in the magnetic field showed intense structural color and responsive visible-light diffractions.[8,120,121]

Although the 3D-printed material with controlled magnetic filler alignment can improve material properties, there is still a big gap between the printed materials and the natural materials.[13,49] The materials fabricated by the magnetic field-assisted printing process need to be further improved to enhance their properties.[13] First, the base matrix can be extended from polymer to other kinds of material such as ceramic and metals. The interface bonding between the magnetic fillers and the base materials can be further enhanced by adding chemical bonds. Second, only limited types of magnetic

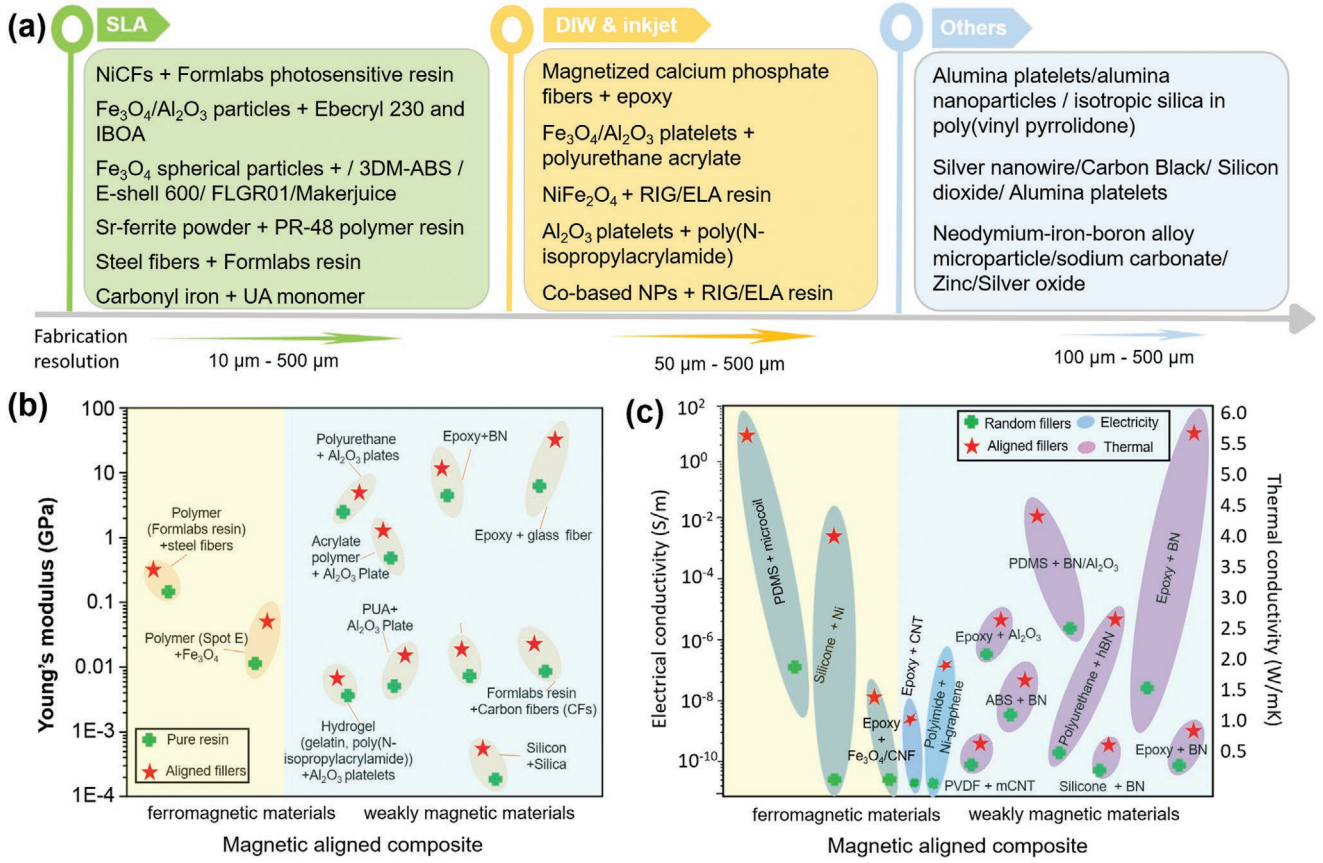

Figure 6. 3D printing of magnetic-aligned composites for properties enhancement. a) Schematic diagram showing the materials, fabrication resolution, and 3D printing processes used to fabricate magnetic-aligned composite; b) the young's modulus of magnetic composite with/without mechanical reinforcement; and c) the electrical and thermal conductivities of magnetic composite with/without alignment.

fillers were used in the current magnetic field-assisted 3D printing processes. Expanding the types of fillers can further enhance the functional properties of 3D-printed composites. The third reason for the limited enhancement of magnetic field assembly is the concentration of magnetic active fillers in the base matrix currently is relatively low to make sure the composite can be 3D printed, such as being cured by light, being extruded from the nozzle, or being spread by the blade. Future research work can be performed on the process optimization to fabricate composite architectures with a higher volume fraction of functional fillers for performance enhancement. Finally, how to disperse the magnetic fillers homogeneously in the base material matrix is another challenge in the 3D printing of magnetic aligned composite. Some research works have been done to enhance the interfacial interaction between the base matrix and the magnetic fillers by modifying fillers' surface characteristics for better dispersion. More studies are needed to better understand the dispersion of functional fillers and their alignment in magnetic fields.

In summary, magnetic field-assisted 3D printing opens intriguing perspectives for designing artificial material based on aligned magnetic fillers to enhance functional performances.[13] The tunable effect of the property is due to the morphologies and concentration of magnetic fillers in the composite. It provides an efficient manufacturing tool to fabricate novel metamaterials based on tunable properties. Considering the enabled anisotropic mechanical/electrical/thermal/optical properties of magnetic field-responsive composites, the fabrication ability of 3D printing technology will create a wide range of potential applications in aerospace engineering, electronics, biomedical engineering, biological science, and civil engineering in the future.

4. 3D Printing of Magnetic-Driven Robots

Magnetic materials have been widely used to design and fabricate various robots due to their excellent mechanical response to an external magnetic field, including magnetic force and torque. In recent years, using an external magnetic field to build robots with designed magnetizations in different areas to achieve complex and controllable motions has been a hot topic. Compared with the traditional fabrication methods, 3D printing technology provides the benefits of fabricating complex structures accurately, enabling the novel design of magnetic-driven robots. Besides, among the external power sources to drive robots remotely, including optical, acoustic, magnetic, and electrical fields, the magnetic field is regarded as the most promising source for powering robots remotely. This section will review the recent developments of

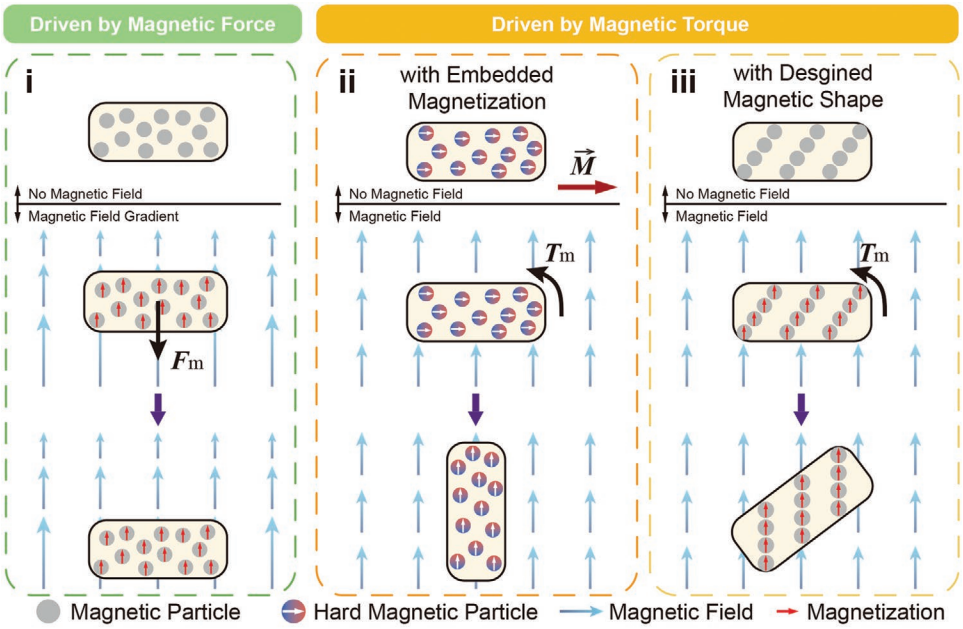

Figure 7. The mechanisms of driving methods for magnetic robots driven by magnetic force or magnetic torque.

mechanisms, materials, applications of 3D-printed magnetic-driven robots.

4.1. Mechanism of Magnetic-Driven Robots

Magnetic-driven robots, regarded as one kind of untethered and off-broad actuated robots, have obtained considerable progress in recent years. However, it remains challenging to apply the magnetic field for actuating robots precisely to realize their functions. The mechanisms of magnetic actuation should be considered when designing magnetic-driven robots. According to the basic principle of magnetic actuation, the magnetic-driven robots are classified as magnetic force-driven robots and magnetic torque-driven robots in this paper, mainly actuated by the quasi-static and periodically changing magnetic field, respectively.

For the magnetic force-driven robots, the controlled motion of a magnetic object originates from the interaction with the gradient of the magnetic field. As shown in **Figure 7**-i, the magnetic particle tends to move toward the strongest magnetic field in the field gradient direction. The principle is also applicable to the 3D-printed objects containing magnetic particles. Therefore, it is feasible to fabricate parts with 3D-printing materials filled with magnetic particles, and the actuation of 3D-printed parts can be realized with a static magnetic field. This actuating method is intuitive and effective. Either a permanent magnet or an electromagnetic coil can be applied to control the robots since the actuating method has no demand for a uniform magnetic field. The actuating force resulting from the gradient of the magnetic field (**H**) is given by:

$$\mathbf{F}_m = V(\mathbf{M}\times\nabla)\mathbf{H} \tag{1}$$

where V is the volume of the magnetic object and $\mathbf{M} = \mathbf{m}/V$ is the magnetization of the object that depends on magnetic properties. **M** is a constant if the object is permanently magnetized, which is determined by the magnetic field and its geometry in the case of a soft-magnetic object. It is convenient and straightforward to propel robots by the magnetic force since the magnetic field gradient can be generated by either permanent magnets or electromagnetic coils.

In comparison, for the magnetic torque-driven robots, the magnetic torque $\mathbf{T}_m$ results from a higher energy state (U_m) when the magnetization **M** of the object is misaligned with the applied magnetic field. For cases in which the material is surrounded by a nonmagnetic medium, $\mathbf{B} = \mu_0 \mathbf{H}$, giving

$$\mathbf{T}_m = -\frac{dU_m}{d\theta} = \mu_0 V\mathbf{M}\times\mathbf{H} \tag{2}$$

The magnetic torque can be established by two methods. The first method can result from the permanent magnetic moment (with constant **M**) within the materials according to Equation (2) (Figure 7-ii). However, for the materials without internal magnetic moment (with $\mathbf{M} = \overline{\chi}\mathbf{H}$, where $\overline{\chi}$ is the shape corrected susceptibility of the object) such as superparamagnetic particles, the required magnetic torque cannot be generated from the relationship of magnetic moment and applied magnetic field.[122] But it is still possible to generate magnetic torque through a designed magnetic shape (Figure 7-iii). The driving source can be derived and quantitatively analyzed using the same deductive methods. The detailed computation method has been reviewed before and will not be further discussed here.[122] For the two magnetic torque generation methods, the former is mainly used to fabricate morph-changing robots, while the latter is more applicable to fabricate microscale magnetic robots.

Compared with the controlled motion driven by magnetic force, the magnetic torque-driven methods can provide a more effective manipulation platform for the magnetic-driven robots

for the following reasons.[122] The soft matter system with embedded magnetization tends to deform in the magnetic field until the magnetization of each domain is collinear with the applied field. This principle can be used to design and fabricate soft shape-morphing robots (Figure 7). It can be induced from the equation that the maximum magnetic torque exists when the object's permanent magnetization is perpendicular ($\theta = 90°$) to the applied magnetic field. In magnetic robots with designed shapes, the magnetic torque is maximal when the applied field is misaligned by 45° from the designed axes of the materials.[122]

Quantitative analysis has been conducted to understand the effect of physical parameters on the magnetic actuation of ideal soft samples with programmed magnetic domains.[21c] For example, when a simple beam with residual magnetization $\mathbf{B}_r = \mu_0 \mathbf{M}$ is placed in a perpendicularly applied magnetic field $\mathbf{B}_{applied}$, the maximum deflection of the bending beam scales can be calculated as:

$$\delta_{max} \propto \frac{B_r B_{applied} L^3}{GH^2} \tag{3}$$

where G is the shear modulus of materials, L and H are the length and height of the beam, respectively. According to Equation (3), several strategies can be applied during the design and manufacturing processes to realize the robot's effective shape-morphing, including 1) the embedded magnetization M can be increased by employing magnetic materials with better properties or increasing the proportions of the magnetic fillers; 2) printing slender structures with large length-to-height ratio L/H can promote the deflection of robots; and 3) the shear modulus G can be reduced by reducing the crosslinking density of the composites.

Second, the object with an integrated magnetization will rotate under magnetic torque then keep still. To continuously propel the object, a rotating or oscillating magnetic field with a certain frequency can be applied to maintain the magnetic torque on the object. Besides actuating the rotation of magnetized objects, magnetic torque can also realize the robots' linear motion coupled with elaborate structures. The most common type of such structures is the helical swimmer. Benefited from its helical body, the rotational motion around the helical axis can be transferred into the translational motion.[123] Swimming robots driven by this method are usually fabricated at a microscale size with a small Reynolds number (<<1), making the viscous forces dominant during motion control. Thus, in such a viscous environment, comparisons between the torque-driven and force-driven methods are concerned. The propulsion matrix relating the velocity and rotational speed to the external force and torque was thoroughly studied.[124] Generally speaking, it can be concluded that the maximum velocity scales with size ($\approx R$) for the torque-driven helical swimmer but $\approx R^2$ for the force-driven equivalent swimmer.[124a] This principle indicates that the torque-driven method is more effective than the force-driven method when actuating microrobots.

Both magnetic force and magnetic torque determine the design and fabrication of magnetic-driven robots, which must be considered carefully according to different applications of magnetic-driven robots. Generally, the magnetic force has a higher efficiency of propulsion and fewer requirements on the applied actuating devices. In comparison, the magnetic torque is more attractive for its comprehensive functions and the advantages of precise control, especially for actuating shape-morphing robots and microrobots in vivo. Notably, these two actuating methods are not mutually extrusive. It is worth further investigation to combine these two methods for the diversified actuating of robots.

Magnetic propulsion raises a high requirement for robots' materials and fabrication methods since the magnetic-driven robots must maintain the magnetic properties and functional structures. It is difficult for the conventional manufacturing processes to realize magnetic-driven robots with controlled magnetic composition. Benefited from the layer-by-layer deposition, 3D printing can overcome the restrictions on processing complex structures. Moreover, various materials ranging from polymers to biocompatible hydrogels can serve as the basic printing inks integrated with magnetic materials to achieve controlled magnetic properties. Based on the mechanisms of magnetic propulsion, different 3D printing technologies can be applied to fabricate magnetic-driven robots with diverse appearances and internal compositions, which enormously expand the functions and applications of robots.

The bodies of 3D-printed magnetic-driven robots are composed of either soft or hard magnetic materials.[125] Typically, NdFeB microparticles, SPIONs,[126] Ni/Ti bilayer coatings,[127] and other magnetic materials are embedded in the robots' bodies or deposited on the body surfaces. Based on different 3D printing technologies and application scenarios, various 3D printing materials are used as the hosting matrix for the magnetic materials, including alginate,[126b] silicone,[128] SU-8,[127] polyethylene-polypropylene glycol,[126c] hydrogel,[20b] and so on.

4.2. 3D Printing of Robots Driven by Magnetic Force

The robots actuated by magnetic force have various morphologies since the propulsion of magnetic force has few limitations on robots' structures. These robots are typically composed of hybrid materials that respond to the applied magnetic field. It is crucial for the fabricated structures to maintain homogeneous magnetic loads. With the help of 3D printing technologies, robots containing different magnetic materials have been developed in the applications of drug delivery,[126c,128] bionics,[20a,129] biomedicine,[127] and so on. Due to its good printability of various composites, DIW was applied to fabricate elastomeric robots driven by magnetic force that undergo complicated reconfiguration and shape change (**Figure 8**a).[128] The soft silicone paste embedding carbonyl iron particles was directly printed in the shape of ultrasoft wavy structures, which is nearly impossible to be fabricated by the traditional manufacturing processes. Under the action of magnetic force, the "elastin-like" structures can contract easily, and the functions such as the switchable water droplet dispenser were demonstrated.[128]

Besides the DIW process, the SLA-based methods were also investigated to print hybrid materials containing magnetic particles due to their fast fabrication speed and high resolution. An artificial fish guided by magnetic force was fabricated using a microscale continuous optical printing (μCOP) system.[130]

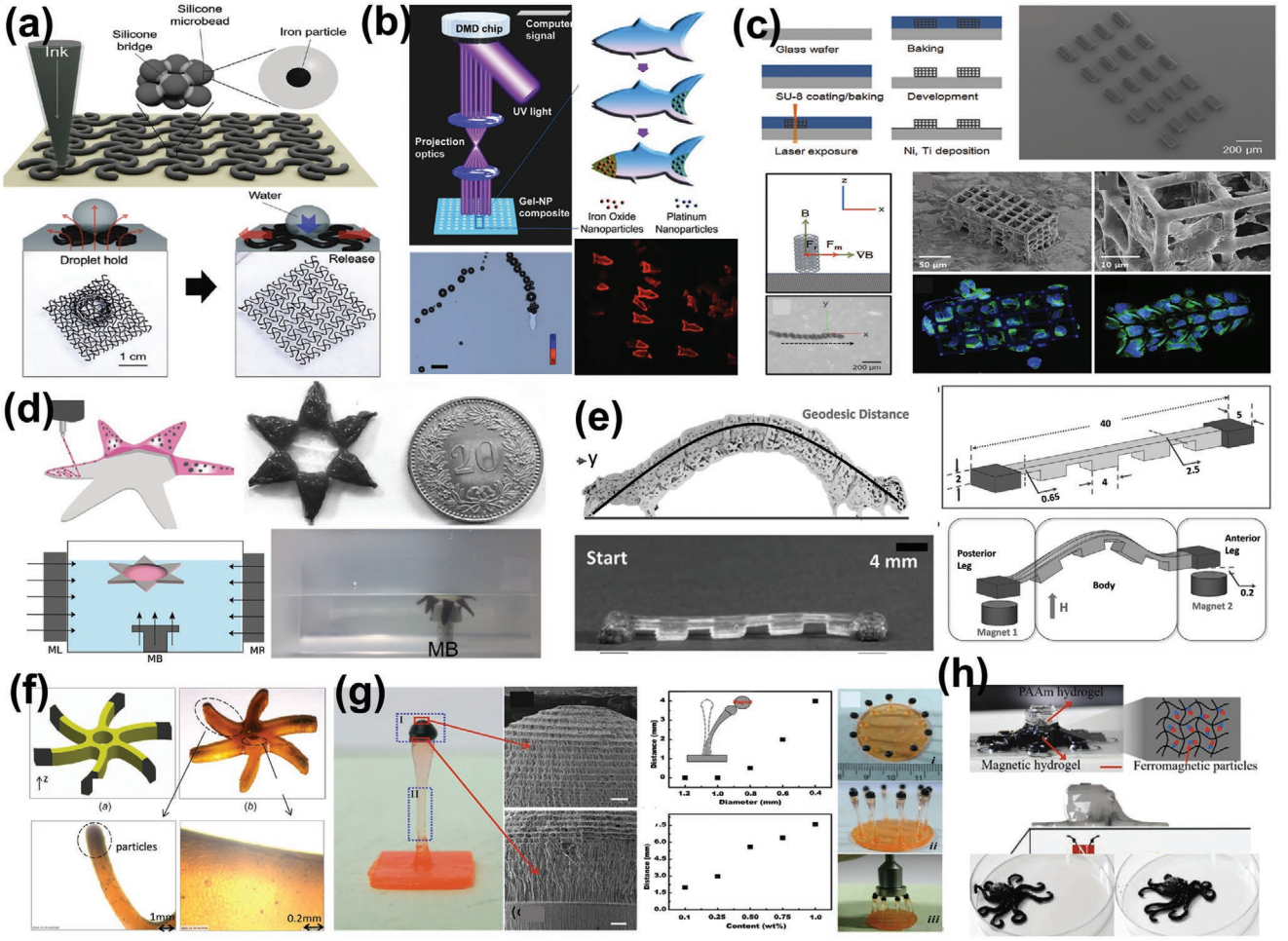

Figure 8. 3D printed magnetic robot driven by magnetic force. a) Elastomeric robots with ultrasoft wavy structures printed by DIW method. Reproduced with permission.[128] Copyright 2019, Wiley VCH. b) Artificial fish printed by high-resolution COP technology can be guided by magnetic force through embedding magnetic Fe_3O_4 nanoparticles. Scale bar, 100 μm. Reproduced with permission.[130] Copyright 2015, Wiley VCH. c) Pictures of porous micro niches for multi-cell culture and transportation. Reproduced with permission.[127] Copyright 2013, Wiley VCH. d) Starfish-inspired robots were actuated by magnetic force. Reproduced with permission.[20a] Copyright 2018, Wiley VCH. e) Inchworm-inspired robots can realize linear locomotion and leg crawling. Reproduced with permission.[129] Copyright 2019, Mary Ann Liebert. f) 3D printed impellers integrating components with different materials. Reproduced with permission.[32] Copyright 2017, American Society of Mechanical Engineers. g) Flexible grippers with embedded magnetic microparticles in the top of the bodies. Reproduced with permission.[126c] Copyright 2017, Wiley VCH. h) Soft octopus robots can move under the driving of a magnetic force. Reproduced with permission.[20b] Copyright 2019, Wiley VCH.

By changing the solutions during 3D printing, the fabricated fish contains different functional particles in the head and tail (Figure 8b). The fish head was polymerized by photocuring matrix material embedding magnetic Fe_3O_4 nanoparticles with a concentration of 5 mg mL^{-1}, which were used to guide the fish motion. Notably, the tail, encapsulated with Pt nanoparticles, enables a self-propulsion motion through the decomposition of the peroxide fuel. In another study, porous micro niches for multi-cell culture and transportation were fabricated using a TPP-based lithography process. The fabricated niches were coated with Ni/Ti bilayers (Figure 8c).[127] The inner coating of Ni can be used for magnetic actuation and the outer coating of Ti can minimize the cytotoxicity to the cells. Considering the requirements for culturing and transporting cells, such a lithography process is one of the best choices to fabricate porous microstructures due to its high resolution and great control over the geometry and porosity. It was indicated that the microrobot had good biocompatibility and cells can adhere, migrate, and proliferate in the porous structures. The 3D-printed microrobot enabled the manipulation by magnetic force since the magnetized body tended to move along the positive gradient of the magnetic field in the DI water with a low Reynolds number. This kind of magnetic-driven robot illustrated the potential of targeted cell or drug transportations for further in vivo applications.

Inspired by mollusks in nature, some biomimetic soft robots, such as the starfish-shaped robot (Figure 8d)[20a] and the inchworm-inspired robot (Figure 8e)[129] driven by magnetic force, were fabricated using 3D printing technologies. An advantage of 3D printing is its ability to build flexible materials that can mimic mollusks' bodies.[13] For the starfish-shaped robots, GelMA mixed with 40% w/v of IOPs were directly printed into

the geometry of the fins of the starfish and then crosslinked by UV exposure. The artificial starfish could realize the basic motions with the help of three electromagnets. Tetherless inchworm-inspired robots were directly printed using SLA, which could ensure linear locomotion and leg crawling. Structures with multi-material composites and locally programmed material compositions are also achievable. Magnetic particles embedded in the anterior and posterior legs had a volume loading fraction of 37.34%, which was sufficient to serve as the actuators. The leg crawling was achieved with the sequential activation of actuators using two permanent magnets. The incorporation of magnetic-responsive materials within the 3D-printed soft materials provides templates for the fabrication of bionic systems.

Compared to other fabricating methods, 3D printing can also integrate components with different materials (Figure 8f–h).[20b,32,126c] For example, in the flexible gripper made by SLA (Figure 8g), the magnetic microparticles were selectively embedded in the top of the bodies, serving as the magnetic responsive parts. As a result, the magnetic force can only impact the bodies' responsive portions to realize the precise control of the robots. The multi-material structures far exceed the conventional fabrication ability, while 3D printing offers more flexibility in selectively printing magnetic materials during the layer-based fabrication process. The integration of multiple materials in 3D-printed structures presents a promising direction for the future magnetic-driven robot development.

4.3. 3D Printing of Robots Driven by Magnetic Torque

Magnetic torque enables the orientation, reconfiguration, and manipulation of magnetic materials, attracting increasing attention in soft robots and microrobots.[131] However, the designs and fabrications of magnetic torque-drive robots present strict requirements. The mechanisms analyzed in Section 3.1 can divide magnetic torque-driven robots into two types: i) Robots with embedded magnetization, and ii) robots with designed magnetic shapes. Combined with 3D printing, both of them expand the applications of magnetic-driven robots. The following sections will discuss them in detail.

4.3.1. 3D Printing of Robots with Embedded Magnetization

Due to magnetic field-assisted 3D printing technologies, magnetically responsive materials can now have anisotropic magnetization profiles generated during the fabricating process. The magnetic-driven robots are no longer limited by homogeneous magnetic materials with uniformly mixed magnetic microparticles. Unlike the 3D printing methods used to fabricate the magnetic force-driven robots, an external magnetic field is now required to regulate magnetization orientations inside robotic bodies during the 3D printing process. Hence robots with programmed magnetization can be actuated by magnetic torque and reconfigured to adapt to various situations.

Many outstanding studies focusing on 3D-printed robots with embedded magnetization have been reported. Notably, Zhao et al.[21a] demonstrated the application of programmed magnetic domains printed using DIW, as shown in **Figure 9**a. An electromagnetic coil was placed around the printing nozzle to generate a uniform magnetic field along the flow direction of the ink. The magnetization of the magnetic ink can be modified by switching the printing path or external magnetic field. This improved DIW configuration provides a universal model for programming magnetizations of robots. The magnetic ink was prepared first by mixing the 20 vol% NdFeB microparticles and silicone-based materials. The ink was then magnetized under a strong magnetic field (≈2.7 T). This ink preparation sequence improved the printability of the composite ink since its yield stress prevented the dispersed magnetized particles from aggregation.[21a] Support ink extruded from another nozzle buttressed the adjacent magnetic ink during printing and 3D structures were constructed layer-by-layer. The 3D-printed structures with programmed magnetizations provided a fast and fully reversible folding process.

Furthermore, guided by the model-based prediction, complex 3D structures with negative Poisson's ratios were designed and fabricated to exhibit shrinkage in both length and width actuated by a magnetic field. The proposed method can be extended to create various soft robots with untethered and fast shape-shifting. Zhao et al. fabricated a ferromagnetic soft continuum robot using the same process (Figure 9b).[69b] The robot's body was composed of soft polymer matrices with embedded hard magnetic microparticles (NdFeB). The outer surface of the robot was covered with hydrogel skin to decrease the surface friction. Controlled by magnetic torque, the continuum robot could navigate through complex and constrained environments, providing an option for minimally invasive robotic surgery in inaccessible lesions like the tortuous cerebrovascular phantom. However, this method was limited by the constant magnetization, and the lack of flexibility in the embedded magnetization density and direction.[69a]

Inspired by origami, a shape-morphing microrobot with encoded magnetization was proposed (Figure 9c).[19b] To fabricate its microscale body, electron beam lithography was used to produce nanomagnets, followed by coatings of thin cobalt films. Since varying aspect ratios of nanomagnets led to different coercive fields, the same microrobot could be programmed with different magnetic configurations through specific arrangements of nanomagnets and consequent magnetization fields. As a result, the magnetic moment can be tuned by modifying the orientations and ratios of different nanomagnet types. An origami-like microscale "bird" with controlled flying modes was designed to demonstrate folding behaviors such as bending and twisting. The proposed magnetic-driven robots based on encoded nanomagnet arrays were tunable in terms of the magnetic configurations, which provided an excellent template for further study of shape-morphing robots.

Another research improved the magnetic-field-assisted DIW to expand the tunability of magnetization by applying voxel-encoding printing (Figure 9d).[69a] Each voxel consisting of hard-magnetic microparticles and silicone-based matrix was considered as the basic element to encode. For the voxel with three layers, the total number of effective magnetization variations can be up to 7. Consequently, the density and direction of magnetization for the entire body can be programmed according to the vector summation of each voxel. Moreover, the

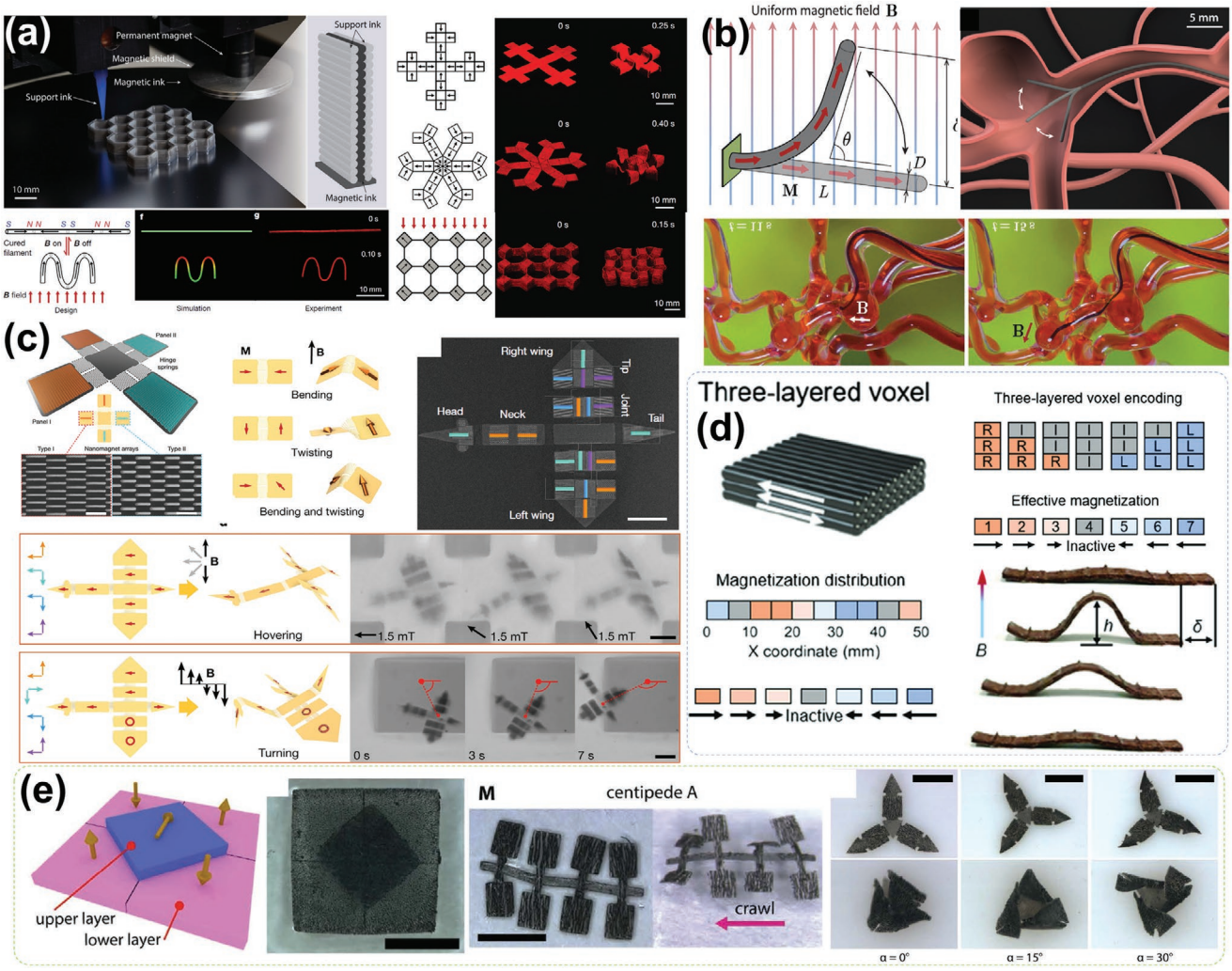

Figure 9. 3D printed magnetic robot with embedded magnetization. a) Robots with programmed magnetizations printed by DIW method using NdFeB particles. Reproduced with permission.[21a] Copyright 2018, Springer Nature. b) Soft continuum robots can navigate through complicated environments. Reproduced with permission.[69b] Copyright 2019, American Association for the Advancement of Science. c) Origami-like micro robots based on encoding nanomagnet arrays. Reproduced with permission.[19b] Copyright 2019, Springer Nature. d) Three-layered voxel expanding the tunability of magnetization for biomimetic robots. Reproduced with permission.[69a] Copyright 2020, Wiley VCH. e) Pictures of different planar magnetic robots with discrete 3D magnetizations printed via SLA-based method. Reproduced with permission.[21b] Copyright 2019, American Association for the Advancement of Science.

evolutionary algorithm was utilized to achieve the most suitable design of magnetization distributions based on the desired shape of deformation. For example, to mimic the crawling motion of the inchworm, the shape of the inchworm body was set as the target shape in the evolutionary algorithm. Following that, the optimum solution of magnetization distribution was obtained, which helped mimic the actual crawling motion of an inchworm successfully. The voxel-encoding method significantly improved the tunability of magnetization in terms of density and direction. The excellent magnetic property tunability will promote the production of magnetic-driven robots with more precise shape-morphing, broadening the application potentials of biomimetic robots in the future.

Besides the aforementioned methods, other 3D printing technologies such as SLA were also developed to arrange the magnetization in the printed structures. For example, an ultraviolet (UV) lithography-based method was reported to encode 3D magnetization,[21b] as shown in Figure 9e. Compared to other 3D printing technologies, the reported UV lithography device could program both horizontal and vertical magnetization in the soft materials by adding a 2-DOF motorized permanent magnet below the curing tank. As a result, the discrete 3D magnetization could promote the performance of magnetic actuators and bring more novel robot designs. The precise and multidimensional programming of embedded magnetization endues robots with much more functions. Such capability will be attractive to the field of magnetic-driven robots, especially the design of shape-morphing robots.

4.3.2. 3D Printing of Robots with Designed Magnetic Shapes

The most conspicuous characteristic of the magnetic-driven robot with designed magnetic shapes is the helical structures.

In the microrobots with helical structures, the applied rotating magnetic field induces the robots' rotation around their helical axes, generating a translational movement. This mode of movement is similar to the motion of bacteria that swims by rotating their flagella. The movement driven by magnetic torque maintains a high efficiency only when the robot size is small enough.[124a] Hence the small-size requirement raises a challenge in fabricating micrometer-scale robots with high accuracies. Benefited from the breakthrough of high-accuracy 3D printing technologies like the TPP process, microrobots with designed magnetic shapes can be fabricated through 3D printing, which significantly lower the barriers of applying the magnetic-driven robots in the biomedical and environmental fields.

One efficient and mature method to fabricate helical microrobots is 3D direct laser writing (DLW), which was proposed by Nelson's group.[132] As a micro and nanoscale fabrication process developed from TPP, DLW has become a versatile and routine tool for precise batch fabrication of complex structures.[131a] As shown in **Figure 10**a, a micro helical structure was produced with a negative photoresist deposited on a substrate by DLW. Subsequently, a thin film of Ni/Ti bilayers was deposited on the surface by electron beam evaporation for magnetic actuation and excellent biocompatibility.[133] The magnetic shape anisotropy effect of a helical robot was explored and plotted by showing the misalignment angle α and helix angle θ. It can be concluded that helical robots with larger helix angles tend to be perpendicular to the direction of the external field.

Some other delicately designed structures were proposed based on the blueprint of helical swimmers,[55b,137] like the syringe-like microtransporter (Figure 10b). This wirelessly controlled robot was designed based on Archimedes screw pumping mechanism. The integrated structure containing two parts, that is, a magnetically driven screw and a hollow cylinder, could move relative to each other under the magnetic field and was manufactured without further assembly. This delicate micro-transporter enables the collection, encapsulation, transportation, and release of microbeads or cells,[55b] which benefits many complicated tasks such as precise drug delivery or diagnostic analysis. Due to the micrometer size of helical swimmers, many trials of in vivo manipulations were demonstrated with impressive results. For example, helical swimmers to monitor the targeted delivery in the body were coupled with NIR-797 isothiocyanate, whose fluorescent signal in the near-infrared (NIR) spectral region could be tracked by optical microscopy (Figure 10c).[132b] The microswimmer was also shown to catch and carry sperms to deliver them to the oocyte for fertilization (Figure 10d).[134] This investigation represents significant progress of accurate control of 3D-printed helical swimmers in the field of microsurgery. It was also reported that helical swimmers could be functionally decorated with lipoplexes containing pDNA (Figure 10e).[135] In this work, the targeted single-cell gene was delivered to human embryonic kidney cells based on the magnetic actuation. The examples mentioned above present the great potential of helical swimmers for in vivo manipulations.

Besides physical vapor deposition, an alternative method to include magnetic shape anisotropy into the helical structure was proposed by embedding superparamagnetic nanoparticles into polymers before the DLW curing process.[23] The superparamagnetic magnetite nanoparticles were dispersed in the photoresist before the printing process. Different from the deposited magnetic layers, the dispersion of aligned magnetic nanoparticles helped set the magnetization axis in the printing process to improve the performance of locomotion.[23,138] The helical structures were printed using a SU-8 negative photoresist with the dispersion of superparamagnetic magnetite nanoparticles (Figure 10f).[23] A uniform magnetic field (≈30 mT) was applied to assemble these nanoparticles in a filamentous structure owing to dipole-dipole magnetic attraction between them.[139] The alignment of particles inside the helical body defined the magnetization axis, enabling the superparamagnetic helical robots with programmed magnetic anisotropy. Due to a large variety of magnetic particles that can be used in the printing process, the functions of 3D-printed objects are enriched, and the biodegradation of microrobots becomes possible. For example, the helical swimmers composed of GelMA and core-shell magnetoelectric nanoparticles (MENPs) were fabricated to be a highly integrated device (Figure 10g).[136] The degradative swimmers were also used to electro-stimulate neuronal cells since MENPs can induce neuronal differentiation of the targeted cells. The microrobots' bodies would degrade after a period bringing few influences on the cell growth. The 3D-printed biodegradable microrobots coupled with embedded functional magnetic nanoparticles provide a promising strategy for controllable drug delivery and disease diagnosis.

4.4. Discussion

Figure 11 shows a comparison of different magnetic-driven robots with related properties. The main challenges for developing magnetic-driven robots lie in the fabrication of complicated multiscale structures with embedded magnetic materials. Benefited from emerging 3D printing technologies such as TPP, MIP-SL, and DIW, it becomes possible to fabricate robots with complex and customized geometry ranging from microscale to macroscale features. Also, a wide variety of 3D printable materials (refer to Figure 11a) enable the flexible integration of diverse magnetic materials in a magnetic-driven robot, laying the foundation for better control of the robot's internal magnetization.

According to the actuating methods, the magnetic-driven robots can be divided into robots driven by magnetic force and magnetic torque. Both maintain diversified shapes and functions. Common 3D printing devices can fabricate magnetic force-driven robots, and the performance under the magnetic force mainly depends on the proportions of magnetic materials. Generally, a larger robot size will lead to a higher proportion of embedded magnetic materials (Figure 11b). The highest proportion of magnetic materials reported (by weight) is around 50 wt% limited by the pastes' viscosity, which raises the requirement of improving magnetic printing processes and materials. For the magnetic torque-driven robots, magnetic field-assisted high-resolution 3D printing is needed depending on robots' size. For instance, with an applied magnetic field around the nozzle, the DIW method can print structures with different magnetizations by tuning the magnetic field direction and the

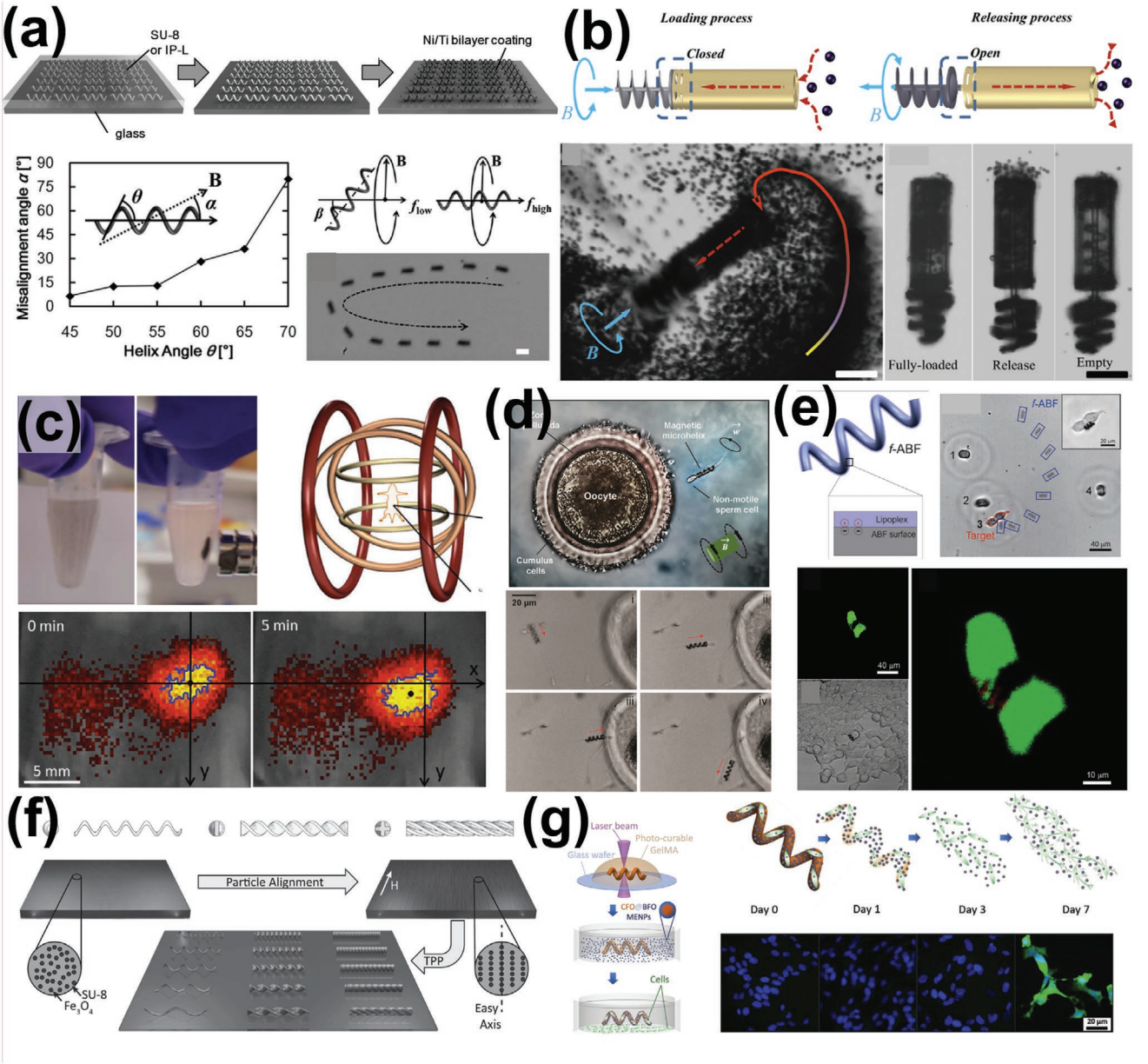

Figure 10. 3D-printed magnetic robots with designed magnetic shapes (organized papers by manufacturing processes and shapes). a) Microscale helical robots printed by DLW with a thin film of Ni/Ti bilayers deposited on the surface. Reproduced with permission.[133] Copyright 2012, Wiley VCH. b) Syringe-like microtransporters for drug delivery or diagnostic analysis. Reproduced with permission.[55b] Copyright 2015, Wiley VCH. c) Helical swimmers whose fluorescent signals could be tracked by optical microscopy. Reproduced with permission.[132b] Copyright 2015, Wiley VCH. d) Micro swimmers designed for fertilization. Reproduced with permission.[134] Copyright 2015, American Chemical Society. e) Helical swimmers decorated with lipoplexes containing pDNA. Reproduced with permission.[135] Copyright 2015, Wiley VCH. f) Helical structures produced by DLW embedding aligned superparamagnetic nanoparticles. Reproduced with permission.[23] Copyright 2014, Wiley VCH. g) Biodegradable swimmers composed of magneto-electric nanoparticles could induce neuronal differentiation. Reproduced with permission.[136] Copyright 2020, Wiley VCH.

moving path.[21a] The SLA method was employed to print 2D soft robots with 3D magnetizations under a magnetic field in the curing plane generated by a 2-DOF motorized permanent magnet.[21b] Micro swimming robots with designed magnetic shapes can be fabricated by DLW followed by physical vapor deposition of magnetic films.[133] In this situation, robots' moving velocity is a primary concern for the researchers. As shown in Figure 11c, robots share a similar movement efficiency since the ratio between velocity and size is close to 1. Hence, how to improve the velocity of magnetic torque-driven robots is still a challenge. Moreover, limited by fluid dynamics, the microscale robots developed so far are mainly helical swimmers. They are less functional and flexible than the morphing-changing robots with programmed magnetizations.

There is still much progress needed in 3D printing magnetic-driven robots to realize their unique advantages for

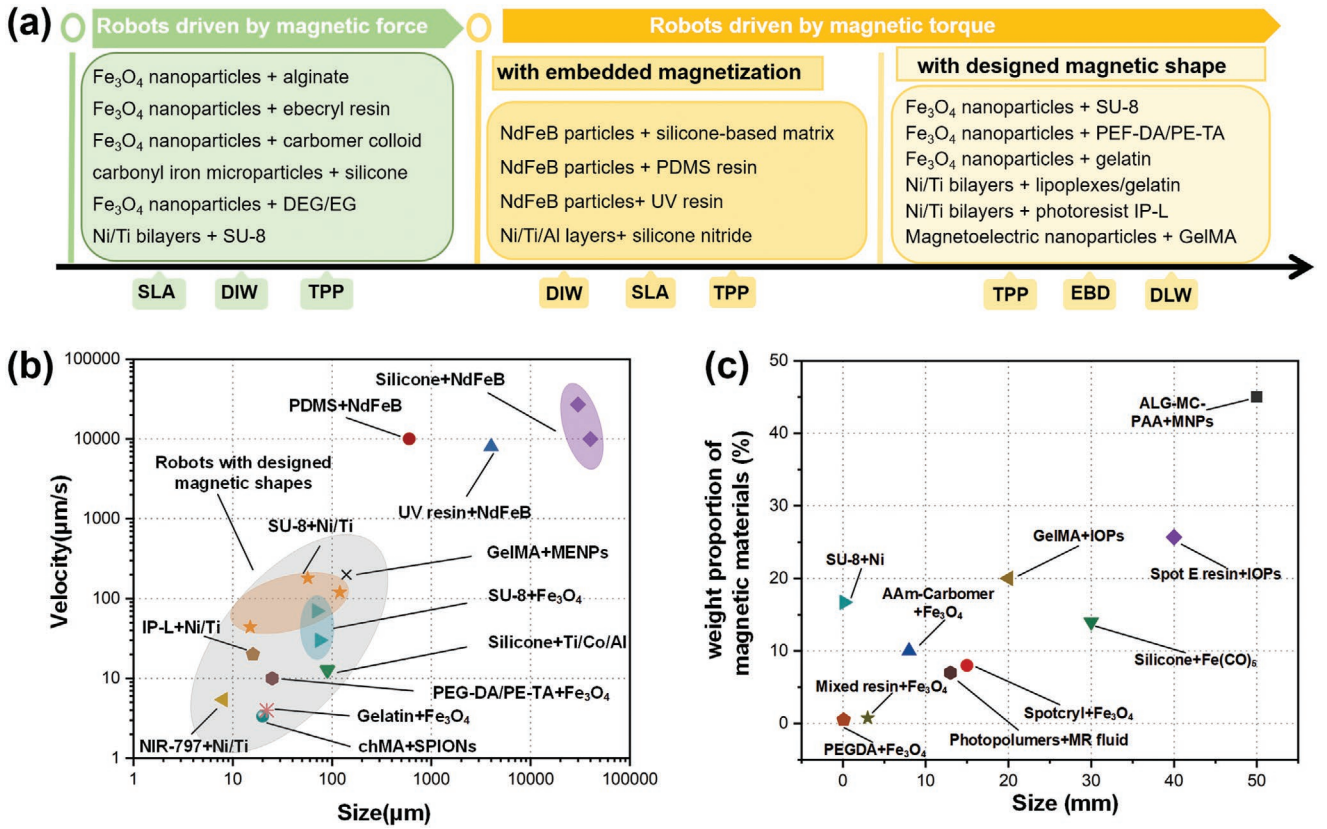

Figure 11. Comparison of various 3D printing magnetic-driven robots. a) Schematic diagram showing the 3D printing technologies, materials, and printing resolutions applied to produce magnetic-driven robots; b) the weight proportion of magnetic materials of force-driven robots with different sizes; and c) the moving velocities of magnetic torque-driven robots with different sizes.

applications in practice. First, there is no 3D printing process to produce structures with complex 3D magnetization, mainly due to the lack of further research on the preparation, regulation, and printing process of magnetic inks. Second, a primary method to improve the performance of magnetic robots is to increase the proportion of magnetic materials. However, the increase of magnetic particles inside the composites will raise the printing difficulty resulting from particle-induced absorption or changing of rheological properties. Moreover, the increased proportion of magnetic materials will reduce the flexibility of robots, which reduces the performance of robots. Hence, the base matrix polymer needs to be optimized for better printability and performance. Finally, the design of magnetic robot structures with maximum performance is another challenge. Research on the prediction of the motion of magnetic robots has emerged. We expect a complete analytical model to be established and perfected to understand the relationship between materials, structures, and performance in the future.

5. 3D Printing of Magnetic Components in Electronics

Besides mechanical property as shown in the reinforced structures and robotic actuation, magnetic materials provide features of interest to electromagnetic devices. Various magnetic components of soft and hard magnetic materials can be efficiently manufactured using 3D printing technology.[31,140] Specific fabrication processes such as the magnetic-field-assisted and laser-sintering-assisted methods were utilized to print components with performance comparable with commercial counterparts.[66,141] Moreover, 3D printing has noticeable advantages in fabricating miniaturized and flexible components with complex structures and multimaterials,[24,142] making it possible to integrate efficient magnetic components into miniaturized devices, flexible electronics, and sensors. This section will review basic principles, recent 3D printing developments, and novel applications of magnetic components in electronics.

5.1. Principle and Mechanism of Magnetic Components in Electronics

Fundamental principles of magnetic components in electronics originate from Faraday's law of induction, that is, electrical energy can be generated by changing magnetic flux through a coil, as shown in Equation (4).

$$\varepsilon = \frac{\Delta \Phi_B}{\Delta t} = \frac{\Delta \int B dA}{\Delta t} \quad (4)$$

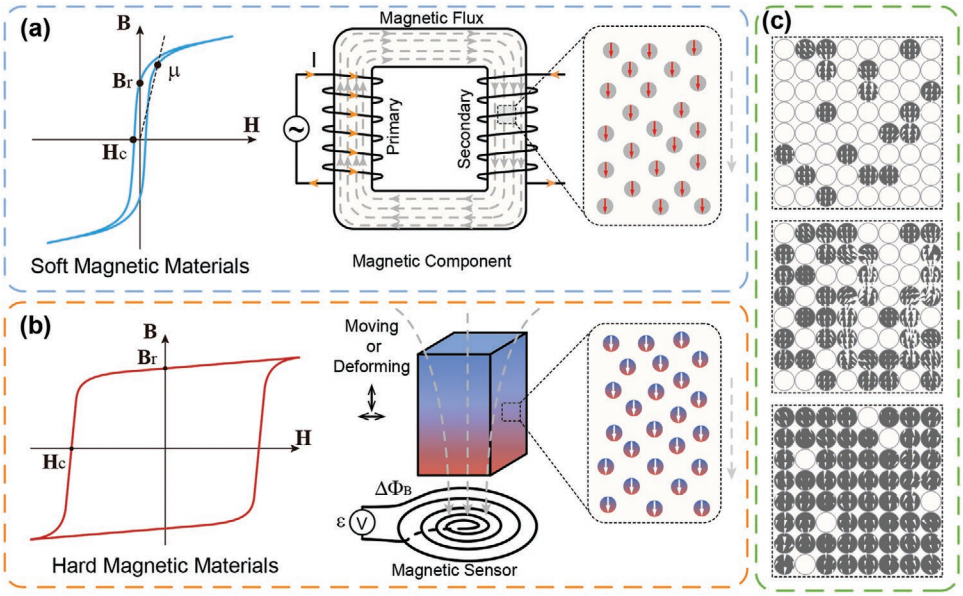

Figure 12. Schematic of typical magnetization and working mechanism of a) soft and b) hard magnetic materials and electronics components. c) Magnetic path and ratio of magnetic particles of composite materials under an external magnetic field applied from top to bottom. Reproduced with permission.[146] Copyright 2003, Elsevier.

The utilization of magnetic materials can concentrate and increase the magnetic flux to maximize the energy transmission efficiency, such as transformer core and electromagnetic shield layers for wireless power transfer (WPT) systems. These devices require a soft magnetic core to achieve high power densities. Another application of magnetic materials is to generate a static magnetic field. The electrical energy can be induced through relative motion between hard magnets and coils. This concept of energy conversion is widely used for 3D-printed magnetic sensors.[143]

Several key magnetic parameters for magnetic materials are important descriptors. The relative magnetic permeability is defined as $\mu_r = B/(\mu_0 H)$, where $\mu_0 = 4\pi \times 10^{-7}$ NAm^2 corresponds to the magnetic permeability of the free space, B is the magnetic flux density, and H is the magnetic field. μ_r is not a constant, as it varies with process parameters, including frequency of magnetic field, domain wall motion, eddy current losses, and rotation of magnetic moments.[31] Saturation magnetization (B_s) is the sample's maximum magnetization. The magnetic remanence (B_r) represents the ability of maintaining magnetization after the external magnetic field is removed. The coercive field (H_c) is the field strength required in the opposing direction to remove the sample's magnetization. H_c is also the parameter that distinguishes hard ($H_c > 1000$ Am^{-1}) and soft ($H_c \leq 1000$ Am^{-1}) magnetic materials. All these parameters can be extracted from the magnetization curve shown in **Figure 12**.

Low coercivity, high saturation magnetizations, and high permeability are three ideal relevant parameters of soft magnetic components. The increase of energy conversion efficiency through employing soft magnetic components is important for modern society (Figure 12a). However, the soft magnetic core becomes a place of inducing energy loss, especially when working frequency increases.[144] One such source is the hysteretic loss associated with dissipative effects in rate-dependent hysteresis. After every full completion of the magnetization process, the magnet will cause energy lost equal to the area inside the curve. Therefore, the increase of frequency can contribute to a massive loss, even for materials with low coercivity. The second source is the eddy current loss caused by the electrical current inside magnetic components generated by the alternative magnetic field. Thus, magnetic materials with low resistivity can be lossy in a time-varying magnetic field. As operating frequency increases, power losses from eddy currents become a dominant source of energy loss.[10] Several methods to tackle this challenge include adding insulating materials to isolate magnetic particles, employing laminated sheet stacks to reduce skin effect, and utilizing soft magnetic materials with high resistivity.[51b,145]

3D printing technology provides a fast manufacturing method to build soft magnetic components with complex structures and multiple materials. The additives in the 3D printing process can reduce the total hysteretic loss in high-frequency applications. The reduction does not come without a cost, as magnetic permeability is sacrificed because the flux has to cross the insulating gaps between magnetic particles,[31] as shown in Figure 12c. The additive content currently used in most 3D printing processes is usually polymers, which is still higher than adequate for a component with appropriate magnetic performance. Thus, 3D printing must bring solutions to provide competitive magnetic properties in a rapid integrated fabricating process. For hard magnetic materials, the properties of 3D-printed hard magnets are not strong enough due to the additives. However, the printed hard magnetic components can be imparted with flexibility and complex structures, making them competent as magnetic sensors (Figure 12b). Manufacturing of multi-materials, such as magnetic materials and conductive materials, or hard magnetic materials and soft magnetic materials, can also be realized through 3D printing

processes to achieve the integration, optimization, and miniaturization of electronics.

The selection of magnetic materials and 3D printing processes ultimately depends on the design requirements of magnetic components in electronic devices. The magnetic properties of 3D-printed components are mainly influenced by three factors: i) Materials selection, ii) structures in both micro and macro scales, and iii) volumetric fraction of magnetic materials. Most materials for 3D-printed magnetic components are iron-rich materials, including various *Fe*-based particles and alloys. Soft magnet components with requirements on concentrating magnetic flux, such as transformers, inductors, and shields, are fabricated with typical soft magnetic materials like ferrite, iron oxide, Fe-Si alloys, etc. Materials with inherent high resistivity are used for high-frequency applications to minimize eddy current loss, while materials with low resistivity are used for low-frequency applications. However, for 3D printing processes that need polymer additives, the insulating additive matrix allows high-frequency applications using low resistivity materials because it eliminates the current paths. 3D printing of multi-materials also provides a potential solution to reduce eddy current loss by integrating magnetic materials and insulating materials.[3] For hard magnetic components with inherent magnetization, such as magnetic sensors and permanent magnets, hard magnetic materials are commonly used due to their high remanence and intrinsic coercivity, including Alnico, SmCo alloys, and NdFeB alloys. Efforts on 3D printing research are mainly concentrated on NdFeB due to its highest magnetic strength at room temperature.

Particle size and orientation are the main factors in microscale structures that affect magnetic properties. Larger particle sizes can increase magnetic properties for the resultant smaller number of non-magnetic discontinuities.[147] Due to the shape anisotropy of magnetic particles, the orientation of particles or grains during printing was proved to be effective in improving magnetic properties.[66,148] The macroscale geometric shapes of magnetic components can also affect the performance. With the help of 3D printing, components with optimized structures, typically complex shapes, can be fabricated to realize better properties in magnetism, flexibility, and mechanical strength.[19c,143,149] Moreover, further increasing the volumetric fractions of magnetic materials leads to improved magnetic properties since magnetic materials are the key functional materials in 3D-printed components.

5.2. 3D Printing of Soft Magnetic Components for Transformers

Soft magnetic components are a type of electric device that can be employed to concentrate magnetic flux when subjected to a static or time-varying magnetic field, such as transformer, antenna, and magnetic shields. Soft magnetic materials can be easily magnetized and demagnetized. Consequently, small energy losses for each cycle of magnetization are indispensable for these applications. Geometric shape is an important factor that affects the performance of a magnetic transformer.[150] 3D printing provides excellent flexibility on the design and fabrication of soft magnetic components with complex structures, which opens the possibility to improve their performance. For example, an efficient transformer structure of toroidal geometry was fabricated using the FDM process by Bollig et al. (**Figure 13**a).[149] Magnetic filament consisting of polylactic acid (PLA) polymer matrix and 40 wt% iron particulate phase was employed to achieve magnetic properties. For the developed FDM-based method, the performance of the 3D-printed transformer core can be increased by utilizing high fill factors and iron contents. The internal pattern of filaments did not appear to affect the performance of the 3D-printed core. However, the magnetic susceptibility of the FDM-printed transformer displayed a surprising improvement when the infill orientation parallel with the applied field due to the absence of air gaps between adjacent printed filaments (Figure 13b).[151] The results exhibit a potential method to tune the magnetic properties of soft magnetic components via the extrusion-based 3D printing processes. Moreover, to further increase the loading of magnetic particles, a printable aqueous magnetic suspension of ≈81 wt% IOPs was developed for DIW.[152] An additive was employed to provide electrostatic and steric repulsion to maintain the rheological properties for printability and to stabilize the suspension of IOPs at its highest loading through the minimum use of a single additive. The printed inks exhibited nearly no deterioration of magnetic behavior than the pure IOPs samples (Figure 13c).

Besides printing parameters, post-processing has been studied for increasing components' performance. A high temperature (950 °C) pressure-less sintered NiZn paste was developed for fabricating high-performance magnetic cores via the DIW process (Figure 13d).[153] Methyacrylamide and *N*,*N*'-methylenebisacrylamide were used as the matrix material, and NiZn ferrite powder was employed as the magnetic filler. Before the printing process, small amounts of dispersant and plasticizer were added to achieve desired particle dispersion and flowability. The characterization of the pressure-less sintered core indicated that the core-loss density of the printed core was around 50% lower than that of the commercial transformer with permeability at 5 MHz.

For transformers in high-frequency applications, soft magnetic alloys, such as FeSi alloys, are also a good choice for their excellent magnetic performance, such as high magnetic saturation, high permeability, and low coercivity. In the conventional manufacturing process, the silicon steels are manufactured into laminations and then stacked to form the laminated cores of transformers with insulation materials between each layer to lower the eddy current loss resulting from high-frequency and low resistivity. Through SLM of multi-alloys, the complex processing can be integrated into one step.[3] To reduce eddy current loss, 3D printing technologies were used to fabricate efficient magnetic cores by taking advantage of their ability to manufacture topology structures and multiple materials (Figure 13e). Layers of FeSi6.7 alloy (thickness at 600 μm) with good magnetic performance and layers of FeAl16 alloy layers (thickness at 140 μm) with high resistivity were alternately fabricated using a SLM machine that had two process chambers containing different materials. The alternating layers of two materials replicated the layered structure of laminated stacks. The slits of the topology structures also guaranteed electrical insulation in the remaining direction. Combining these two strategies, the loss amount reduced to 28% of the layered structure, or 7% of the sample without layers.

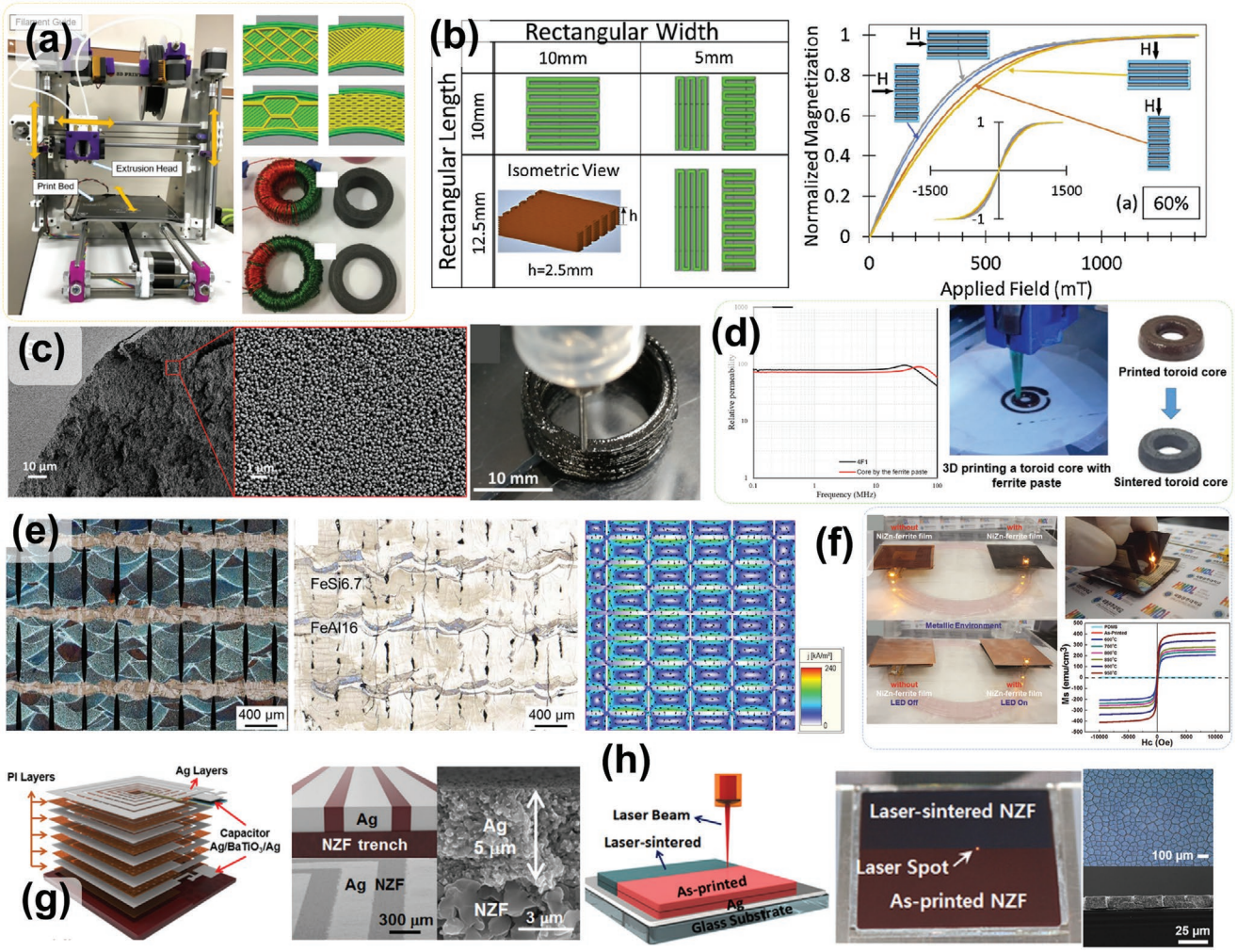

Figure 13. 3D printing of soft magnetic components. a) Different transformer cores with different filling patterns, percent fill, and structures printed by a FDM printer. Reproduced with permission.[149] Copyright 2017, Elsevier. b) Normalized magnetization versus applied field for rectangular samples printed with non-equivalent aspect ratios for 60% infill percentage via FDM. Reproduced with permission.[151] Copyright 2019, Elsevier. c) 3D printing of thin-walled toroidal magnetic core using the suspension of highly loaded IOPs by DIW. Reproduced with permission.[152] Copyright 2018, American Chemical Society. d) Relative permeability versus frequency of a core printed by NiZn ferrite paste and a commercial 4F1 core. Reproduced with permission.[153] Copyright 2018, IEEE. e) Design, prototype, and simulation of a SLM-printed sample using combined strategies of alternating materials and slits structures. Reproduced with permission.[3] Copyright 2019, Elsevier. f) A NZF film manufactured by IJP and the sintering process shows good performance of the flexible WPT near metallic components. Reproduced with permission.[24] Copyright 2017, Wiley VCH. g) Magnetic 3D trench structure and the built-in coils of multiple PI/Ag bilayers are printed via IJP to reduce resistance. Reproduced with permission.[19c] Copyright 2019, Elsevier. h) Schematic of a laser-assisted 3D printing technology and a picture of the laser-sintered NZF film surface. Reproduced with permission.[141] Copyright 2018, Elsevier.

Soft magnetic components in flexible electronics also received numerous attentions for their ability to increase efficiency in transferring electromagnetic energy. For flexible electronics applications, a sufficiently thin geometrical form of the magnetic layer is required to minimize the strain for a given bending radius due to the linear relationship between bending-induced strain and thickness.[154] Therefore, a flexible NiZn-ferrite (NZF) ceramic film working as a magnetic substrate for WPT can be achieved by a thin film 3D printing technique using IJP.[24] The flexibility of the film was imparted by embedding it into PDMS. The magnetize saturation was improved to a high value of 412 emu cc^{-1} after sintering in 950 °C compared to the as-printed film (≈200 emu cc^{-1}) due to the increasing packing density. The fabricated ferrite layers with the thickness from 5 to 25 μm were proved with excellent flexibility and mechanical robustness through a bending test with a 10 mm bending radius. The printed magnetic film also maintained good WPT performance in a conductive environment under compressive or tensile stress conditions (Figure 13f). Moreover, a 3D NZF trench structure with the spiral coil was fabricated by the IJP process to achieve a high-aspect-ratio coil.[19c] With the multi-material printing ability, the IJP process was also employed to build both the magnetic 3D trench structure and the built-in coils with multiple PI/Ag bilayers (Figure 13g). The coils' WPT efficiency in 3D magnetic structures (≈34%) improved by more than 100% at a zero-gap compared to the 2D

coils (≈15%) due to the reduction of resistance. However, the processes of NZF materials mentioned above require sintering in a high-temperature furnace. To evade this high-cost and time-consuming process, 3D printing based on laser-assisted sintering was explored as an alternative method.[141] Microcracks on the film surface induced by laser sintering were used to impart flexibility (Figure 13h). The 3D-printed receiving coils kept a competitive WPT efficiency value of 22%. The control of microcracks during the laser sintering process presents an option to improve the flexibility of 3D-printed magnetic films.

5.3. 3D Printing of Hard Magnetic Components for Sensors

An electromagnetic sensor is a device that converts changes in the magnetic properties of sensitive components induced by magnetic fields, currents, stresses, strains, temperatures, and light into electrical signals and detects the corresponding physical quantities accordingly. Such sensors are widely used in infrastructure health monitoring and damage detection.[155] Magnetic materials are the core components of an electromagnetic sensor. Their development is essential and indispensable for improving the efficiency and performance of devices in electric power generation, conditioning, conversion, transportation, and other energy-use sectors of the economy.[156] Conventional magnet manufacturing is a significant bottleneck in developing magnet-based products because of the long lead times required for every design adaption and production step.

3D printing of magnetic components delivers the opportunity to shift to agile and test-driven development in early prototyping stages, as well as new possibilities for complex designs.[157] For example, Li et al.[54a] developed a big area 3D printing of high-performance bonded NdFeB magnets based on a nozzle deposition process as shown in **Figure 14**a. The fabricated isotropic near-net-shape NdFeB bonded magnets with magnetic and mechanical properties comparable to or even better than traditional injection molded magnets. The starting polymer magnet composite pellets consist of 65 vol% isotropic NdFeB powder and 35 vol% polyamides (Nylon-12). The density of the 3D-printed magnet product reached 4.8 g/cm^3, and the magnetic properties at room temperature were intrinsic coercivity H_{ci} = 688.4 kA/m, remanence B_r = 0.51 T, and energy product (BH)max = 43.49 kJ m^{-3} (5.47 MGOe). Also, tensile yielded an average ultimate tensile strength of 6.60 MPa and an average failure strain of 4.18%. The present process significantly simplifies the manufacturing of near-net-shape bonded magnets. Huber et al.[54b] also presented a method to 3D print polymer-bonded isotropic hard magnets with a low-cost, end-user 3D printer based on the extrusion process (Figure 14b). The presented fabrication method using dual extruder was used to print magnets composed of locally different polymer matrix materials and different magnetic powders ranging from soft magnetic alloys to hard magnetic NdFeB or ferrite alloys. Commercially available isotropic NdFeB powder inside a PA11 matrix was used for the printing process. An example of a 3D-printed magnet with a complex shape designed to generate a specific stray field was presented. The same group further developed a similar 3D printing of polymer-bonded rare-earth magnets with a variable magnetic compound fraction for a predefined stray field (Figure 14c).[158]

Among these classes of materials, advanced permanent magnets play an important role in providing high efficiency and reliability, improved compactness, low cost, and low maintenance solutions for renewable energy technologies, including wind turbines, hydroelectric power generators, and wave power buoys. The main attempts of permanent magnets printing are held with NdFeB magnets,[54a,58b,60,158,163] as mentioned above, because of their outstanding magnetic characteristics. Additionally, conventional permanent magnet synthesis typically involves complex multi-step processing.[164] Developing new or improving permanent magnet alloys with decreased amounts of critical materials requires accelerating both the alloy synthesis and property characterization. Therefore, Meng et al.[159] reported bulk combinatorial synthesis via the laser engineered net shaping (LENS) process coupled with high-throughput characterization techniques to rapidly identify potential permanent magnet alloy compositions in the Ce-Co-Fe-Cu quaternary system (Figure 14d). Bulk sample libraries synthesized by LENS proved ideal for high-throughput characterization techniques of magnetic, thermal, and structural properties. Using this approach, researchers have rapidly identified promising compositions and prepared those with more conventional melt processing and casting synthesis. Combined structures of ferrite-based soft ($NiFe_2O_4$) and hard ($BaFe_{12}O_{19}$) bulk magnetic with 3D morphologies were also developed by Peng et al.[160] They successfully used inexpensive metal oxide powder (NiO/Fe_2O_3 and $BaCO_3/Fe_2O_3$) precursors in a simple extrusion free-forming technique coupled with a high-temperature solid-state reaction process (Figure 14e). The 3D-printed structures exhibited either soft or hard magnetic material behavior with i) saturation magnetization values up to approximately 86% and 95% of the $NiFe_2O_4$ and $BaFe_{12}O_{19}$ theoretical bulk magnetization values, respectively, and ii) high densities up to ≈93% of their respective theoretical bulk density.

Advances in magnetic materials and their processing technology are revolutionizing the preparation and application of devices, especially electromagnetic sensors. For instance, Leigh et al. demonstrated an impeller flow sensor by multi-material FDM printing technology.[161] To maintain the impeller's structural integrity, standard ABS material was utilized to fabricate the main body of the sensor, and several layers of formulated magnetite composite are deposited afterward on the top surface. A paddle of the impeller was magnetized to improve the magnitude of magnetic fluctuations for detection using a Hall effect sensor to measure flow velocity during rotation (Figure 14f). The printed magnetic flow sensor exhibited good linear response over an extensive range of flow rates and demonstrated good robustness. The utilization of magnetic materials in this application showed that 3D printing would be a promising method to manufacture functional devices by customized design and multi-material printing when the raw materials may be scarce.

Additionally, a material combination concept to realize 4D-printed products with newly emerging property/functionality was proposed by Wu et al.[4] Traditional 3D printing technologies can generate complex-structural products in one step; however, it fails to endow the products with a "smart" feature. 4D printing shows the capability of additively manufacturing structures whose shape, property, and

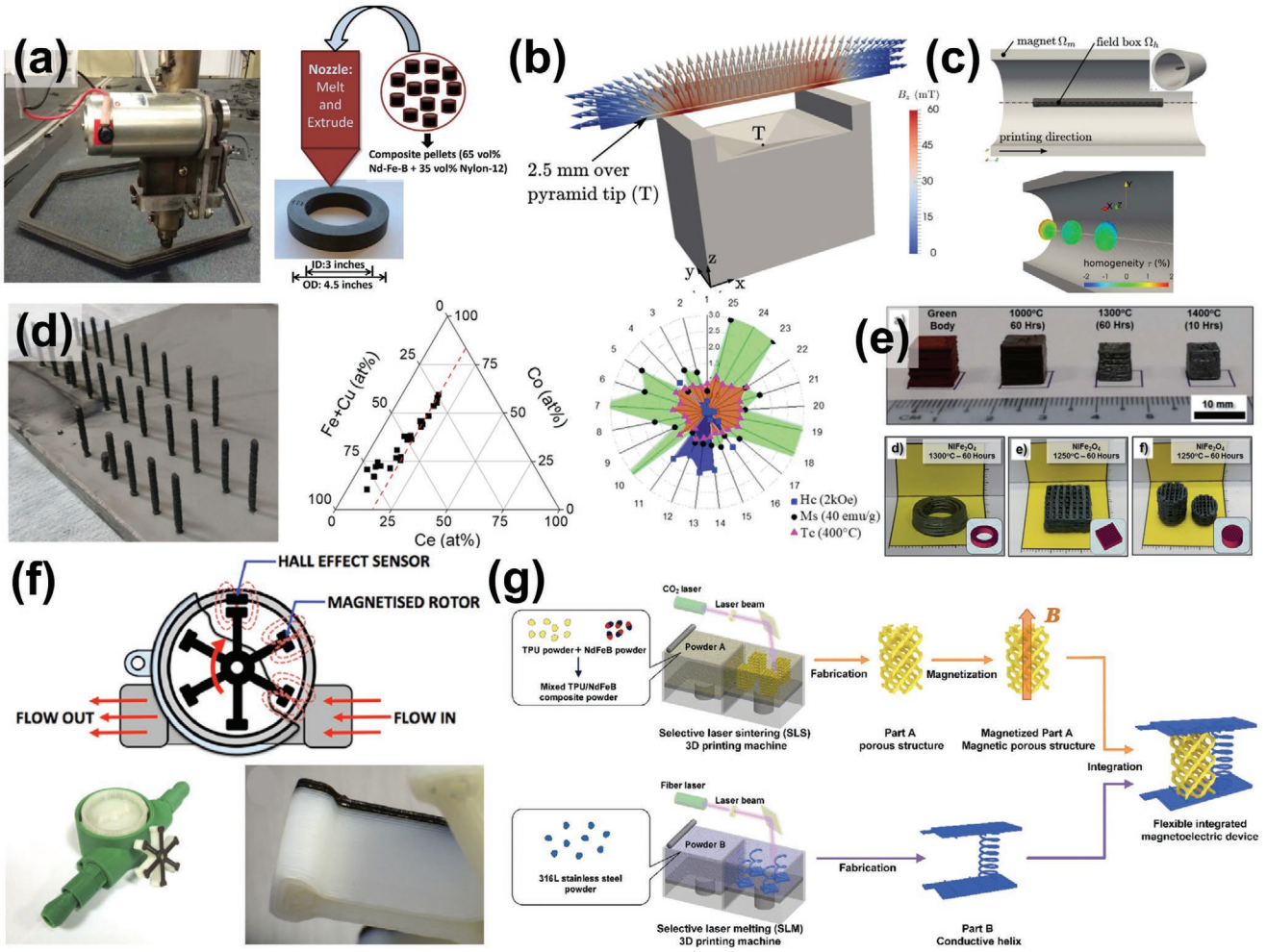

Figure 14. 3D printing of magnetic sensors. a) Images of fabricating isotropic near-net-shape NdFeB bonded magnet using a big area additive manufacturing method. Reproduced with permission.[54a] Copyright 2016, Springer Nature. b) Picture of area scan of a magnetic field with a step size of 0.1 mm in the middle of the printed magnet via a commercial FDM printer. Reproduced with permission.[54b] Copyright 2016, AIP Publishing. c) Images of a model of hollow cylinder magnet with a predefined stray field, the homogeneity within a radius of 2.5 mm on three planes in the field box ($d = 2$ mm, $L = 30$ mm) is lower than 2%. Reproduced with permission.[158] Copyright 2017, Springer Nature. d) As-printed bulk Ce-Co-Fe-Cu rods using the laser engineered net shaping method and the samples' chemical deposition distributions after heat treatment. To help identify compositions for permanent magnet applications with appropriate properties, the compositions that met normalized properties are plotted on the radar plot. Reproduced with permission.[159] Copyright 2018, Minerals, Metals & Materials Society. e) Pictures of bulk samples printed via extrusion free-forming technique coupled with high-temperature solid-state reaction process using NiO/Fe_2O_3 and $BaCO_3/Fe_2O_3$. Reproduced with permission.[160] Copyright 2017, Royal Society of Chemistry. f) The operation of a flow sensor and the printed magnetic flow sensor by multi-material printing. Reproduced with permission.[161] Copyright 2014, IOP Publishing. g) Schematic of the fabrication process of flexible integrated magnetoelectric sensors: A porous structure printed using TPU/NdFeB composite and a helix structure with two flat plates printed using conductive steel powders. Both structures were printed by the SLM process. Reproduced with permission.[162] Copyright 2020, Wiley VCH.

functionality can be varied with time under external stimuli.[162] Here, a material combination concept was proposed to construct 4D-printed devices whose property and functionality can be modulated in a programmable manner. The 4D-printed devices consist of conductive and magnetic parts, enabling the integrated devices to show a piezoelectric property even neither part is piezoelectric individually (Figure 14g). Consequently, the devices' functionality is endowed to transfer mechanical to electrical energy based on the electromagnetic introduction principle, laying the foundation for performance-changed and functionality-changed 4D printing by putting forward a material combination concept. This work extends the applications of the 4D-printed magnetoelectric device. The future development of 3D/4D printing of magnetic sensors will benefit from the novel combination of multiple mechanisms and applications such as thermoelectric/piezoelectric/photoelectric/ultrasound required to enhance the sensors' efficiency.[165]

5.4. Discussion

Figure 15a shows the 3D printing processes and the related magnetic materials used to fabricate magnetic components. Since 3D printing is a relatively new manufacturing technology,

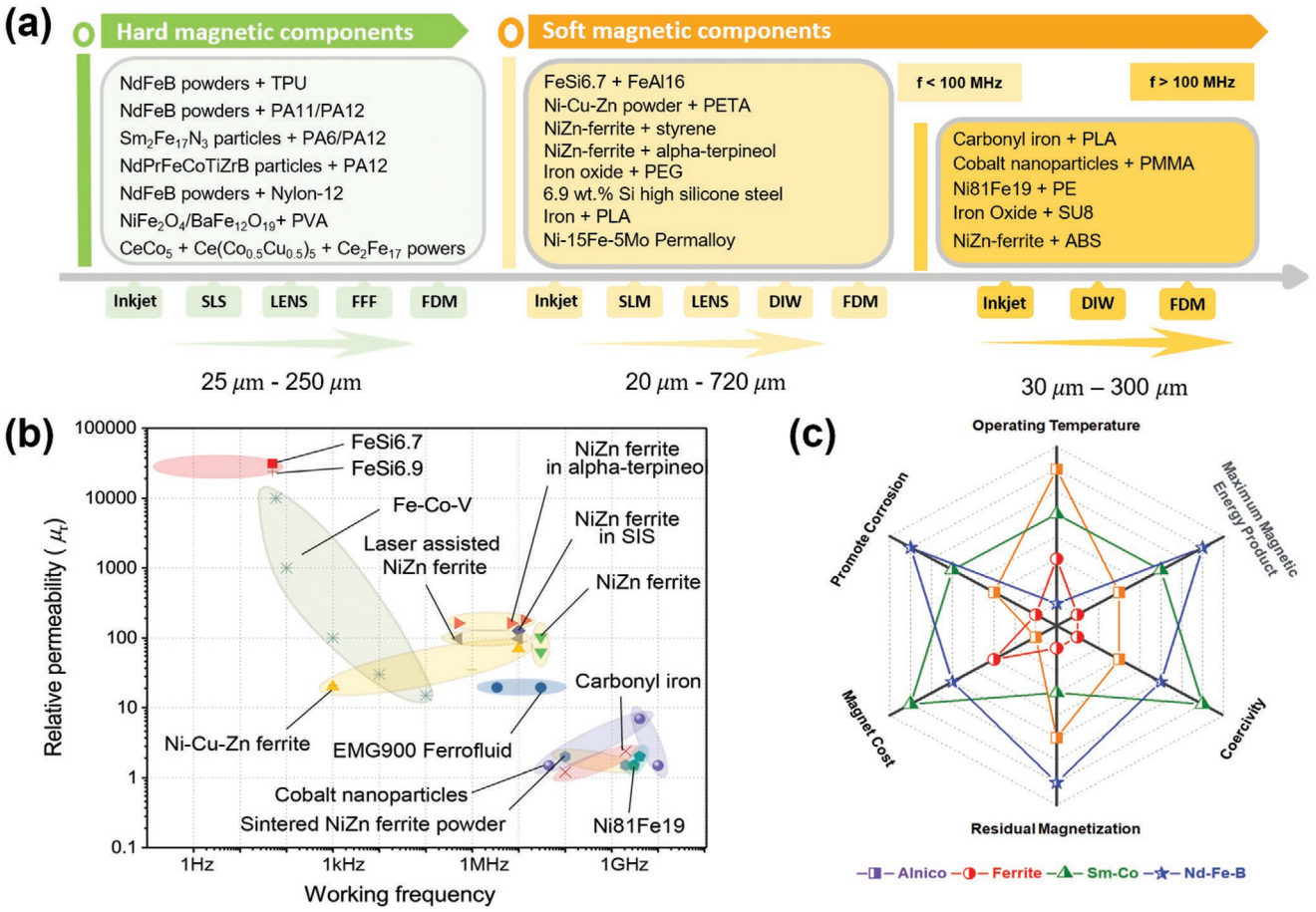

Figure 15. Magnetic components by 3D printing technology. a) Schematic diagram showing the materials and 3D printing methods and their resolutions in fabricating magnetic components. b) The relative permeability with working frequency relationship of typical soft magnetic materials employed in 3D printing. c) Radar plot of comparison between four typical hard magnetic materials.

the magnetic components' design and fabrication using 3D printing are still in their infancy. There are many optimizations to be explored for the best performance of the 3D-printed magnetic materials. Some primary challenges lie in the fabrication of magnetic materials with controlled orientation and high pack density. Meanwhile, many efforts have been spent on manufacturing an electronic device that contains diverse components/materials using 3D printing.[4,166] The surface finish and accuracy of 3D-printed components with small feature sizes is another challenge. However, compared to the tedious fabrication and assembly process of the conventional methods, 3D printing opens new avenues in rapidly manufacturing novel designed prototypes, which will accelerate the future development of electronics.

Magnetic components in electronic devices can benefit from 3D printing techniques due to their ability of fabricating complex geometry and controlling microscale structures to improve magnetic performance. Figure 15b shows the relative permeability of 3D-printed soft magnetic components and their working frequencies. 3D printing techniques that aim at fully dense metal manufacturing have also been explored. In addition, properties of flexibility and mechanical strength can be imparted into 3D-printed components through geometric shape optimization. Hard magnetic materials have great potential for novel magnetic sensors due to their high magnetization remanence. Figure 15c shows six important factors of different hard magnetic materials, including magnetic properties, operating temperature, chemical stability, and cost. 3D printing for permanent magnetic materials mainly focuses on building a strong permanent magnet. The main methods are to increase the proportion of magnetic particles and induce crystallographic anisotropy, which can be used to guide the manufacturing of high-performance magnetic sensors. However, how to use the advantages of 3D printing to build complex structures and control microscale structures to achieve novel magnetic sensors has become a mainstream research direction. 3D printing also provides benefits in integrating magnetic components and electronic circuits by the multimaterial fabrication processes. The 3D-printed hybrid objects can also expand potential applications such as medical devices, miniaturized electronics, and intelligent sensors.

6. 3D Printing of Magneto-Thermal Materials

Heat generation of materials and structures is an essential method for property control and shape changing. Recently,

research on magnetically induced heating methods utilized the magnetothermal effect as a unique heat source in hyperthermia therapy, cell signaling, stem cell cryogenic recovery, and actuation of SMP.[167] Magneto-thermal devices have the benefits of molecular-level heating selectivity, nanoscale spatial resolution, and the ability of indirect actuation, providing a less invasive, less toxic, and more precise heat control compared to the conventional heat sources. For example, Yoo et al. reported a hyperthermia therapy conducted by magneto-thermal devices to destruct cancer cells via apoptosis and necrosis. In this study, resistance-free apoptosis-inducing magnetic nanoparticles triggered by AMF generate heat to release geldanamycin and create protein inhibition. It achieves high efficacy of apoptotic hyperthermia at a mild temperature without affecting normal cells.[168] Moreover, the thermal effect of magnetic nanoparticles can act as a controller of drug release in chemotherapy. Kakwere et al. introduced a PNIPAm polymer-based smart material, which triggered drug release in chemotherapy by actuating the surface functionalization of the cubic-IOPs. It was shown 90% of the drug could be released by magnetothermal effect in 5 hours. The release rate was much faster than the control without the magnetothermal effect (8%).[169]

Besides the direct use of thermal energy, the magneto-thermal effect can be converted to the shape change of SMP composites. By incorporating magnetic nanoparticles in thermoplastic SMP, the magnetically induced recovery process can be triggered by inductive heating in an AMF. Mohr et al. reported a TFX composite mixed with 10 wt% Fe_2O_3 nanoparticles presenting a 65% shape recovery rate in a magnetic field f = 258 kHz and H = 30 kA · m^{-1}.[170] Although magnetic thermal devices have broad applications in biomedical fields, the fabrication capability limits the design freedom and the commercializing of magneto-thermal devices. Due to its ability to fabricate composite material with complex geometry, multiple materials, and novel shape-changing behaviors, 3D printing technology with an integrated magnetic field has shown its fabrication potential for magneto-thermal devices.

6.1. Mechanism of Magneto-Thermal Effect

The mechanisms of magnetothermal effect on magnetic fillers are mainly governed by hysteresis loss and Néel-Brownian relaxations when magnetic materials are exposed to an AMF.[171] In the former case, if a magnetic field ($H > H_c$) is applied in the direction antiparallel to the easy axis of magnetization of magnetic particles, the magnetization reverses. Consequently, the Zeeman energy falls and causes heat dissipation.[172] The area within the hysteresis loop shows the energy required to complete a full cycle of magnetization and reverse, which represents the energy dissipated during this process. For the cured magnetic particles inside a 3D-printed structure, it is hard to apply H parallel to the easy axis. According to the Stoner-Wohlfarth model, the hysteresis loop becomes narrower when the angle θ between applied field H and the easy axis increases, as shown in **Figure 16**a. Therefore, to efficiently improve heat generation through hysteresis loss, the alignment of magnetic particles should be uniform, and the amplitude of AMF should be adjusted to H_c.

When the magnetic particles become relatively small (usually < 50 nm), thermal fluctuation becomes predominant, and the direction of the easy axis is randomly reversed. In that case, Néel-Brownian relaxation loss contributes to the heat generation of magnetic nanoparticles. The Néel relaxation process dominates when the size of magnetic nanoparticles decreases below a certain critical domain wall thickness, as shown in Figure 16b. In this case, the barrier of magnetocrystalline anisotropy energy that separates the axis of the magnet is low and can be overcome by the external magnetic field. When an applied external magnetic field is sufficient to overcome the energy barrier, the magnetic spins are flipped. Their magnetization direction is reversed, and the provided magnetic energy is released as heat. It is the only relaxation process occurring in immobilized magnetic nanoparticles.[171a] As the particle size increases, the magnetic anisotropy energy barrier becomes high enough to block the Néel relaxation process, and then the Brownian relaxation

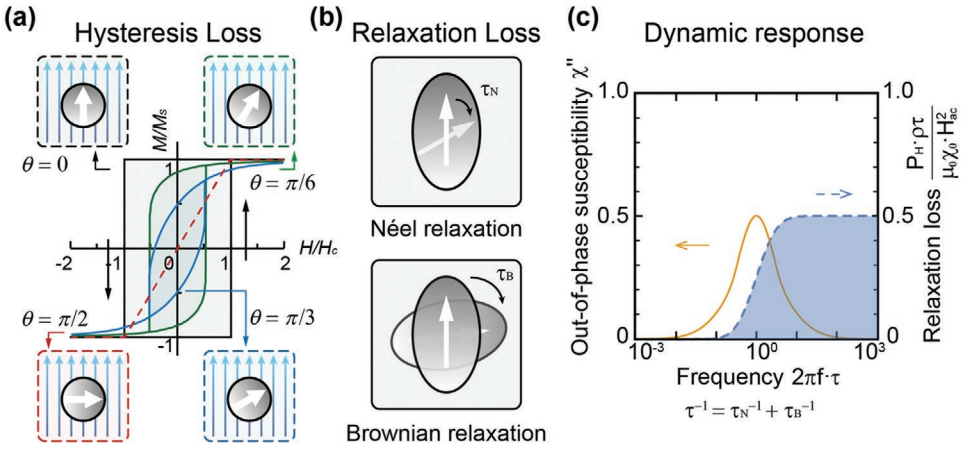

Figure 16. Representative working principles of the magneto-thermal effect due to hysteresis loss and relaxation loss. a) Magnetic hysteresis loop of magnetic single-domain particles in the magnetic field applied in different directions to the easy axis of magnetization. b) Schematic diagram of Néel relaxation and Brownian relation. c) Frequency dependence of AC susceptibility and relaxation loss P_H. Reproduced with permission.[172] Copyright 2019, Elsevier.

dominates. The applied magnetic field leads the particles to rotate in the surrounding medium with the magnetic spin directions. When the particles rotate, the heat is emitted by the rotational friction between the particles and the medium, known as Brownian relaxation. These two relaxation processes have been discussed in detail in former research.[171a,172]

Considering the reversal and rotation when responding to an applied AMF, a magnetic nanoparticle's relaxation time could be expressed using Equation (5), where τ_N and τ_B represent the relaxation time of Néel relaxation and Brownian relaxation, respectively. The power loss P_H corresponding to relaxation can be calculated by Equation (6), where χ_0 is the initial static susceptibility of nanoparticles, ρ is the mass density, and H_{ac} is the amplitude of AMF. The frequency of AMF should be adjusted to a suitable value ($2\pi f = \tau^{-1}$) to maximize the heat generation due to the relaxation loss. As shown in Figure 16c, the out-of-phase susceptibility of nanoparticles (solid yellow line) has its maximum, and accordingly, the dependence of losses on frequency shows a sharp maximum.[172,173] According to Equation (6), H_{ac} should be increased to the maximum possible value for maximizing P_H.

$$\tau^{-1} = \tau_N^{-1} + \tau_B^{-1} \tag{5}$$

$$P_H = \frac{\mu_0 \chi_0 H_{ac}^2}{2\rho\tau} \times \frac{(2\pi f\tau)^2}{1+(2\pi f\tau)^2} \tag{6}$$

Research on the magnetothermal effect has been done to study the relationship between the parameters of magnetic nanoparticles and the heating effect. The heating effect was mainly affected by particle size, particle shape, and particle material.[174] Designed experiments showed the thermal energy generated by γ-Fe_2O_3 magnetic nanoparticles measured under an applied AMF of 25 kA m^{-1} at 700 kHz was gradually increased from 4 to 275 W g^{-1} when the magnetic nanoparticle diameter was increased from 5 to 10 nm.[175] The size effect of Fe_3O_4 MNPs was also studied. The thermal energy was increased from 30 to 61 W g^{-1} when the size was increased from 10 to 16.2 nm under an AMF of 21 kA m^{-1} at 170 kHz.[176] Besides particle size, the particle shape is also crucial to the magnetic heating effect. Cubic Fe_3O_4 nanoparticles generated higher thermal energy than nanoparticles with a spherical shape under the identical stimulus.[177] Furthermore, the heating effect can be improved by modifying the material of magnetic nanocomposite. For instance, $MnFe_2O_4$ nanoparticles exhibited a more substantial heating effect due to their unpaired electrons. Experiments also showed that $Zn_xMn_{1-x}Fe_2O_4$ nanoparticles showed much higher thermal energy (432 W g^{-1}) than conventional IOPs (115 W g^{-1}).[178] It can be drawn based on the previous experiment results that higher AMF intensity and frequency generate increased heat effect per unit mass. And the selection of nanoparticles also has a significant impact on the heat effect.

By integrating magneto-thermal materials and shape-memory materials, a new type of composite material can convert magnetic energy to heat energy and finally to mechanical energy. This hybrid material is categorized as magneto-thermal shape memory material. Most of the magneto-thermal shape memory devices use PLA as a SMP. PLA is compounded with TPU, a supporting material to maintain ductile behavior at room temperature.[179] When the deformation happens, the strain energy will be stored in the system until the temperature increased above the glass transition temperature (T_g) of PLA. In the glassy state, PLA regains mobility and returns to its original shape when the temperature is higher than T_g. 3D printing can be applied to fabricate composites with changeable dynamic properties. For example, by combining hard magnetic materials with soft PNIPAm, researchers achieved hybrid magnetic responsive devices under AMF, leading to new design freedom.[5a]

6.2. 3D Printing of Magneto-Thermal Response Devices and Applications

The magnetic nanoparticle-mediated heating system has become an effective strategy to finely control biological systems from high temperature to cell signal transmission in a time-space controlled manner.[180] In magnetic-induced heating, magnetic NPs play a major role in converting external electromagnetic energy (i.e., AMF) to heat via Néel-Brownian relaxations.[174] The material selection of matrix polymer is mainly based on the applications. For example, for magnetic hyperthermia therapy purposes, biodegradable materials are commonly used to avoid second surgery of removing the implanted device. A polycaprolactone (PCL) mat was used for the anti-cancer magneto-thermal device.[22] In another magnetic hyperthermia application, 3D-printed Akermanite/Fe_3O_4/CaO_2 scaffolds aimed at realizing the subsequent tissue regeneration.[5b] To obtain satisfactory performance, advanced design concepts enabled by 3D printing have been developed to customize the property of magneto-thermal response devices to directly control the nanoparticles' heating characteristics and their therapeutic effect.

Magnetic hyperthermia therapy is a promising method for treating tumors due to its effectiveness and only mild side effects. Zhang et al. reported a study of 3D-printed magnetic Fe_3O_4/MBG/PCL composite scaffolds to achieve multifunctionality of bone regeneration, local anticancer drug delivery, and hyperthermia (**Figure 17**a).[22] Regular macros porous structures with 0° and 90° angle steps between two successive layers were fabricated via a 3D Bioplotter. The fabricated composite scaffolds ($6 \times 6 \times 6$ mm^3) containing mesoporous bioactive glass (MBG) and PCL with magnetic Fe_3O_4 nanoparticles. The results showed that the 3D-printed scaffolds had uniform macropores of 400 μm, high porosity of 60%, and excellent compressive strength of 13–16 MPa. The addition of Fe_3O_4 nanoparticles into MBG/PCL scaffolds did not affect their apatite mineralization ability but provided excellent magnetic heating ability. Such heating ability significantly stimulated proliferation and alkaline phosphatase activity. For instance, the scaffolds induced the temperature increase from 20 to 43 °C at an AC frequency of 409 kHz and magnetic strength of 180 G within 2 min, suggesting considerable potential for their use in the treatment.

Critical requirements for administering magnetic nanoparticles for in vivo therapy include selecting a secure pathway to deliver carriers explicitly targeting the tumor and retaining those carriers in the tumor region in a sufficient

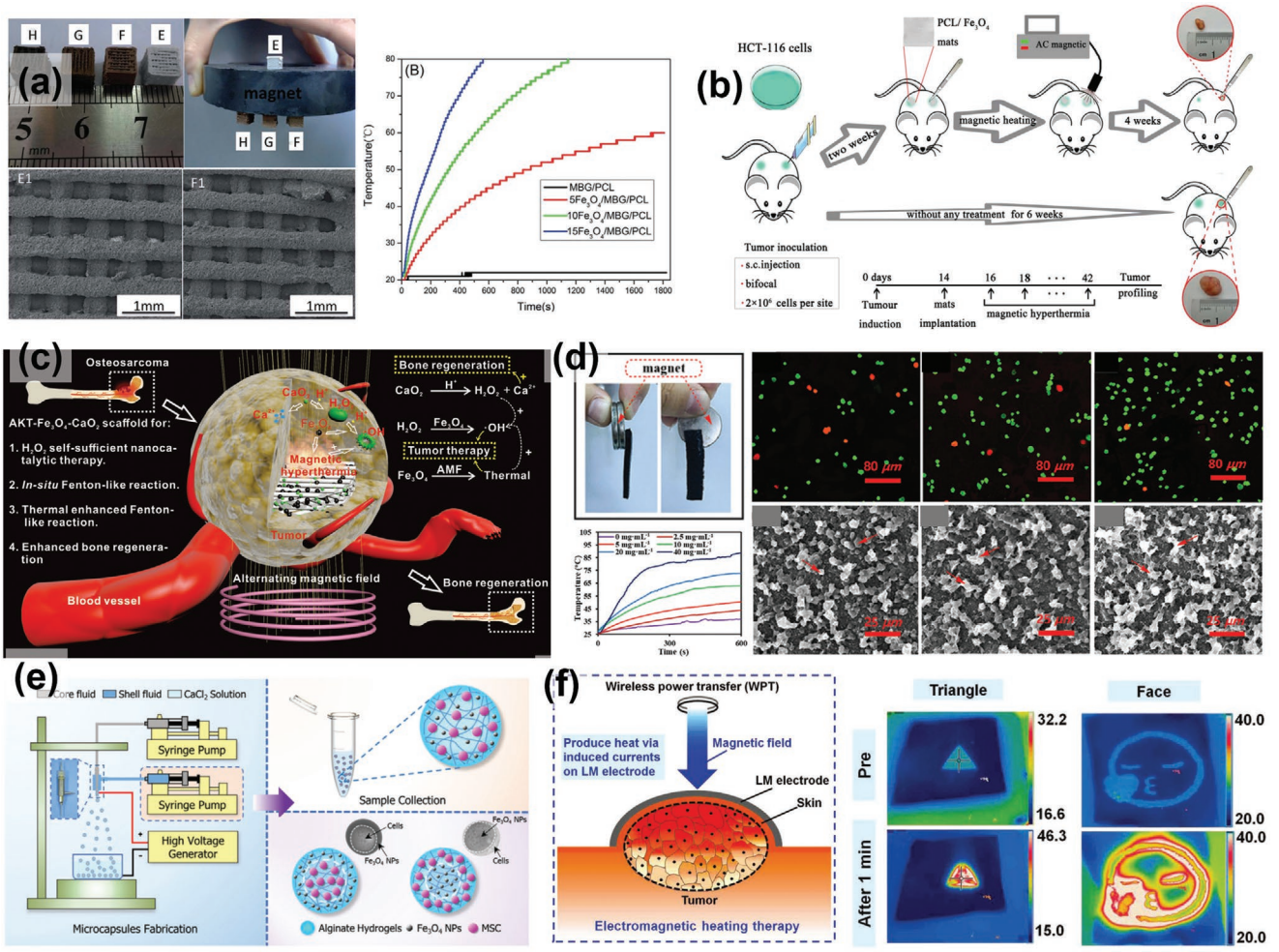

Figure 17. 3D printing of magnetothermal devices for hyperthermia therapy. a) Photograph of different 3D-printed scaffolds, including (E) MBG/PCL, (F) $5Fe_3O_4$/MBG/PCL, (G) $10Fe_3O_4$/MBG/PCL, and (H) $15Fe_3O_4$/MBG/PCL, and their temperature changes under an AMF of 409 kHz. Reproduced with permission.[22] Copyright 2014, Royal Society of Chemistry. b) Schematic description of experimental design using magnetic hyperthermia for tumor treatment. Reproduced with permission.[181] Copyright 2017, Wiley Periodicals. c) Schematic illustration of 3D-printed scaffolds co-loaded with Fe_3O_4 and CaO_2 nanoparticles for bone regeneration and tumor therapy under AMF. Reproduced with permission.[5b] Copyright 2019, Wiley VCH. d) Heat-induction properties and cytocompatibility of magnetic hydrogels with different iron concentrations. Reproduced with permission.[182] Copyright 2019, Royal Society of Chemistry. e) Schematic of electrostatic spraying system and the microcapsules with different structures. Reproduced with permission.[183] Copyright 2018, Royal Society of Chemistry. f) Schematic and thermal IR pictures of the electromagnetic heating process of O-GaIn e-skin. Reproduced with permission.[184] Copyright 2019, Wiley VCH.

concentration. Recently, a novel method of preparing magnetic heating mats for high-performance hyperthermia was developed using electrohydrodynamic jet (E-jet) printing (Figure 17b).[181] When Fe_3O_4 nanoparticles were used in the mats at a concentration of 6 mmol L^{-1}, the mats with 0.07 g PCL/Fe_3O_4 were able to increase the temperature peripherally to 45 °C under an AMF within 45 min. The artificially induced hyperthermia close to a tumor caused tumor cell death. Therefore, in vivo experiments indicated clear signs of tumor growth inhibitory and prolonged survival time of tumor-bearing mice after four weeks of treatment. Furthermore, the main advantage of such implantable magnetic mats is the local and precise delivery of Fe_3O_4 NPs, ideal for the hyperthermia treatment of easily accessible tumors.

Recently developed nanocatalysts based on Fenton-like reactions for catalytic therapy demonstrated a high potential to eliminate chemotherapeutic-insensitive tumors.[185] However, the insufficient concentration of intrinsic hydrogen peroxide (H_2O_2) and low intra-tumoral penetrability hinder their applications and therapeutic efficiency. The synchronous enriching intratumor H_2O_2 amount or nano agents and promoting osteogenesis are intriguing strategies to solve the dilemma in osteosarcoma therapy. Therefore, Dong et al.[5b] proposed a multifunctional "all-in-one" biomaterial platform that was constructed by co-loading calcium peroxide (CaO_2) and iron oxide (Fe_3O_4) nanoparticles into a 3D-printed akermanite scaffold (AKT-Fe_3O_4-CaO_2) (Figure 17c). The loaded CaO_2 nanoparticles acted as H_2O_2 sources to achieve H_2O_2 self-sufficient nano catalytic osteosarcoma therapy as catalyzed by coloaded Fe_3O_4 nano agents. They also provided calcium ion (Ca^{2+}) pools to enhance bone regeneration. The synergistic osteosarcoma-therapeutic effect was achieved from both magnetic hyperthermia (>50 °C)

(frequency, 500 kHz; output current, 22 A; coil diameter, 100 mm) as enabled by Fe_3O_4 nanoparticles under AMF and hyperthermia-enhanced Fenton-like nano catalytic reaction for producing highly toxic hydroxyl radicals.

A better understanding of therapeutic principles against bone tumors, designing restorative biomaterials of bone defects, and further developing bio-application of 3D-printed scaffolds can all profit from the magneto-thermal method and the related biomaterial platform. Gang et al.[182] developed a robust magnetic double-network hydrogel with self-healing, MR imaging, cytocompatibility by 3D printing (Figure 17d). First, Fe_3O_4 nanoparticles of about 40–50 nm were fabricated with relatively few surface groups and proved to be suitable for in situ surface coating and reaction. Then, AA, AM, and DAm monomers were chemically polymerized by APS in the presence of chitosan and nano-Fe_3O_4 to form a physically and chemically crosslinked polyolefin—chitosan double network hydrogel. The hydrogel exhibited enhanced heating ability at higher intensity AMF. The hydrogel with heat-induction properties was used to treat tumors and drug-controlled release,[186] offering superior functionalities than previously reported. A similar study on cryogenic recovery of stem cell-laden alginate-Fe_3O_4 nanocomposite hydrogels by magnetothermal heating has also been reported (Figure 17e).[183]

In addition to the magnetic nanoparticle-loaded composite materials for magneto-thermal therapy, 3D-printed conformable liquid metals for electronic skin (e-skin) have been investigated for wireless multisite tumor therapy.[184] Gallium-based functional liquid metals (LMs) have been increasingly evaluated for biomedical applications, especially as e-skin, due to their inherent flexibility, high electroconductivity, excellent thermal conductivity, and easy printability. A new biomedical application of e-skin with bioelectromagnetic thermal effect to spatiotemporally controlled wireless multisite tumor treatment was introduced (Figure 17f). The heat was generated by eddy current under an AMF due to good conductivity of LM electrode rather than magnetic hysteresis loss or relaxation loss. Due to its super thermal and electroconductivity, excellent softness, biosafety, and easy printability, oxidized GaIn (O-GaIn) LM material was directly printed on the skin surface with customized patterns as a conformable bioelectrode covering an abnormal tumor. After 1 min of electromagnetic, thermal induction, the temperature of the skin-LM rose to around 42 °C, while the temperature of skin without the LM remained unchanged (≈17 °C). Based on the effective electromagnetic, thermal induction of O-GaIn e-skin, temperature-controlled DOX-loaded chitosan (CS) hydrogel was introduced under an AMF for electromagnetic hyperthermia and chemotherapy. This engineered LM e-skin, which serves as an excellent bioelectromagnetic agent, can successfully achieve WPT for multisite tumor treatment, which is promising for expanding tumor therapeutics.

6.3. 3D Printing of Magneto-Thermal Shape Memory Polymer

3D printing of SMP is being developed for biocompatible actuators and personalized implant devices. The shape-changing and recovery properties actuated by the magneto-thermal effect have advantages in low invasive, remote intervention, and indirect control. For the shape-changing purpose, SMPs such as PLA, PEGDA, and PNIPAm are often used. The SMP recovers to its original shape due to external stimuli such as temperature, plasticizing effect, and chemical effect. The temperature change induced by the magneto-thermal effect can be used as a "switch" for the temperature-responsive shape memory material. For instance, Lin et al. reported a 3D printed biocompatible shape memory occluders actuated by AMF as an accurate and controllable treatment of the atrial septal defect (**Figure 18**a).[187] Occluders with 3/4/6 arms and the size of 16 mm in diameter were printed using the PLA-based magnetic nanocomposites. The occluders can be remotely actuated to expand and block the defect in a heart chamber within 22 s magnetic stimulus (AMF, 7.5 kHz, 4 kA m^{-1}) due to the heat generated from embedded 10 wt% Fe_3O_4 nanoparticles. After implantation, the occluder will serve as a temporary platform for cell growth and adhesion to complete the defect's closure. The occluding membranes were prepared by an electrospinning technology that uses shape memory PLA, whose fiber porous structure can be used as a substrate to guide cell adhesion, growth, and proliferation. Tang et al. reported an approach to achieve the shape morphing of magnetic hydrogels in an AMF by combining magnetic polymer structures with 2D and 3D origami structures (Figure 18b).[188] The shape-changing composite fabricated by NPNIPAm and Fe_3O_4 nanoparticles can respond to static field and AMF.

The device navigation, shape-changing, and fixation can be achieved by the noncontact magnetic stimulus method. This approach can be readily incorporated in 3D/4D printing technologies to have novel applications in biomedical devices and soft robots. Wei et al. developed a magnetically controlled and guided vessel stent with a length of 30 mm and a diameter of 1 mm (Figure 18c).[189] The authors first printed a multilayer scaffold with a width of 2 mm using a DIW nozzle of 150 μm inner diameter under a pressure of 1.4 MPa and a velocity of 2 mm s^{-1}. The 3D-printed scaffold was deformed into a spiral structure before being sent to the target location in the vessel. After applying the magnetic stimulus, the spiral structure changed from 1 to 2.7 mm within 10 s, which presented a great potential to be used as a self-expandable intravascular stent. The key strategy of the devices is that the recovery shape triggered in a restrictive circumstance will keep the deformed spiral structure with a larger diameter. Moreover, Zhang et al. fabricated a 3D-printed shape-changing structure for personalized bone repairment since different bone sizes can be printed as required to fit the bone defect (Figure 18d).[25] PLA composite with 15 wt% Fe_3O_4 printed by a 1.75 mm nozzle and with the temperature set as 175 °C showed a 95.6% shape recovery ratio within 5 s under 24.7 kHz. Noticeably, the working surface temperature of the 3D-printed shape-changing polymer was distributed from 20 to 40 °, indicating that the material and structural design is suitable for tissue engineering.

Furthermore, the magneto-thermal SMP can be served as the external supporting structure in tissue engineering. For instance, Zhao et al. designed a tracheal scaffold with bidirectional spiral ridge and porous holes structure whose shape can be remotely controlled by AMF (Figure 18e).[19d] The 3D-printed tracheal scaffolds, compared with traditional tracheal scaffolds, have increased conformable fixation, larger cell tissue load

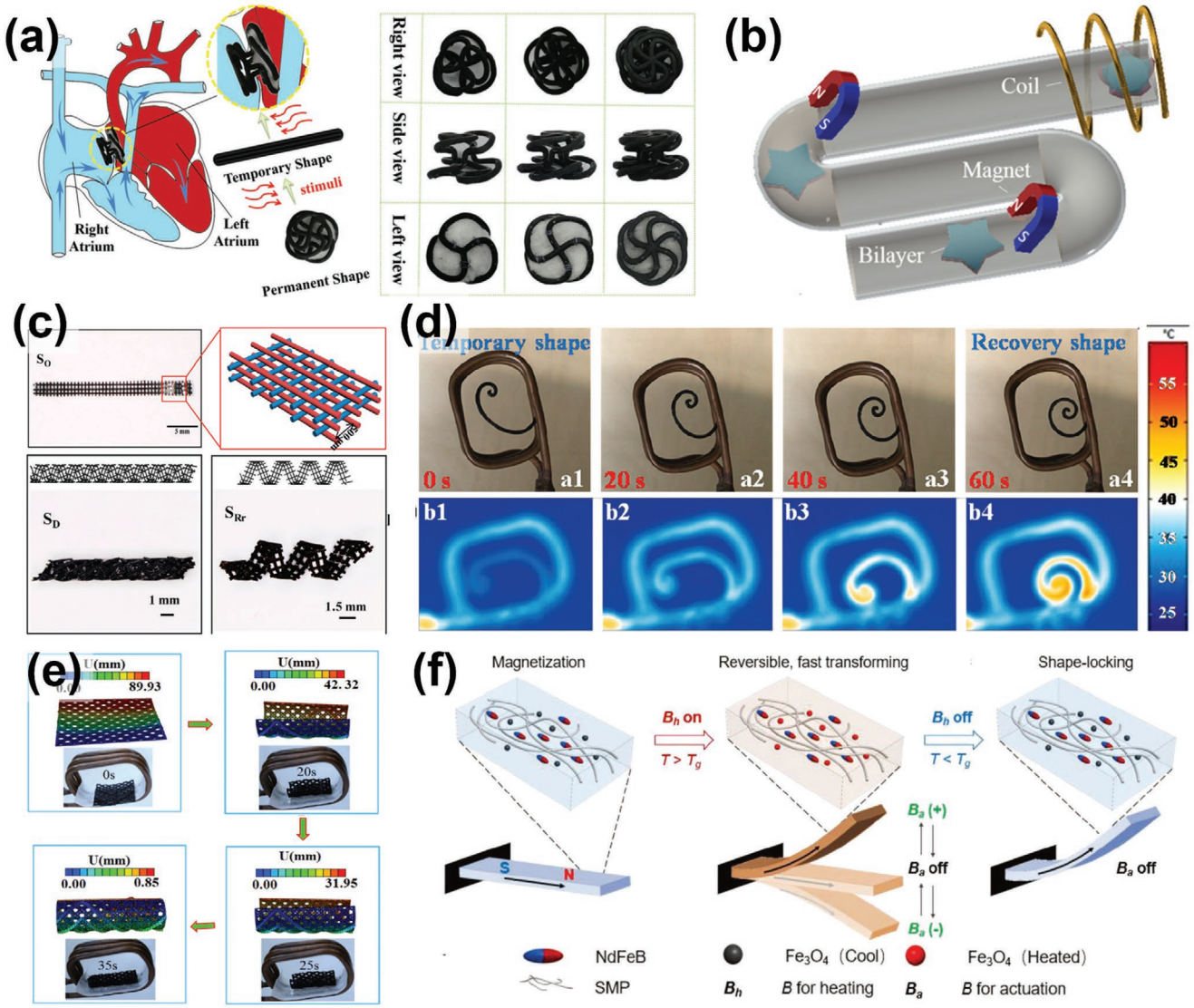

Figure 18. 3D printing of magnetothermal SMP devices. a) Interventional therapy for ASD using 3D-printed magnetic occluders. Reproduced with permission.[187] Copyright 2019, Wiley VCH. b) Schematic for the magnetic navigation of a starlike magnetic bilayer and its shape morphing in AMF. Reproduced with permission.[188] Copyright 2019, American Chemical Society. c) A 3D-printed magnetic multilayer scaffold deforming under magnetically induced heating and recover under a restrictive condition. Reproduced with permission.[189] Copyright 2016, American Chemical Society. d) Shape recovery of a 3D-printed structure using PLA and 15wt% Fe_3O_4 under 27.5 kHz AMF. Reproduced with permission.[25] Copyright 2019, Elsevier. e) Photographs showing the shape recovery of a bioinspired tracheal scaffold in 35 s under 30 kHz AMF. Reproduced with permission.[19d] Copyright 2019, Elsevier. f) The working mechanism of magnetic shape memory polymers by embedding soft (Fe_3O_4) and hard (NdFeB) magnetic particles. Reproduced with permission.[5a] Copyright 2019, Wiley VCH.

capacity, and biocompatibility. Fe_3O_4 and PLA composite with a ratio of 3:17 was extruded out by a 0.4 mm FDM nozzle at the printing speed of 50 mm min^{-1} at 210 ° and the bed temperature at 60 °C. The 3D-printed tracheal scaffolds wrapped the patient tracheal under shape memory deformation that served as tissue growth support, solving the scaffold migration and facture led by traditional tracheal scaffolds. The researchers also demonstrated the 3D-printed shape memory had a gradient structure that responded to various types of SMPs through different sources of stimuli such as contact and noncontact triggering. In the study, monomer (BMA) mixed with a crosslinker (PEGDMA) and photoinitiator (phenyl-bis (2,4,6-trimethyl benzoyl) phosphine oxide) were mixed mechanically and cured by UV light. The SMPs under investigation have high mechanical strength and thermal stability compared to traditional SMP, which can be applied in numerous fields, from medical devices to soft robotics with contact and noncontact triggering stimuli.

Taking advantage of 3D printing materials that have different mechanical properties, multi-material 3D printing methods can further improve shape-changing performance. For example, Ze et al. developed a hard-magnetic powder and soft SMP composite material, completing the reprogrammable, untethered, fast, and reversible actuation and shape locking (Figure 18f).[5a] Both Fe_3O_4 and NdFeB were in acrylate-based amorphous SMP

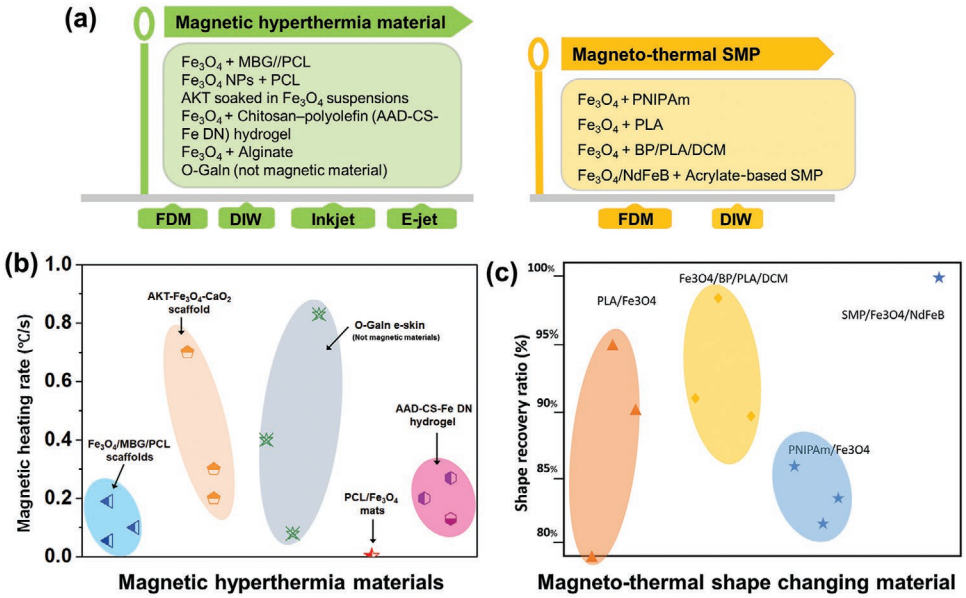

Figure 19. a) Summary of 3D printing methods and materials in fabricating magnetothermal devices. b) The heating rate of magnetic hyperthermia materials in 3D printing. c) Comparison of shape recovery ratio between different SMP materials under AMF stimuli.

that can be 3D printed. Although the acrylate-based amorphous SMP was not prepared by 3D printing, similar materials such as PNAPAm are known to be 3D printable. The Fe_3O_4 particles enable inductive heating under a high-frequency AMF and thus can be employed to change the stiffness of materials for shape locking and unlocking. The NdFeB particles were magnetized with predetermined magnetization profiles for programmable deformation under a low-frequency actuation magnetic field. The 3D-printed devices utilizing two types of embedded magnetic particles for inductive heating and magnetic actuation can provide effective lock and unlock control for functions such as soft robotic grippers, employable/reconfigurable antennas, sequential actuation devices, and digital logic circuits.

6.4. Discussion

Broad design freedom for magnetothermal devices has been enabled by 3D printing technology, benefited from its ability of complex shape, multiscale fabrication, and multi-material printing of magnetic materials and other functional materials. **Figure 19**a shows the representative 3D printing methods and the related magnetic materials. As a low toxic therapy for tumors, magnetic hyperthermia has the increasing need of fabricating personally customized devices with well-designed structures and embedded magnetic nanoparticles. Benefits from the multi-material fabrication enabled by 3D printing, the ability of in-situ heat generation of implants may attract more attention in the fields of drug delivery, bone regeneration, and cancer treatment.[139]

In SMP applications, 3D printing is a widely used fabrication method for its excellent ability to build complex and accurate structures. The high porosity structure such as hyperthermia mat, smart material with switchable dynamic properties, and biocompatible SMP with complex geometry such as tracheal and heart scaffolds can be fabricated. By introducing magnetic materials, SMP could be heated in a noninvasive method, making it possible to achieve controllable shape morphing in an enclosed environment. The SMP structures can perform more sophisticated shape-changing behaviors by combining multi-material and high precision fabrication presented by 3D printing technology.

On the other hand, as a newly emerged field, 3D-printed magnetothermal devices still encounter challenges in response speed, heating rate, energy efficiency, and fabrication cost. The heating rate of magnetothermal devices varies from 0.1 to 1.0 °C s^{-1} (Figure 19b). Although it has the advantages of uniform and non-invasive heating, a higher heating rate needs to be achieved in the future for the cancer surgery application. A higher heating rate can significantly reduce surgery time and increase the number of surgeries per day. Another essential factor for magnetothermal devices is the shape recovery ratio (Figure 19c). The larger shape recovery ratio indicates the material's capability of recovering to the original shape. A larger shape recovery ratio is needed for the accurate control of shape-changing devices. Current shape recovery ratios vary from 80% (PNIPAm) to 98% (SMP-NdFeB composite polymer). To further increase the shape recovery ratios, the development of magnetothermal devices with new materials, shape structures, and microstructure are some potential research directions.

7. Conclusions and Outlook

In summary, the development of 3D printing technology and the profound understanding of magnetic mechanisms have prompted the exploration of functional magnetic materials for various applications. Particularly, functional magnetic materials can benefit from 3D printing in many areas, such as property enhancement, microrobots, electronics, and heat generation. In anisotropic alignment, magnetic field-assisted 3D printing technology is a promising method to orientate magnetic

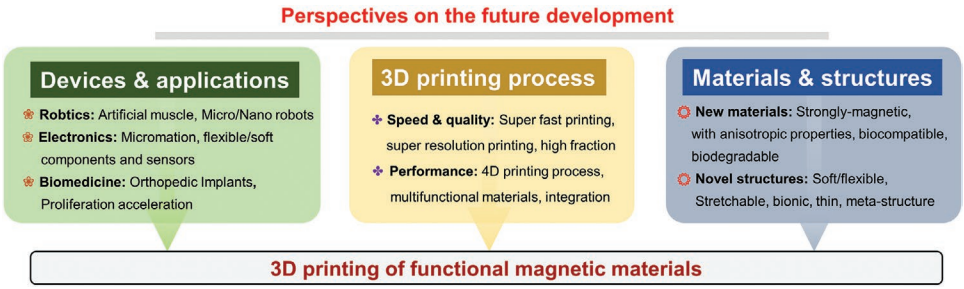

Figure 20. Perspectives on the future development of 3D printing functional magnetic materials and devices.

micro fillers. This novel fabrication method with non-contact alignment can duplicate the excellent mechanical properties of natural materials[1a] and provide potential opportunities to reproduce smart materials for electrical, thermal, and optical applications with tunable properties. In microrobots, advanced 3D printing technologies are employed to build well-designed magnetic robots with high driving efficiency. For example, the TPP method was used to build micrometer swimming robots because robots with helical structures have the best swimming performance on such a small scale.[133,138,190] Also, 3D printing technology facilitates the fabrication of electronic devices that can be integrative and flexible in the future. The performance of 3D-printed magnetic devices can be improved by optimizing geometry and structure. As for heat generation, 3D printing technology is a powerful tool in fabricating magnetically heating materials and precisely depositing such materials in a designed structure. Novel non-invasive heating devices using hyperthermia materials and biocompatible shape memory structures can significantly benefit from 3D printing's precise geometry building and multi-material printing ability.

Although the research in 3D printing functional magnetic materials has progressed significantly, many challenges need to be well addressed before broad uses in more practical applications. Specifically, the concentrations of magnetic active fillers in the base matrix in current research are still relatively low. Such low concentrations of magnetic fillers are mainly to ensure the current 3D printing methods can deposit the magnetic composite. The lack of research on the optimization of preparation, control, and printing of magnetic composites hinders the fabrication of composite architectures with a high-volume fraction of magnetic fillers. Also, selecting magnetic materials with strong magnetic-response and preparing them to better integrate with the matrix materials need to be explored for improved functions.

Some additional research directions to promote 3D printing functional magnetic materials and their applications are identified (**Figure 20**). First, the research on miniaturization and integration of 3D-printed parts needs to be developed. With improved shape and material control enabled by 3D printing technology, high-precision fabrication of multi-material components has become a trend. 3D-printed magnetic materials combined with other functional materials will allow engineers to realize more complex and diverse functions. Second, the design of 3D-printed magnetic robots with improved performance and more functions is a new research direction. At present, research on accurate motion analysis and prediction for magnetic robots has emerged. We expect a complete multi-scale model and simulation framework will be established to understand the relations between materials, mechanism, structure, and performance of 3D-printed magnetic devices. With such improved understanding and established computational framework, the design of geometry, the choice of materials, and the selection of 3D printing methods will be more well-guided to realize given functions. Third, new 3D printing methods that can handle composites with high magnetic filler concentrations are needed to produce a compound structure with a much higher volume fraction of magnetic fillers.

This review emphasizes the potential of novel 3D printing technologies to build functional parts using magnetic materials. 3D printing of magnetic materials is still in its infancy and needs tremendous contributions and extensive collaborations from multiple disciplines, such as electromagnetism, materials science, physics, and mechanics. The collaboration of scientists and engineers will lead to further advancements in 3D printing of magnetic materials to satisfy myriads of functional applications, including, but not limited to, robots, electronics, thermology, and biomedicine. With increasing progresses obtained to address the identified limitations, the 3D printing of functional magnetic materials may exert a promising alternative for advanced applications, such as anisotropy for property enhancement, magnetic robots, magnetic components in electronics, and magneto-thermal devices.

Acknowledgements

The authors at USC would like to acknowledge the visiting scholar program at the University of Southern California. The authors at ZJU would like to acknowledge the National Natural Science Foundation of China (grant numbers 51635006, 51875519, 51821093) and the Natural Science Foundation of Zhejiang Province (grant number LZ18E050002).

Conflict of Interest

The authors declare no conflict of interest.

Keywords

additive manufacturing, composite, magnetic, robot, sensor

Received: March 22, 2021
Revised: May 9, 2021
Published online:

[1] a) X. J. Li, W. Shan, Y. Yang, D. Joralmon, Y. Zhu, Y. Chen, Y. Yuan, H. Xu, J. Rong, R. Dai, Q. Nian, Y. Chai, Y. Chen, *Adv. Funct. Mater.* **2020**, *31*, 2003725; b) J. J. Martin, B. E. Fiore, R. M. Erb, *Nat. Commun.* **2015**, *6*, 8641.
[2] W. Q. Hu, G. Z. Lum, M. Mastrangeli, M. Sitti, *Nature* **2018**, *554*, 81.
[3] D. Goll, D. Schuller, G. Martinek, T. Kunert, J. Schurr, C. Sinz, T. Schubert, T. Bernthaler, H. Riegel, G. Schneider, *Addit. Manuf.* **2019**, *27*, 428.
[4] H. Wu, X. Zhang, Z. Ma, C. Zhang, J. Ai, P. Chen, C. Yan, B. Su, Y. Shi, *Adv. Sci.* **2020**, *7*, 1903208.
[5] a) Q. J. Ze, X. Kuang, S. Wu, J. Wong, S. M. Montgomery, R. D. Zhang, J. M. Kovitz, F. Y. Yang, H. J. Qi, R. K. Zhao, *Adv. Mater.* **2020**, *32*, 1906657; b) S. Dong, Y. Chen, L. Yu, K. Lin, X. Wang, *Adv. Funct. Mater.* **2020**, *30*, 1907071.
[6] A. Boudenne, Y. Mamunya, V. Levchenko, B. Gamier, E. Lebedev, *Eur. Polym. J.* **2015**, *63*, 11.
[7] K. Kim, J. Kim, *Composites, Part B* **2016**, *93*, 67.
[8] M. S. Wang, L. He, S. Zorba, Y. D. Yin, *Nano Lett.* **2014**, *14*, 3966.
[9] Z. Li, F. Yang, Y. Yin, *Adv. Funct. Mater.* **2020**, *30*, 1903467.
[10] J. M. Silveyra, E. Ferrara, D. L. Huber, T. C. Monson, *Science* **2018**, *362*, eaao0195.
[11] E. A. Perigo, G. Hemery, O. Sandre, D. Ortega, E. Garaio, F. Plazaola, F. J. Teran, *Appl. Phys. Rev.* **2015**, *2*, 041302.
[12] A. Zhakeyev, P. Wang, L. Zhang, W. Shu, H. Wang, J. Xuan, *Adv. Sci.* **2017**, *4*, 1700187.
[13] Y. Yang, X. Song, X. Li, Z. Chen, C. Zhou, Q. Zhou, Y. Chen, *Adv. Mater.* **2018**, *30*, 1706539.
[14] M. A. Skylar-Scott, J. Mueller, C. W. Visser, J. A. Lewis, *Nature* **2019**, *575*, 330.
[15] A. Marino, C. Filippeschi, V. Mattoli, B. Mazzolai, G. Ciofani, *Nanoscale* **2015**, *7*, 2841.
[16] J. R. Tumbleston, D. Shirvanyants, N. Ermoshkin, R. Janusziewicz, A. R. Johnson, D. Kelly, K. Chen, R. Pinschmidt, J. P. Rolland, A. Ermoshkin, E. T. Samulski, J. M. DeSimone, *Science* **2015**, *347*, 1349.
[17] a) T. D. Ngo, A. Kashani, G. Imbalzano, K. T. Nguyen, D. Hui, *Composites, Part B* **2018**, *143*, 172; b) W. Du, X. Ren, C. Ma, Z. Pei, presented at ASME 2017 International Mechanical Engineering Congress and Exposition, Tampa, November **2017**.
[18] L. Y. Zhou, J. Fu, Y. He, *Adv. Funct. Mater.* **2020**, *30*, 2000187.
[19] a) D. Kokkinis, M. Schaffner, A. R. Studart, *Nat. Commun.* **2015**, *6*, 8643; b) J. Z. Cui, T. Y. Huang, Z. C. Luo, P. Testa, H. R. Gu, X. Z. Chen, B. J. Nelson, L. J. Heyderman, *Nature* **2019**, *575*, 164; c) M. Bissannagari, T.-H. Kim, J.-G. Yook, J. Kim, *Nano Energy* **2019**, *62*, 645; d) W. Zhao, F. Zhang, J. Leng, Y. Liu, *Compos. Sci. Technol.* **2019**, *184*, 107866.
[20] a) R. Tognato, A. R. Armiento, V. Bonfrate, R. Levato, J. Malda, M. Alini, D. Eglin, G. Giancane, T. Serra, *Adv. Funct. Mater.* **2019**, *29*, 1804647; b) Z. Chen, D. H. Zhao, B. H. Liu, G. D. Nian, X. K. Li, J. Yin, S. X. Qu, W. Yang, *Adv. Funct. Mater.* **2019**, *29*, 1900971.
[21] a) Y. Kim, H. Yuk, R. K. Zhao, S. A. Chester, X. H. Zhao, *Nature* **2018**, *558*, 274; b) T. Q. Xu, J. C. Zhang, M. Salehizadeh, O. Onaizah, E. Diller, *Sci. Rob.* **2019**, *4*, eaav4494; c) R. K. Zhao, Y. Kim, S. A. Chester, P. Sharma, X. H. Zhao, *J. Mech. Phys. Solids* **2019**, *124*, 244.
[22] J. H. Zhang, S. C. Zhao, M. Zhu, Y. F. Zhu, Y. D. Zhang, Z. T. Liu, C. Q. Zhang, *J. Mater. Chem. B* **2014**, *2*, 7583.
[23] C. Peters, O. Ergeneman, P. D. W. García, M. Müller, S. Pané, B. J. Nelson, C. Hierold, *Adv. Funct. Mater.* **2014**, *24*, 5269.
[24] M. Bissannagari, W. Lee, W. Y. Lee, J. H. Jeong, J. Kim, *Adv. Funct. Mater.* **2017**, *27*, 1701766.
[25] F. Zhang, L. Wang, Z. Zheng, Y. Liu, J. Leng, *Compos. Part A-Appl. S.* **2019**, *125*, 105571.
[26] P. Y. Chen, J. McKittrick, M. A. Meyers, *Prog. Mater. Sci.* **2012**, *57*, 1492.
[27] Z. Zhao, R. Fang, Q. Rong, M. Liu, *Adv. Mater.* **2017**, *29*, 1703045.
[28] A. R. Studart, *Chem. Soc. Rev.* **2016**, *45*, 359.
[29] P. Ball, in *Photobiological Sciences Online* (Ed: K. C. Smith), American Society for Photobiology **2012**.
[30] M. D. Shawkey, N. I. Morehouse, P. Vukusic, *J. R. Soc., Interface* **2009**, *6*, S221.
[31] E. A. Perigo, B. Weidenfeller, P. Kollar, J. Fuzer, *Appl. Phys. Rev.* **2018**, *5*, 031301.
[32] L. Lu, P. Guo, Y. Pan, *J. Manuf. Sci. Eng.* **2017**, *139*, 071008.
[33] S. Safaee, R. Chen, *Procedia Manuf.* **2019**, *34*, 731.
[34] P. M. Enriquez-Navas, M. L. Garcia-Martin, in *Frontiers of Nanoscience*, Vol. *4*, (Eds: J. M. Fuente, V. Grazu), Elsevier, Amsterdam, The Netherlands **2012**, Ch. 9.
[35] J. H. Lee, Y. M. Huh, Y. Jun, J. Seo, J. Jang, H. T. Song, S. Kim, E. J. Cho, H. G. Yoon, J. S. Suh, J. Cheon, *Nat. Med.* **2007**, *13*, 95.
[36] M. S. Wang, L. He, Y. D. Yin, *Mater. Today* **2013**, *16*, 110.
[37] P. S. Antonel, C. L. P. Oliveira, G. A. Jorge, O. E. Perez, A. G. Leyva, R. M. Negri, *J. Nanopart. Res.* **2015**, *17*, 294.
[38] A. C. Wright, M. Faulkner, *J. Vac. Sci. Technol., B* **2012**, *30*, 021603.
[39] C. Y. Du, M. Li, M. Cao, S. C. Feng, H. Guo, B. A. Li, *Carbon* **2018**, *126*, 197.
[40] X. Xu, H. Li, Q. Q. Zhang, H. Hu, Z. B. Zhao, J. H. Li, J. Y. Li, Y. Qiao, Y. Gogotsi, *ACS Nano* **2015**, *9*, 3969.
[41] L. Q. Ren, X. L. Zhou, Q. P. Liu, Y. H. Liang, Z. Y. Song, B. Y. Zhang, B. Q. Li, *J. Mater. Sci.* **2018**, *53*, 14274.
[42] a) A. S. Sokolov, V. G. Harris, *J. Eur. Ceram. Soc.* **2018**, *38*, 5257; b) R. M. Erb, J. S. Sander, R. Grisch, A. R. Studart, *Nat. Commun.* **2013**, *4*, 1712.
[43] Z. Y. Lin, Y. Liu, S. Raghavan, K. S. Moon, S. K. Sitaraman, C. P. Wong, *ACS Appl. Mater. Interfaces* **2013**, *5*, 7633.
[44] Y. D. Xu, Y. Q. Yang, D. X. Yan, H. J. Duan, C. Y. Dong, G. Z. Zhao, Y. Q. Liu, *J. Mater. Sci.: Mater. Electron.* **2017**, *28*, 9126.
[45] J. J. Martin, A. Caunter, A. Dendulk, S. Goodrich, R. Pembroke, D. Shores, R. M. Erb, *Proc. SPIE* **2017**, *10194*, 258.
[46] C. Y. Liang, C. Y. Liu, H. Wang, L. N. Wu, Z. H. Jiang, Y. J. Xu, B. Z. Shen, Z. J. Wang, *J. Mater. Chem. A* **2014**, *2*, 16397.
[47] P. Guillamat, J. Ignes-Mullol, F. Sagues, *Proc. Natl. Acad. Sci. USA* **2016**, *113*, 5498.
[48] N. Suksangpanya, N. A. Yaraghi, D. Kisailus, P. Zavattieri, *J. Mech. Behav. Biomed. Mater.* **2017**, *76*, 38.
[49] Y. S. Leung, T. H. Kwok, X. Li, Y. Yang, C. C. L. Wang, Y. Chen, *J. Comput. Inf. Sci. Eng.* **2019**, *19*, 021013.
[50] P. Calvert, *Chem. Mater.* **2001**, *13*, 3299.
[51] a) M. Vaseem, F. A. Ghaffar, M. F. Farooqui, A. Shamim, *Adv. Mater. Technol.* **2018**, *3*, 1700242; b) M. Bissannagari, J. Kim, *Ceram. Int.* **2015**, *41*, 8023.
[52] T. Wang, R. Patel, B. Derby, *Soft Matter* **2008**, *4*, 2513.
[53] B. N. Turner, R. Strong, S. A. Gold, *Rapid Prototyping J.* **2014**, *20*, 192.
[54] a) L. Li, A. Tirado, I. Nlebedim, O. Rios, B. Post, V. Kunc, R. Lowden, E. Lara-Curzio, R. Fredette, J. Ormerod, *Sci. Rep.* **2016**, *6*, 36212; b) C. Huber, C. Abert, F. Bruckner, M. Groenefeld, O. Muthsam, S. Schuschnigg, K. Sirak, R. Thanhoffer, I. Teliban, C. Vogler, *Appl. Phys. Lett.* **2016**, *109*, 162401.
[55] a) C. A. Koepele, M. Guix, C. Bi, G. Adam, D. J. Cappelleri, *Adv. Intell. Syst.* **2020**, *2*, 1900147; b) T. Y. Huang, M. S. Sakar, A. Mao, A. J. Petruska, F. M. Qiu, X. B. Chen, S. Kennedy, D. Mooney, B. J. Nelson, *Adv. Mater.* **2015**, *27*, 6644.
[56] I. C. Yasa, A. F. Tabak, O. Yasa, H. Ceylon, M. Sitti, *Adv. Funct. Mater.* **2019**, *29*, 1808992.
[57] A. Mostafaei, E. L. Stevens, J. J. Ference, D. E. Schmidt, M. Chmielus, *Addit. Manuf.* **2018**, *21*, 63.
[58] a) A. Mostafaei, K. A. Kimes, E. L. Stevens, J. Toman, Y. L. Krimer, K. Ullakko, M. Chmielus, *Acta Mater.* **2017**, *131*, 482; b) M. P. Paranthaman, C. S. Shafer, A. M. Elliott, D. H. Siddel,

M. A. McGuire, R. M. Springfield, J. Martin, R. Fredette, J. Ormerod, *JOM* **2016**, *68*, 1978.
[59] M. Brandt, *Laser Additive Manufacturing: Materials, Design, Technologies, and Applications*, Woodhead Publishing, Cambridge **2016**.
[60] F. Bittner, J. Thielsch, W.-G. Drossel, *Prog. Addit. Manuf.* **2020**, *5*, 3.
[61] a) C. Mikler, V. Chaudhary, T. Borkar, V. Soni, D. Jaeger, X. Chen, R. Contieri, R. Ramanujan, R. Banerjee, *JOM* **2017**, *69*, 532; b) J. Geng, I. Nlebedim, M. Besser, E. Simsek, R. Ott, *JOM* **2016**, *68*, 1972; c) C. Mikler, V. Chaudhary, V. Soni, B. Gwalani, R. Ramanujan, R. Banerjee, *Mater. Lett.* **2017**, *199*, 88.
[62] J. J. Martin, M. S. Riederer, M. D. Krebs, R. M. Erb, *Soft Matter* **2015**, *11*, 400.
[63] a) X. J. Li, Y. Yang, B. S. Xie, M. Chu, H. F. Sun, S. Y. Hao, Y. Y. Chen, Y. Chen, *Adv. Mater. Technol.* **2019**, *4*, 1800476; b) Y. Yang, X. J. Li, X. Zheng, Z. Y. Chen, Q. F. Zhou, Y. Chen, *Adv. Mater.* **2018**, *30*, 1704912; c) X. J. Li, Y. Chen, *J. Manuf. Process.* **2017**, *28*, 531.
[64] J. A. Lewis, *Adv. Funct. Mater.* **2006**, *16*, 2193.
[65] H. L. Ferrand, F. Bouville, T. P. Niebel, A. R. Studart, *Nat. Mater.* **2015**, *14*, 1172.
[66] H. Song, J. Spencer, A. Jander, J. Nielsen, J. Stasiak, V. Kasperchik, P. Dhagat, *J. Appl. Phys.* **2014**, *115*, 17E308.
[67] Y. Q. Liu, X. P. Zhang, Y. N. Xia, H. Yang, *Adv. Mater.* **2010**, *22*, 2454.
[68] A. J. Bandodkar, C. S. Lopez, A. M. V. Mohan, L. Yin, R. Kumar, J. Wang, *Sci. Adv.* **2016**, *2*, e1601465.
[69] a) S. Wu, C. M. Hamel, Q. Ze, F. Yang, H. J. Qi, R. Zhao, *Adv. Intell. Syst.* **2020**, *2*, 2000060; b) Y. Kim, G. A. Parada, S. D. Liu, X. H. Zhao, *Sci. Rob.* **2019**, *4*, eaax7329.
[70] B. Derby, *Annu. Rev. Mater. Res.* **2010**, *40*, 395.
[71] C. L. Zhang, K. P. Lv, N. Y. Hu, L. Yu, X. F. Ren, S. L. Liu, S. H. Yu, *Small* **2012**, *8*, 2936.
[72] R. R. Sondergaard, M. Hosel, F. C. Krebs, *J. Polym. Sci., Part B: Polym. Phys.* **2013**, *51*, 16.
[73] L. Zhang, B. J. Nelson, L. Dong, in *Encyclopedia of Nanotechnology* (Ed: B. Bhushan), Springer, Dordrecht, Netherlands **2012**, p. 1264.
[74] J. Billaud, F. Bouville, T. Magrini, C. Villevieille, A. R. Studart, *Nat. Energy* **2016**, *1*, 16097.
[75] K. Thorkelsson, P. Bai, T. Xu, *Nano Today* **2015**, *10*, 48.
[76] Z. Q. Liu, Z. F. Zhang, R. O. Ritchie, *Adv. Funct. Mater.* **2020**, *30*, 1908121.
[77] a) S. H. Hiew, A. Miserez, *ACS Biomater. Sci. Eng.* **2017**, *3*, 680; b) M. Eder, S. Amini, P. Fratzl, *Science* **2018**, *362*, 543.
[78] H. N. Hayenga, H. Aranda-Espinoza, *Biomaterial Mechanics,* CRC Press, Boca Raton **2017**.
[79] B. Pokroy, E. Zolotoyabko, *J. Mater. Chem.* **2003**, *13*, 682.
[80] F. Barthelat, H. Tang, P. D. Zavattieri, C. M. Li, H. D. Espinosa, *J. Mech. Phys. Solids* **2007**, *55*, 306.
[81] A. H. Barber, D. Lu, N. M. Pugno, *J. R. Soc., Interface* **2015**, *12*, 20141326.
[82] J. McKittrick, P. Y. Chen, L. Tombolato, E. E. Novitskaya, M. W. Trim, G. A. Hirata, E. A. Olevsky, M. F. Horstemeyer, M. A. Meyers, *Mater. Sci. Eng., C* **2010**, *30*, 331.
[83] M. A. Jansen, J. Williams, N. Chawla, N. M. Franz, *Adv. Mater.* **2019**, *31*, 1903526.
[84] J. C. Weaver, G. W. Milliron, A. Miserez, K. Evans-Lutterodt, S. Herrera, I. Gallana, W. J. Mershon, B. Swanson, P. Zavattieri, E. DiMasi, D. Kisailus, *Science* **2012**, *336*, 1275.
[85] M. L. Snead, D. H. Zhu, Y. P. Lei, S. N. White, C. M. Snead, W. Luo, M. L. Paine, *Mater. Sci. Eng., C* **2006**, *26*, 1296.
[86] V. Imbeni, R. K. Nalla, C. Bosi, J. H. Kinney, R. O. Ritchie, *J. Biomed. Mater. Res., Part A* **2003**, *66A*, 1.
[87] Y. Yang, X. J. Li, M. Chu, H. F. Sun, J. Jin, K. H. Yu, Q. M. Wang, Q. F. Zhou, Y. Chen, *Sci. Adv.* **2019**, *5*, eaau9490.
[88] B. G. Compton, J. A. Lewis, *Adv. Mater.* **2014**, *26*, 5930.
[89] Y. Si, L. H. Wang, X. Q. Wang, N. Tang, J. Y. Yu, B. Ding, *Adv. Mater.* **2017**, *29*, 1700339.
[90] J. H. Holtz, S. A. Asher, *Nature* **1997**, *389*, 829.
[91] a) K. Yu, N. X. Fang, G. Huang, Q. Wang, *Adv. Mater.* **2018**, *30*, 1706348; b) J. A. Jackson, M. C. Messner, N. A. Dudukovic, W. L. Smith, L. Bekker, B. Moran, A. M. Golobic, A. J. Pascall, E. B. Duoss, K. J. Loh, C. M. Spadaccini, *Sci. Adv.* **2018**, *4*, eaau6419.
[92] L. Q. Ren, B. Q. Li, Z. Y. Song, Q. P. Liu, L. Ren, X. L. Zhou, *Composites, Part B* **2019**, *164*, 458.
[93] F. L. Bargardi, H. L. Ferrand, R. Libanori, A. R. Studart, *Nat. Commun.* **2016**, *7*, 13912.
[94] X. J. Li, Y. Yuan, L. Y. Liu, Y. E. S. Leung, Y. Y. Chen, Y. X. Guo, Y. Chai, Y. Chen, *Bio-Des. Manuf.* **2020**, *3*, 15.
[95] E. B. Joyee, L. Lu, Y. Y. Pan, *Composites, Part B* **2019**, *173*, 106840.
[96] L. Hu, R. R. Zhang, Q. W. Chen, *Nanoscale* **2014**, *6*, 14064.
[97] X. L. Xie, Y. W. Mai, X. P. Zhou, *Mater. Sci. Eng., R* **2005**, *49*, 89.
[98] N. A. C. Lah, M. N. M. Zubir, M. A. L. Samykano, in *Handbook of Nanomaterials for Industrial Applications* (Ed: C. M. Hussain), Elsevier, Amsterdam **2018**, p. 324.
[99] T. Kimura, H. Ago, M. Tobita, S. Ohshima, M. Kyotani, M. Yumura, *Adv. Mater.* **2002**, *14*, 1380.
[100] E. S. Choi, J. S. Brooks, D. L. Eaton, M. S. Al-Haik, M. Y. Hussaini, H. Garmestani, D. Li, K. Dahmen, *J. Appl. Phys.* **2003**, *94*, 6034.
[101] N. Choudhary, S. Hwang, W. Choi, in *Handbook of Nanomaterials Properties*, Springer, Berlin **2014**, p. 709.
[102] M. Yoonessi, J. R. Gaier, J. A. Peck, M. A. Meador, *Carbon* **2015**, *84*, 375.
[103] S. Y. Wu, R. B. Ladani, J. Zhang, A. J. Kinloch, Z. H. Zhao, J. Ma, X. H. Zhang, A. P. Mouritz, K. Ghorbani, C. H. Wang, *Polymer* **2015**, *68*, 25.
[104] X. H. Li, J. Cai, Y. Y. Shi, Y. Yue, D. Y. Zhang, *ACS Appl. Mater. Interfaces* **2017**, *9*, 1593.
[105] a) A. Kamyshny, S. Magdassi, *Small* **2014**, *10*, 3515; b) B. H. Lu, H. B. Lan, H. Z. Liu, *Opto-Electron Adv* **2018**, *1*, 170004.
[106] S. Jegadheeswaran, A. Sundaramahalingam, S. D. Pohekar, *J. Therm. Anal. Calorim.* **2019**, *138*, 1137.
[107] C. Yuan, B. Duan, L. Li, B. Xie, M. Y. Huang, X. B. Luo, *ACS Appl. Mater. Interfaces* **2015**, *7*, 13000.
[108] a) Y. Kim, J. Kim, *Compos. Sci. Technol.* **2020**, *188*, 107961; b) K. Kim, J. Kim, *Int. J. Therm. Sci.* **2016**, *100*, 29.
[109] a) M. Liu, S.-W. Chiang, X. Chu, J. Li, L. Gan, Y. He, B. Li, F. Kang, H. Du, *Ceram. Int.* **2020**, *46*, 20810; b) J. C. Liu, W. W. Li, Y. F. Guo, H. Zhang, Z. Zhang, *Composites, Part A* **2019**, *120*, 140.
[110] H. Y. Yan, Y. X. Tang, W. Long, Y. F. Li, *J. Mater. Sci.* **2014**, *49*, 5256.
[111] O. Kose, A. Tran, L. Lewis, W. Y. Hamad, M. J. MacLachlan, *Nat. Commun.* **2019**, *10*, 510.
[112] J. Y. Chung, J. G. Lee, Y. K. Baek, P. W. Shin, Y. K. Kim, *Composites, Part B* **2018**, *136*, 215.
[113] Z. X. Zhang, J. Y. Qu, Y. Y. Feng, W. Feng, *Compos. Commun.* **2018**, *9*, 33.
[114] R. Xiong, J. Y. Luan, S. Kang, C. Ye, S. Singamaneni, V. V. Tsukruk, *Chem. Soc. Rev.* **2020**, *49*, 983.
[115] a) V. Sharma, M. Crne, J. O. Park, M. Srinivasarao, *Science* **2009**, *325*, 449; b) S. Vignolini, P. J. Rudall, A. V. Rowland, A. Reed, E. Moyroud, R. B. Faden, J. J. Baumberg, B. J. Glover, U. Steiner, *Proc. Natl. Acad. Sci. USA* **2012**, *109*, 15712.
[116] J. P. F. Lagerwall, C. Schutz, M. Salajkova, J. Noh, J. H. Park, G. Scalia, L. Bergstrom, *NPG Asia Mater* **2014**, *6*, e80.
[117] F. Kimura, T. Kimura, M. Tamura, A. Hirai, M. Ikuno, F. Horii, *Langmuir* **2005**, *21*, 2034.
[118] K. Yao, Q. Meng, V. Bulone, Q. Zhou, *Adv. Mater.* **2017**, *29*, 1701323.
[119] S. N. Fernandes, P. L. Almeida, N. Monge, L. E. Aguirre, D. Reis, C. L. P. de Oliveira, A. M. F. Neto, P. Pieranski, M. H. Godinho, *Adv. Mater.* **2017**, *29*, 1603560.
[120] T. Ding, K. Song, K. Clays, C. H. Tung, *Adv. Mater.* **2009**, *21*, 1936.

[121] J. P. Ge, L. He, Y. X. Hu, Y. D. Yin, *Nanoscale* **2011**, *3*, 177.
[122] R. M. Erb, J. J. Martin, R. Soheilian, C. Z. Pan, J. R. Barber, *Adv. Funct. Mater.* **2016**, *26*, 3859.
[123] a) E. Lauga, T. R. Powers, *Rep. Prog. Phys.* **2009**, *72*, 096601; b) J. Lighthill, *J. Eng. Math.* **1996**, *30*, 35.
[124] a) J. J. Abbott, K. E. Peyer, M. C. Lagomarsino, L. Zhang, L. X. Dong, I. K. Kaliakatsos, B. J. Nelson, *Int. J. Rob. Res.* **2009**, *28*, 1434; b) E. M. Purcell, *Proc. Natl. Acad. Sci. USA* **1997**, *94*, 11307.
[125] I. Cooperstein, E. Sachyani-Keneth, E. Shukrun-Farrell, T. Rosental, X. F. Wang, A. Kamyshny, S. Magdassi, *Adv. Mater. Interfaces* **2018**, *5*, 1800996.
[126] a) S. Lantean, G. Barrera, C. F. Pirri, P. Tiberto, M. Sangermano, I. Roppolo, G. Rizza, *Adv. Mater. Technol.* **2019**, *4*, 1900505; b) D. Podstawczyk, M. Nizioł, P. Szymczyk, P. Wiśniewski, A. Guiseppi-Elie, *Addit. Manuf.* **2020**, *34*, 101275; c) Z. Ji, C. Yan, B. Yu, X. Wang, F. Zhou, *Adv. Mater. Interfaces* **2017**, *4*, 1700629.
[127] S. Kim, F. M. Qiu, S. Kim, A. Ghanbari, C. Moon, L. Zhang, B. J. Nelson, H. Choi, *Adv. Mater.* **2013**, *25*, 5863.
[128] S. Roh, L. B. Okello, N. Golbasi, J. P. Hankwitz, J. A. C. Liu, J. B. Tracy, O. D. Velev, *Adv. Mater. Technol.* **2019**, *4*, 1970021.
[129] E. B. Joyee, Y. Y. Pan, *Soft Rob.* **2019**, *6*, 333.
[130] W. Zhu, J. X. Li, Y. J. Leong, I. Rozen, X. Qu, R. F. Dong, Z. G. Wu, W. Gao, P. H. Chung, J. Wang, S. C. Chen, *Adv. Mater.* **2015**, *27*, 4411.
[131] a) H. Wang, M. Pumera, *Chem. Rev.* **2015**, *115*, 8704; b) X. Z. Chen, M. Hoop, F. Mushtaq, E. Siringil, C. Z. Hu, B. J. Nelson, S. Pane, *Appl. Mater. Today* **2017**, *9*, 37.
[132] a) F. M. Qiu, R. Mhanna, L. Zhang, Y. Ding, S. Fujita, B. J. Nelson, *Sens. Actuators, B* **2014**, *196*, 676; b) A. Servant, F. M. Qiu, M. Mazza, K. Kostarelos, B. J. Nelson, *Adv. Mater.* **2015**, *27*, 2981.
[133] S. Tottori, L. Zhang, F. M. Qiu, K. K. Krawczyk, A. Franco-Obregon, B. J. Nelson, *Adv. Mater.* **2012**, *24*, 811.
[134] M. Medina-Sanchez, L. Schwarz, A. K. Meyer, F. Hebenstreit, O. G. Schmidt, *Nano Lett.* **2016**, *16*, 555.
[135] F. M. Qiu, S. Fujita, R. Mhanna, L. Zhang, B. R. Simona, B. J. Nelson, *Adv. Funct. Mater.* **2015**, *25*, 1666.
[136] M. Dong, X. P. Wang, X. Z. Chen, F. Mushtaq, S. Y. Deng, C. H. Zhu, H. Torlakcik, A. Terzopoulou, X. H. Qin, X. Z. Xiao, J. Puigmarti-Luis, H. Choi, A. P. Pego, Q. D. Shen, B. J. Nelson, S. Pane, *Adv. Funct. Mater.* **2020**, *30*, 1910323.
[137] S. Tottori, B. J. Nelson, *Biomicrofluidics* **2013**, *7*, 061101.
[138] C. Peters, O. Ergeneman, B. J. Nelson, C. Hierold, presented at 2013 IEEE 26th International Conference on Micro Electro Mechanical Systems (MEMS), Taipei, January **2013**.
[139] K. Hu, J. Sun, Z. Guo, P. Wang, Q. Chen, M. Ma, N. Gu, *Adv. Mater.* **2015**, *27*, 2507.
[140] a) R. Magisetty, N. S. Cheekuramelli, *Appl. Mater. Today* **2019**, *14*, 35; b) E. Périgo, J. Jacimovic, F. Ferré, L. M. Scherf, *Addit. Manuf.* **2019**, *30*, 100870; c) V. Chaudhary, S. Mantri, R. Ramanujan, R. Banerjee, *Prog. Mater. Sci.* **2020**, *114*, 100688.
[141] K. Rajaram, J. Kim, *Nano Energy* **2019**, *57*, 317.
[142] Y. Gu, D. Park, S. Gonya, J. Jendrisak, S. Das, D. R. Hines, *Addit. Manuf.* **2019**, *30*, 100843.
[143] Z. Ma, J. Ai, X. Zhang, Z. Du, Z. Wu, K. Wang, D. Chen, B. Su, *Adv. Intell. Syst.* **2020**, *2*, 1900140.
[144] A. H. Taghvaei, H. Shokrollahi, K. Janghorban, H. Abiri, *Mater. Des.* **2009**, *30*, 3989.
[145] a) H. Hamzehbahmani, P. Anderson, J. Hall, D. Fox, *IEEE Trans. Power Delivery* **2014**, *29*, 642; b) A. Hamler, V. Gorican, B. Sustarsic, A. Sirc, *J. Magn. Magn. Mater.* **2006**, *304*, e816.
[146] J. L. Mattei, M. L. Floc'h, *J. Magn. Magn. Mater.* **2003**, *257*, 335.
[147] M. Anhalt, *J. Magn. Magn. Mater.* **2008**, *320*, e366.
[148] J. Zou, Y. Gaber, G. Voulazeris, S. Li, L. Vazquez, L. F. Liu, M. Y. Yao, Y. J. Wang, M. Holynski, K. Bongs, M. M. Attallah, *Acta Mater.* **2018**, *158*, 230.
[149] L. M. Bollig, P. J. Hilpisch, G. S. Mowry, B. B. Nelson-Cheeseman, *J. Magn. Magn. Mater.* **2017**, *442*, 97.
[150] R. A. Jabr, *IEEE Trans. Magn.* **2005**, *41*, 4261.
[151] M. V. Patton, P. Ryan, T. Calascione, N. Fischer, A. Morgenstern, N. Stenger, B. B. Nelson-Cheeseman, *Addit. Manuf.* **2019**, *27*, 482.
[152] A. Hodaei, O. Akhlaghi, N. Khani, T. Aytas, D. Sezer, B. Tatli, Y. Z. Menceloglu, B. Koc, O. Akbulut, *ACS Appl. Mater. Interfaces* **2018**, *10*, 9873.
[153] C. Ding, L. B. Liu, Y. H. Mei, K. D. T. Ngo, G. Q. Lu, presented at *2018 IEEE Applied Power Electronics Conference and Exposition (APEC)*, San Antonio, March **2018**.
[154] S. I. Park, J. H. Ahn, X. Feng, S. Wang, Y. Huang, J. A. Rogers, *Adv. Funct. Mater.* **2008**, *18*, 2673.
[155] M. L. Wang, J. P. Lynch, H. Sohn, *Sensor Technologies for Civil Infrastructures*, Vol. *2*, Elsevier, Amsterdam **2014**.
[156] V. Popov, A. Koptyug, I. Radulov, F. Maccari, G. Muller, *Procedia Manuf.* **2018**, *21*, 100.
[157] V. Petersdorff-Campen, Y. Hauswirth, J. Carpenter, A. Hagmann, S. Boës, M. S. Daners, D. Penner, M. Meboldt, *Appl. Sci.* **2018**, *8*, 1275.
[158] C. Huber, C. Abert, F. Bruckner, M. Groenefeld, S. Schuschnigg, I. Teliban, C. Vogler, G. Wautischer, R. Windl, D. Suess, *Sci. Rep.* **2017**, *7*, 9419.
[159] F. Meng, R. P. Chaudhary, K. Gandha, I. Nlebedim, A. Palasyuk, E. Simsek, M. J. Kramer, R. T. Ott, *JOM* **2018**, *70*, 872.
[160] E. Peng, X. Wei, T. S. Herng, U. Garbe, D. Yu, J. Ding, *RSC Adv.* **2017**, *7*, 27128.
[161] S. J. Leigh, C. P. Purssell, D. R. Billson, D. A. Hutchins, *Smart Mater. Struct.* **2014**, *23*, 095039.
[162] X. Kuang, D. J. Roach, J. Wu, C. M. Hamel, Z. Ding, T. Wang, M. L. Dunn, H. J. Qi, *Adv. Funct. Mater.* **2019**, *29*, 1805290.
[163] a) L. Pigliaru, M. Rinaldi, L. Ciccacci, A. Norman, T. Rohr, T. Ghidini, F. Nanni, *Functional Composite Materials* **2020**, *1*, 4; b) T. F. V. Silva, M. H. Stoppa, *J. Thermoplast. Compos. Mater.* **2019**, 0892705719886894, https://doi.org/10.1177/0892705719886894; c) M. Skalon, M. Görtler, B. Meier, S. Arneitz, N. Urban, S. Mitsche, C. Huber, J. Franke, C. Sommitsch, *Materials* **2020**, *13*, 139.
[164] K. Kumar, *J. Appl. Phys.* **1988**, *63*, R13.
[165] a) Y. Yang, H. Hu, Z. Chen, Z. Wang, L. Jiang, G. Lu, X. Li, R. Chen, J. Jin, H. Kang, *Nano Lett.* **2020**, *20*, 4445; b) L. Jiang, Y. Yang, R. Chen, G. Lu, R. Li, J. Xing, K. K. Shung, M. S. Humayun, J. Zhu, Y. Chen, *Adv. Funct. Mater.* **2019**, *29*, 1902522; c) L. Jiang, Y. Yang, R. Chen, G. Lu, R. Li, D. Li, M. S. Humayun, K. K. Shung, J. Zhu, Y. Chen, *Nano Energy* **2019**, *56*, 216; d) L. Jiang, R. Chen, J. Xing, G. Lu, R. Li, Y. Jiang, K. K. Shung, J. Zhu, Q. Zhou, *J. Appl. Phys.* **2019**, *125*, 214501; e) H. Peng, X. Qian, L. Mao, L. Jiang, Y. Sun, Q. Zhou, *Appl. Phys. Lett.* **2019**, *115*, 203701.
[166] a) B. Heer, A. Bandyopadhyay, *Mater. Lett.* **2018**, *216*, 16; b) N. Lazarus, S. S. Bedair, G. L. Smith, *Addit. Manuf.* **2019**, *26*, 15.
[167] a) M. Y. Razzaq, M. Behl, K. Kratz, A. Lendlein, *Adv. Mater.* **2013**, *25*, 5730; b) K. Maier-Hauff, F. Ulrich, D. Nestler, H. Niehoff, P. Wust, B. Thiesen, H. Orawa, V. Budach, A. Jordan, *J. Neuro-Oncol.* **2011**, *103*, 317; c) J. Moon, M. G. Christiansen, S. Y. Rao, C. Marcus, D. C. Bono, D. Rosenfeld, D. Gregurec, G. Varnavides, P. H. Chiang, S. Park, P. Anikeeva, *Adv. Funct. Mater.* **2020**, *30*, 2000577.
[168] D. Yoo, H. Jeong, S. H. Noh, J. H. Lee, J. Cheon, *Angew. Chem.* **2013**, *125*, 13285.
[169] H. Kakwere, M. P. Leal, M. E. Materia, A. Curcio, P. Guardia, D. Niculaes, R. Marotta, A. Falqui, T. Pellegrino, *ACS Appl. Mater. Interfaces* **2015**, *7*, 10132.
[170] R. Mohr, K. Kratz, T. Weigel, M. Lucka-Gabor, M. Moneke, A. Lendlein, *Proc. Natl. Acad. Sci. USA* **2006**, *103*, 3540.
[171] a) S. Dutz, R. Hergt, *Int. J. Hyperthermia* **2013**, *29*, 790; b) R. M. Fratila, J. M. De La Fuente, *Nanomaterials for Magnetic and Optical Hyperthermia Applications*, Elsevier, Amsterdam **2018**.

[172] H. Mamiya, B. Jeyadevan, in *Nanomaterials for Magnetic and Optical Hyperthermia Applications*, Elsevier, Amsterdam **2019**, p. 13.
[173] R. Hergt, W. Andra, C. G. d'Ambly, I. Hilger, W. A. Kaiser, U. Richter, H. G. Schmidt, *IEEE Trans. Magn.* **1998**, *34*, 3745.
[174] N. Lee, D. Yoo, D. Ling, M. H. Cho, T. Hyeon, J. Cheon, *Chem. Rev.* **2015**, *115*, 10637.
[175] J.-P. Fortin, C. Wilhelm, J. Servais, C. Ménager, J.-C. Bacri, F. Gazeau, *J. Am. Chem. Soc.* **2007**, *129*, 2628.
[176] L. Lartigue, C. Innocenti, T. Kalaivani, A. Awwad, M. d. M. S. Sanchez Duque, Y. Guari, J. Larionova, C. Guérin, J.-L. G. Montero, V. Barragan-Montero, *J. Am. Chem. Soc.* **2011**, *133*, 10459.
[177] C. Martinez-Boubeta, K. Simeonidis, A. Makridis, M. Angelakeris, O. Iglesias, P. Guardia, A. Cabot, L. Yedra, S. Estradé, F. Peiró, *Sci. Rep.* **2013**, *3*, 1652.
[178] J. T. Jang, H. Nah, J. H. Lee, S. H. Moon, M. G. Kim, J. Cheon, *Angew. Chem., Int. Ed.* **2009**, *48*, 1234.
[179] X. Jing, H. Y. Mi, X. F. Peng, L. S. Turng, *Polym. Eng. Sci.* **2015**, *55*, 70.
[180] S. H. Noh, S. H. Moon, T. H. Shin, Y. Lim, J. Cheon, *Nano Today* **2017**, *13*, 61.
[181] Y. K. Yang, C. Y. Tong, J. C. Zhong, R. Y. Huang, W. H. Tan, Z. K. Tan, *J. Biomed. Mater. Res., Part B* **2018**, *106*, 1827.
[182] F. L. Gang, H. Yan, C. Y. Ma, L. Jiang, Y. Y. Gu, Z. Y. Liu, L. Y. Zhao, X. M. Wang, J. W. Zhang, X. D. Sun, *Chem. Commun.* **2019**, *55*, 9801.
[183] X. Z. Zhang, G. Zhao, Y. Cao, Z. S. Haider, M. Wang, J. P. Fu, *Biomater. Sci.* **2018**, *6*, 3139.
[184] X. L. Wang, L. L. Fan, J. Zhang, X. Y. Sun, H. Chang, B. Yuan, R. Guo, M. H. Duan, J. Liu, *Adv. Funct. Mater.* **2019**, *29*, 1907063.
[185] E. G. Garrido-Ramirez, B. K. G. Theng, M. L. Mora, *Appl. Clay Sci.* **2010**, *47*, 182.
[186] a) J. J. Hu, Y. H. Chen, Y. Q. Li, Z. J. Zhou, Y. Y. Cheng, *Biomaterials* **2017**, *112*, 133; b) G. He, S. Chen, Y. J. Xu, Z. H. Miao, Y. Ma, H. S. Qian, Y. Lu, Z. B. Zha, *Mater. Horiz.* **2019**, *6*, 711.
[187] C. Lin, J. X. Lv, Y. S. Li, F. H. Zhang, J. R. Li, Y. J. Liu, L. W. Liu, J. S. Leng, *Adv. Funct. Mater.* **2019**, *29*, 1906569.
[188] J. D. Tang, Q. F. Yin, Y. C. Qiao, T. J. Wang, *ACS Appl. Mater. Interfaces* **2019**, *11*, 21194.
[189] H. Q. Wei, Q. W. Zhang, Y. T. Yao, L. W. Liu, Y. J. Liu, J. S. Leng, *ACS Appl. Mater. Interfaces* **2017**, *9*, 876.
[190] K. E. Peyer, L. Zhang, B. J. Nelson, *Nanoscale* **2013**, *5*, 1259.

Chengqian Zhang is a doctoral student in the School of Mechanical Engineering at Zhejiang University. He received his B.S. degree at Zhejiang University (2016). His research interests include magnetic levitation, magnetic-driven manipulation, and their applications in density measurement, soft robotics, and biomedical engineering.

Xiangjia Li is an Assistant Professor in the Department of Aerospace and Mechanical Engineering at the School for Engineering of Matter, Transport and Energy at Arizona State University. She received her Ph.D. degree in industrial and systems engineering from the University of Southern California in 2019. Her research focuses on the development of ultra-fast multiscale and multimaterial 3D printing with bioinspired design methodologies and programmable functional materials for potential applications in aerospace, interfacial engineering, biomedical devices, and flexible sensor.

Yong Chen is a Professor in the Epstein Department of Industrial and Systems Engineering and Department of Aerospace and Mechanical Engineering at the University of Southern California. He received his Ph.D. degree in mechanical engineering from Georgia Institute of Technology in 2001. Before joining USC in 2006, he was a Senior Research and Development Engineer at 3D Systems Inc. His research focuses on additive manufacturing (3D printing) in micro- and mesoscales and related modeling, control, material, and application. He is a Fellow of the American Society of Mechanical Engineers.